
Star clusters in unperturbed spiral galaxies

Marcelo Mora



München, November 2008

Star clusters in unperturbed spiral galaxies

Marcelo Mora

DISSERTATION

an der Fakultät für Physik
der Ludwigs-Maximilians-Universität München

zur Erlangung des Grades
Doktor der Naturwissenschaften

Dr. rer. nat.

vorgelegt von

Marcelo Mora
aus Santiago, Chile

München, November 2008

1. Gutachter: Prof. Dr. R. Bender
 2. Gutachter: Dr. A. Weiss
- Tag der mündlichen Prüfung: 4 November 2008

To my wife Carolina.

Zusammenfassung

Sterne werden nicht isoliert sondern in Gruppen, bekannt als Sternhaufen geboren. Sternhaufen sind beobachtet worden in einer Vielzahl von Galaxien und unterschiedlichsten Umgebungen. Ihre Existenz enthält Informationen über die Geschichte der jeweiligen Galaxie und der entsprechenden Sternentstehungsprozesse. In den letzten Jahren sind Sternhaufen in aktiven Umgebungen detailliert untersucht worden während solche in ruhigeren Umgebungen weniger Beachtung fanden. Unter allen ungestörten Umgebungen konzentrieren wir uns hier auf 5 Spiralgalaxien die keine Anzeichen von externer Störung aufweisen: NGC 45, NGC 1313, NGC 4395, NGC 5236 and NGC 7793. Sternhaufen in diesen Galaxien wurden photometrisch beobachtet mit dem Hubble Space Telescope (HST) und spektroskopisch mit dem Very Large Telescope (VLT). Die Analyse der Sternhaufen, ihrer Masse, ihres Alters und ihrer Ausdehnung zeigt dass die Bildung von Sternhaufen ein noch nicht abgeschlossener Prozess ist, der von den lokalen Bedingungen abhängt. Die beobachteten Leuchtkraftfunktionen der Sternhaufen weisen Werte auf die in Übereinstimmung mit dem erwarteten Wert $\alpha \sim -2$ sind. Wir konnten eine wichtige Anzahl von Sternhaufen in NGC 45 identifizieren. Ihre Eigenschaften wurden photometrisch und spektroskopisch analysiert. Die Ergebnisse der Photometrie deuten darauf hin, dass diese Kugelsternhaufen zu einer einzigen metallarmen Population gehören. Die spektroskopischen Beobachtungen bestätigten dies für die 8 hellsten Haufen. Die gemessenen Geschwindigkeiten deuten auf Halo oder Bulge Kinematik hin. Eigenschaften des Absorptionsspektrums lassen Alter von der Größenordnung Gigajahre und $[\alpha/\text{Fe}]$ Werte geringer als in der Milchstraße aber ähnlich zu denen in anderen Zwerggalaxien in der lokalen Gruppe vermuten.

Abstract

Stars do not form in isolation, they form in groups known as star clusters. Star clusters are seen in a wide range of galaxies and environments. Their presence reveals the history of the host galaxy and the processes of its star formation. During the last years star clusters have been deeply investigated in violent environments, while the properties of star clusters in more quiet environments have received less attention. Among all unperturbed environments we focus on 5 spiral galaxies with no signs of external perturbations: NGC 45, NGC 1313, NGC 4395, NGC 5236 and NGC 7793. Star clusters lying in these galaxies were observed through HST imaging and VLT spectroscopy. The analysis of star cluster masses, ages, sizes, and their positions on the galaxies, showed that star cluster formation is an ongoing process that depends on the local conditions. The observed star cluster luminosity functions show values consistent with the expected $\alpha \sim -2$. We found an important number of globular clusters in NGC 45. Their properties are analyzed through photometry and spectroscopy. Photometry suggests that these globular clusters belong to a single metal poor population. Spectroscopy confirmed this for the 8 brightest ones. Velocities indicate halo or bulge kinematics. Absorption spectrum features indicate ages of the order of Gyr and $[\alpha/\text{Fe}]$ values lower than the Milky Way globular clusters, but similar to dwarf galaxies in the local group.

Contents

Zusammenfassung	v
Abstract	vi
1 Introduction	1
1.1 Star clusters	3
1.1.1 Star cluster formation and disruption	3
1.1.2 Properties and applications of star clusters	7
1.1.3 The environments of the star clusters	9
1.1.4 Deriving ages	12
2 Imaging of star clusters in unperturbed spiral galaxies with the Advanced Camera for Surveys: I. The low luminosity galaxy NGC 45	18
2.1 Introduction	20
2.2 Data and reductions	21
2.2.1 Photometry	21
2.2.2 Object sizes	23
2.2.3 Aperture corrections	24
2.2.4 Artificial object experiments	25
2.3 Selection of cluster candidates	28
2.3.1 Young clusters vs globular clusters	29
2.4 Young star clusters	32
2.4.1 Colors	32
2.4.2 Ages and masses	32
2.4.3 Sizes	35
2.4.4 Cluster disruption time	37
2.4.5 Luminosity function	38
2.5 Globular clusters	39
2.5.1 Sizes and color distribution	40
2.5.2 Globular-cluster specific frequency	40
2.6 Discussion and conclusions	42

3	ACS Imaging of Star clusters in unperturbed spiral galaxies: II. The relative properties of star clusters in five late type spirals	54
3.1	Introduction	56
3.2	Observation and reductions	58
3.2.1	Photometry	59
3.2.2	Size measurements	60
3.2.3	Completeness tests	60
3.3	Star cluster selection	60
3.3.1	Sample selection by size and brightness limit	60
3.3.2	Selection of old star cluster in the colour–magnitude diagrams	62
3.4	Colour–colour distributions	63
3.5	Ages, masses and sizes	66
3.5.1	Fitting ages, masses and internal extinction simultaneously	66
3.5.2	Internal extinction	68
3.5.3	Cumulative age distributions	69
3.5.4	Sizes	70
3.6	Luminosity functions	73
3.7	Cluster disruption	75
3.8	Radial distributions	77
3.8.1	Spatial completeness correction	78
3.8.2	Radial distribution of the surface density	78
3.9	Globular clusters	79
3.9.1	Total number of globular clusters	79
3.10	Summary and discussion	82
4	Spectroscopy of globular clusters in the low luminosity spiral galaxy NGC 45	86
4.1	Introduction	88
4.2	Candidates selection, observation and, reductions	89
4.2.1	Globular cluster selection	89
4.2.2	Observations and reductions	89
4.3	Radial velocities	90
4.4	Lick index calibrations	93
4.5	Results	96
4.5.1	Age diagnostic plots	96
4.5.2	Comparison with photometric ages	98
4.6	Discussion and conclusion	100
5	Conclusions	105
5.1	Synopsis	105
5.2	Outlook	106
5.3	Concluding remarks	107

List of Figures

1.1	Star cluster examples	2
1.2	Age distributions	7
1.3	Interacting galaxy	8
1.4	Spectral Energy Distribution (SED)	14
1.5	Graphical Lick index definition	16
2.1	NGC 45 ACS and WFPC2 pointings.	22
2.2	Photometry errors.	23
2.3	Artificial objects.	26
2.4	Completeness profiles.	27
2.5	Size errors.	27
2.6	Size distribution histograms.	28
2.7	Magnitude versus FWHM.	29
2.8	Color-magnitude diagram.	30
2.9	Spatial distribution.	31
2.10	Color-color diagrams.	33
2.11	Reddening-corrected color-color diagram.	34
2.12	Mass as a function of cluster age.	35
2.13	Effective radius vs mass and age.	36
2.14	Age distribution and mass distributions.	37
2.15	Detection limit.	39
2.16	B_{F435W} band luminosity function.	40
2.17	Histogram of the $V - I$ color distribution.	41
3.1	ACS and WFPC2 images.	57
3.2	Completeness and FWHMs	61
3.3	Size distributions.	62
3.4	Color-magnitude diagrams	64
3.5	Colour-colour diagrams	65
3.6	Mass as function of age.	67
3.7	GALEV normalized distributions.	70

3.8	Normalized cumulative cluster distributions I.	71
3.9	Normalized cumulative cluster distributions II.	72
3.10	Radius versus mass.	73
3.11	Luminosity functions.	75
3.12	Age distributions.	77
3.13	Radial surface density profiles.	78
3.14	Globular cluster candidate stamps.	80
4.1	Sample of the spectra.	91
4.2	Distributions of velocity measurements.	92
4.3	Globular cluster velocities versus H I velocity field.	94
4.4	Calibration of Lick indice.	96
4.5	Age diagnostic plots.	97
4.6	Iron versus Mgb and Mg2 plots	99

List of Tables

2.1	Aperture corrections as a function of FWHM.	25
2.2	Young star clusters.	44
2.3	Globular clusters with 4 band photometry.	50
2.4	Globular clusters with 3 band photometry.	52
3.1	Pointing coordinates and exposure times.	58
3.2	Summary of galaxy properties.	58
3.3	Number of selected star clusters.	63
3.4	Median internal extinction $E(B-V)$ towards the star clusters.	68
3.5	Young star cluster median effective radii.	71
3.6	Size coefficients.	72
3.7	Luminosity function coefficients.	74
3.8	Derived values from Eq. 3.8.	79
3.9	Total number of globular clusters and specific frequencies.	81
3.10	Red star cluster mean effective radii.	82
3.11	Derived star cluster properties for all the galaxies (Sample).	84
4.1	Log of the observations	90
4.2	Globular cluster velocities.	93
4.3	Lick indice calibration summary.	95
4.4	Metallicities from age diagnostic plots.	100
4.5	Ages from diagnostic plots.	100
4.6	Measured indice.	102

Chapter 1

Introduction

During the XVII century astronomers started to observe several nebulous objects. Due to the limitations of visual observations with telescopes of that time, their nature was unknown. It was in 1755 when Immanuel Kant in his book “Universal Natural History and the Theory of Heavens” suggested the possibility of the existence of entities of stars, which later Alexander Von Humboldt on his book *Kosmos* (1845), called *Island Universes*.

In 1784 the comet hunter Charles Messier compiled a catalog of non stellar objects (nebulous objects) in order to avoid confusion with possible new comets. Sir William Herschel was the first to study the properties of those nebulous objects. In 1850 Rosse suggested that some of the nebulous objects could be composed of stars. Nowadays it is known that some of the nebulous objects are star ensembles not related with the Milky way (i.e. galaxies) and the rest are objects which belong to our Galaxy (mostly planetary nebulae and star clusters). Since then, star clusters in the Milky Way have been extensively studied, however we still do not know if the Milky Way star clusters are typical for a spiral galaxy or just a special case.

In this manuscript a star cluster is considered as an ensemble of stars gravitationally bound, sharing common properties such as ages and abundances. Historically, in the Milky Way, star clusters have been separated in two apparently different classes : globular clusters and open star clusters.

Globular clusters are roughly spherical with $10^4 - 10^6$ members and mass ranges from 10^4 up to 10^6 Solar Masses (M_{\odot}) (Kissler-Patig 2000a). Milky Way globular clusters can be divided into two sub-populations. One population (metal-poor) is associated with the halo, (e.g. Morgan 1959; Kinman 1959; Zinn 1985; Ashman & Bird 1993; Barmby et al. 2000) and the other one (metal-rich) associated with the bulge/thick disk (e.g. Minniti 1995; Côté 1999). Although the origin of these populations is still a matter of debate, it is believed that each population is associated with different epochs or mechanisms of star and star cluster formations (Kissler-Patig 2000a).

Open star clusters are star ensembles with almost no central concentration, with a few tens to thousand of stars, with masses lower than 10^3 solar masses and mainly observed

in the galaxy disk.

However, it is not very clear where one classification ends and where the other begins. Examples of ambiguous classification (see Fig. 1.1) are listed in Stetson (1993). The panorama beyond the Milky Way is even less clear. Globular/Blue clusters in the Large Magellanic Cloud show ages and masses which have no counterpart in the Milky Way (Elson & Fall 1985). Beyond the local group there are several examples of star clusters which have no counterpart in the Milky Way. For example, Holtzman et al. (1992) found several star clusters in the starburst galaxy NGC 1275 (galaxy which is a recent merger), with ages of the order of 10^8 yr and masses in the range of $10^5 - 10^8 M_{\odot}$. In a galaxy merger (the Antennae galaxies) Whitmore & Schweizer (1995) observed blue massive star clusters. They interpreted them as the younger counterpart of the Milky Way globular clusters and eventually, if they live long enough, they would be expected to evolve into globular clusters.



Figure 1.1: **Left:** Typical Milky Way globular cluster: NGC 6093 (Image obtained from the Hubble heritage). **Center:** NGC 6791. This star cluster was considered to be neither globular cluster, nor an open star cluster (Image from Bernhard Hubl web page: <http://www.astrophoton.com/>). **Right:** One of the most known open star cluster since ancient times: The Pleiades (Image courtesy of Robert Gendler from astronomical picture of the day 2006 January 9).

Among the several environments in which star clusters have been found, the properties of star clusters in isolated spiral galaxies are least known. This lack of knowledge does not allow us to understand if the Milky Way star cluster population corresponds to a typical population for a spiral galaxy or if it is a rare case.

While many works have focused on massive star clusters and their environments, the properties of the low mass star clusters (i.e. open star clusters) are almost unknown outside the Local Group. Although, they are not as bright as the massive star clusters, they are still observable by the HST. Several questions remain unanswered i.e. How long do they survive? What are the mechanisms that trigger their formation? What are the relations between star clusters and their host galaxy? How do they compare among other similar galaxies? Is there any relation between the formation of the massive star clusters and the low mass ones? Do they show any relation between their sizes, masses and the original dust cloud from which were formed? Do the star clusters located in the same galaxy show similar or different properties?

In order to address these questions, and achieve insights of those questions, this thesis focuses on five unperturbed late type galaxies and their star cluster populations through

HST imaging and VLT spectroscopy. It is structured in the following way:

Chapter 2 focuses on a faint and isolated galaxy: NGC 45. Because of the isolation of this galaxy it is used for investigating how unperturbed an environment can be and still trigger star cluster formation. It is in this galaxy where the boundary condition of the star cluster selection criteria are tested and adopted for the entire sample. We found a modest population of star clusters not very massive showing masses at the lower limit comparable with the open star clusters of the Milky Way. Also we investigate how long will the star cluster live in this galaxy, although the results are not very conclusive due to the small number of detected star clusters. The discovery of 19 globular clusters is analyzed and the specific frequency¹ derived $S_N = 1.4 - 1.9$ which is high for the galaxy type.

In chapter 3 the analysis is extended to 4 more spiral galaxies. All galaxies have similar spiral classification, similar distance and no obvious sign of external perturbations. We look at ages and masses of the star clusters on each galaxy and we compare their local and global properties (i.e. galaxy to galaxy comparisons and different areas in the same galaxy). From this is concluded that the star cluster formation is a very localized process. We also analyze the luminosity function (and we found no different results compared with previous studies). The presence of most massive clusters was analyzed and corresponds to size of sample effects. Also a shallow increase in the star clusters mass versus size is seen. We were not able to derive confident estimations of the disruption times from the age distribution, nor give a definitive answer whether cluster disruption is predominantly mass-dependent or mass-independent.

In chapter 4 the thesis focuses in the analysis of the old globular cluster population previously found in NGC 45. The analysis is done by spectroscopy and it is concluded that the globular clusters have sub-solar metallicities with similar values found in previous work in galaxies near by NGC 45 (e.g. Olsen et al. 2004). In this chapter we close the circle getting a general understanding of the properties of the old and young star cluster populations in NGC 45.

1.1 Star clusters

Before to start with the chapters where the work is written, I would like to give a small review on what is relevant to this work.

1.1.1 Star cluster formation and disruption

Formation

One of the first ideas about the origin of globular clusters was formulated by Peebles & Dicke (1968). They suggested that the smallest gravitationally unstable clouds, produced just after recombination from isothermal perturbations, could be identified as the progenitors of globular clusters. Later, Fall & Rees (1985) argued that globular clusters are formed in the collapsing gas of a protogalaxy. Searle & Zinn (1978) suggest that star clusters are formed in transient protogalactic fragments that fall into the galaxy. Schweizer

¹For the definition of the Specific Frequency see Eq. 1.1

(1987) poses that some of the star clusters (and globular clusters) may form in galaxy mergers. Ashman & Zepf (1992) suggest that some of the globular clusters are formed during the interaction or mergers of galaxies. Harris & Pudritz (1994) argued that globular clusters formed out of dense cores within supergiant molecular clouds. Elmegreen (1994) suggested the possibility of star cluster formation as consequence of the molecular cloud formation from the compressing waves of the arms of the spiral galaxies. Evidence favoring this scenario is seen in NGC 45 where star clusters were found in a galaxy without evidence of external perturbation (see chapter 2). Lee et al. (1995) proposed that star clusters form in bursts at the merging interfaces as protogalactic clouds collide.

It is still a matter of debate if there is an unique mechanism that triggers the molecular cloud collapse, and therefore star cluster formation. The merger scenario would explain the several globular cluster populations found in ellipticals (e.g. Côté et al. 2004) as well as the young massive clusters in interacting systems (e.g. Schweizer 1987; Ashman & Zepf 1992; Zepf & Ashman 1993; Kumai et al. 1993; Whitmore 2003). However, young massive star clusters have been found in spiral galaxies (e.g. Larsen & Richtler 1999) indicating that galaxy mergers (i.e. violent environments) are not the only mechanism which leads to massive star cluster formation.

While the mechanism considered to cause cloud collapse differs from author to author, there is a general consensus that the mechanism by which star clusters (i.e. open star clusters, young massive star clusters, and globular clusters) are formed is the same, and their apparent differences are only due to the different conditions (Elmegreen & Efremov 1997) in the environment of the molecular clouds. Under this assumption, a massive star cluster will be formed in a high pressure environment, while a low mass star cluster will be formed in a low pressure environment.

Therefore, the origin of star clusters is in the molecular clouds which initially are in equilibrium between the gravitational force (gravitational potential energy) and the internal pressure (mostly kinetic energy). When molecular clouds are compressed, they become unstable and start to collapse. Dense regions turn into stars first. The less dense regions of the surrounding cloud will be blown up as a consequence of the young massive stars, stellar winds and, supernova explosions. With the expelling of the surrounding cloud, the star formation ends. This scenario is supported by observations of star forming regions and star clusters hidden inside the dust cloud, known as embedded star clusters. For a review of embedded star clusters see Lada & Lada (2003).

Disruption

Several mechanisms are involved in star cluster disruptions. The first one in the life of a star cluster is the gas removal phase on which the stellar winds expel the remanent gas, reducing the cluster mass and the binding energy, expanding the cluster and, eventually dissolving it (e.g. Goodwin 1997). Lada & Lada (2003) suggest by comparing the number of embedded star clusters with the open star clusters in the Milky Way, that 90–95% of the embedded star clusters will emerge from molecular clouds as unbound systems. This early disruption stage in the star cluster life is known as “infant mortality”. However, the “infant mortality” phase is not the only stage in star cluster lives that may disrupt them.

Since star clusters do not live isolated they have to face gravitational interactions with the galactic bulge, or disk crossing (Spitzer 1987). Also they are affected by spiral arms crossing (e.g. Gieles et al. 2007a) and interactions with molecular clouds (e.g. Spitzer & Harm 1958; Gieles et al. 2006b).

These processes increase the kinetic energy of the stars in the clusters, expanding the cluster sizes, decreasing the binding energy and, as a direct consequence, some of the stars in the cluster will reach the escape velocity and will leave the cluster. This will reduce the star cluster mass and, eventually will disrupt the star cluster.

Since observations are snap-shots of the current star cluster evolution of the host galaxies, it is necessary to look at the entire properties of the star clusters in order to derive the rate of star cluster disruption. This is achieved by looking at the number of star clusters versus star cluster ages and masses. These quantities are compared with models and empirical laws. Three major assumption are taken into account:

- The Initial Mass Function (IMF) (i.e. the initial distribution in mass of the star clusters). Observations suggest (Elmegreen & Efremov 1997; Hunter et al. 2003; Bik et al. 2003; de Grijs et al. 2003; Zhang & Fall 1999) that the cluster Initial Mass Function (IMF) is a power law of index $\alpha \sim -2$.
- The star cluster formation rate (i.e. how many clusters form per unit of time), which could be, for example, a constant rate (e.g. Boutloukos & Lamers 2003) or a Gaussian burst (e.g. Whitmore et al. 2007).
- The third assumption is how clusters are disrupted. Two different approaches are currently adopted. The mass-dependent approach from the “Utrecht group” (e.g. Boutloukos & Lamers 2003; Gieles et al. 2006b; Lamers et al. 2005b,a) and mass-independent from the “Baltimore group” (e.g. Fall et al. 2005; Chandar et al. 2006; Whitmore et al. 2007).

The “Utrecht group” considers a magnitude limited sample on which the star cluster disruption time depends on the initial mass of a cluster as M_i^γ , where $\gamma = 0.62$ (Lamers et al. 2005b). It also considers the decrease of the cluster mass due to stellar evolution (i.e. mass lost due to the stellar winds) and tidal effects (i.e. encounter with other objects in the star cluster orbits such as the galaxy disk, molecular clouds, etc) for a cluster older than 10^7 yr which already survived the infant mortality. The expected slope of the age distribution of a bandpass-dependent star cluster sample goes from ~ -0.8 up to ~ -1.4 . Initially, it was assumed that clusters disrupt instantaneously at t_{dis} (Boutloukos & Lamers 2003), but later on the disruption was treated in a more realistic way on which star clusters loss mass in gradual form (Lamers et al. 2005a).

The “Baltimore group” considers that star clusters are disrupted in two phases. A rapid mass-independent phase for the first 10^8 yr, modeled as a constant number loss $dN/d\tau \propto \tau^\gamma$, where $\gamma = -1$; which is defined as 90% of infant mortality. And a longer term mass-dependent phase mimicking the effects of two body-evaporation (i.e. constant mass loss), modeled as the time dependence resulting from two-body relaxation for a cluster in the tidal field of the host galaxy $M = M_0 - \mu_{ev}\tau$, where $\mu_{ev} \sim 2 \times 10^{-5} M_\odot \text{yr}^{-1}$

(Fall & Zhang 2001). The main observational support for the “Baltimore group” are observations from the Antennae galaxies (Whitmore & Schweizer 1995), the only galaxy where it is possible to make mass and magnitude selection criteria considering a high percentage of completeness of the sample.

In figure 1.2 both groups analyzed the same data, obtaining similar results, differing in their interpretations. Data corresponds to star clusters in the Small Magellanic Cloud. In the left panel the original data from Rafelski & Zaritsky (2005) is shown. Central panel corresponds to the “Baltimore group” (Chandar et al. 2006) analysis and, the right panel corresponds to the analysis done by the “Utrecht” group. Rafelski & Zaritsky (2005) found a slope of $dN(t)/dt = -2.1$. They normalized the sample with the number of field stars that were formed at each bin. The “Baltimore group” found a slope $dN/dt \propto -0.85$ (Chandar et al. 2006) and, the “Utrecht group” found a slope $dN/dt \propto -0.84$ (Gieles et al. 2007b). Both groups did not normalize the distributions as Rafelski & Zaritsky (2005) did. The “Baltimore group” interpreted the slope dN/dt as evidence of constant star cluster mass loss, and the value of the slope was directly compared with the Antennae and Milky Way dN/dt values (~ -1), concluding that star clusters these three galaxies follow similar disruption behaviors.

The “Utrecht group” interpreted the dN/dt slope as result of the magnitude limitation of the Rafelski & Zaritsky (2005) sample. They also pointed out that is not possible to compare the Rafelski & Zaritsky (2005) sample with the Antennae sample because the Antennae sample is mass limited, while Rafelski & Zaritsky (2005) sample is magnitude limited.

Independent of the mass-limited or magnitude-limited sample, the key point is whether the star cluster disruption is mass dependent or mass independent. Distinguishing between these two scenarios is not possible nowadays. Most of the observations are magnitude limited and the only galaxy where is possible to use a mass limited sample is the Antennae galaxy.

It is important to discriminate whereas the sample is magnitude-limited or mass-limited. Direct comparison of both samples without further considerations will lead to non valid conclusions. Chandar et al. (2006) considered star clusters with masses greater than $10M_{\odot}$ but ignoring that the sample from (Rafelski & Zaritsky 2005) is limited by magnitude and therefore, it is not possible to compare with the Antennae data (Whitmore & Schweizer 1995), which is mass limited.

The “Utrecht group” does not consider that often observations are not limited only by one filter magnitude (like in the case of these thesis) and usually is a mixture of two or more magnitude limitations. In the other hand the data of the “Baltimore group” is mainly based in the Antennae, which is a very special galaxy and to obtain a mass limited sample in a different galaxy is a challenging task due to the actual instrument limitations.

In this thesis in Chapter 3 we tried to elucidate these two groups disruption scenarios, however considering the present data, we were not able to give a conclusive answer. Thus, the disruption controversy will not be solved until extremely deep data can be acquired in a galaxy with high star cluster formation rate (i.e. a starburst galaxy). It will be necessary to cover a wide range of star cluster masses considering extremely low masses from a few hundred of solar masses (M_{\odot}) up to $10^6 - 10^7 M_{\odot}$. With a wide range in mass and high

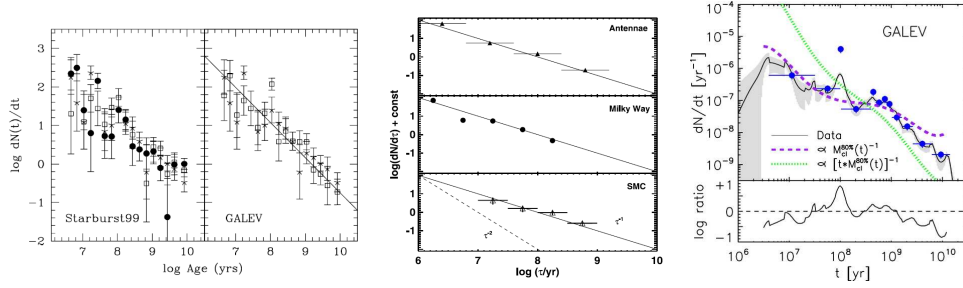


Figure 1.2: Left: Number of star clusters versus age (age distribution) for star clusters in the Small Magellanic Cloud (SMC) considering two Simple Stellar Population models: GALEV and Starburst99 from Rafelski & Zaritsky (2005). Center: Age distributions of star clusters in SMC (open triangles), the Milky Way (filled circles) and the Antennae (filled triangles) from Chandar et al. (2006). Note that the three age distributions are described by power law τ^{-1} and is the main argument in favor of constant star cluster mass loss. Right: Age distribution of the SMC star clusters based on Rafelski & Zaritsky (2005) sample from Gieles et al. (2007b)

number of clusters it will be possible to make a selection in mass as well as in magnitude and therefore, compare both scenarios.

1.1.2 Properties and applications of star clusters

At the distance of the galaxies which have been studied in this thesis, the stars that compose the star clusters are not resolved and each star cluster is seen as a single source. Therefore, instead of focusing on the individual properties of the star clusters, this thesis focuses on their collective properties, revealing information about their host galaxies and, making possible comparisons between them. Some of the star and globular cluster applications and properties are:

- **Star clusters as star formation and galaxy environment tracers:** Stars do not form in isolation, they form in associations which are the star clusters. Therefore, by studying the star cluster ages it is possible to reconstruct the past star formation i.e. the star formation history in the host galaxy. However, there are limitations which must be considered, such as the completeness of the sample (i.e. the limit until the sample is reliable). By looking at the number of clusters versus age it is possible to derive how much time a star cluster of $10^4 M_{\odot}$ will live. This time is known as the star cluster disruption time (Boutloukos & Lamers 2003). The disruption time is an indirect measurement of the violence of the environment in which star clusters are located in their host galaxy. The disruption time is expected to be shorter for violent environments because two body encounters are more likely in interacting galaxies (e.g. tidal waves, cloud encounters, etc) than in more quiet (e.g. non interacting) galaxies. The determination of the disruption time is important for the study of the past star cluster formation in the galaxies because most of the old star clusters will be disrupted. If this effect is not taken into account, the past star cluster formation will be underestimated. Therefore, by considering the star

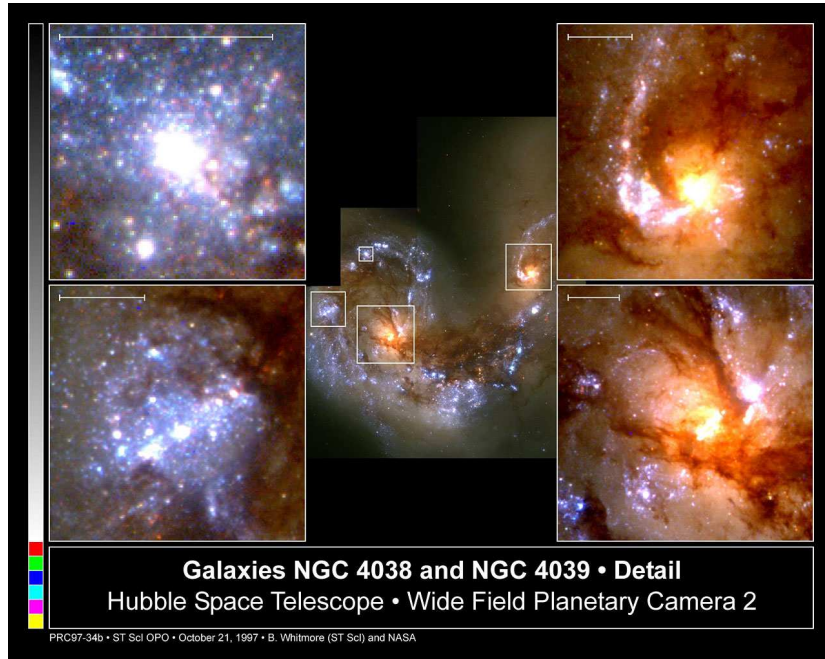


Figure 1.3: One of the most famous interacting galaxies: NGC 4038 and NGC 4039, The Antennae. This figure shows how star cluster formation blooms in galaxy mergers due to the compression of the interstellar media, triggering the molecular cloud collapse and star cluster formation. Most of the objects shown here are star clusters. Blue objects are young star clusters and the orange ones are young star clusters lying behind the dust. Since those clusters are formed in this highly perturbed environment most of them will be disrupted by interactions with the surrounding environment and the nearby star clusters.

cluster formation rate, the star cluster disruption rate, the time that a cluster will remain bound, the observed star cluster ages and, the limitations of the sample; it is possible to reconstruct part of the past star cluster formation. We attempted this for our five galaxies, but unfortunately with the present space telescope (HST) plus the distance of our galaxy, we were not able to calculate a good estimation of this time. Nevertheless, we were able to reconstruct (under the data limitation) part of the past star cluster formation on our galaxies.

- **Luminosity functions:** This property quantifies the number of objects per luminosity unit. For young star clusters, the luminosity function is often expressed as the number of star clusters versus magnitude (logarithmic luminosity) and it is described by a power-law distribution: $N(L)dL \propto L^{-\alpha}$ with $-\alpha \sim -2$. It is a powerful tool that gives indirect information about the range in masses of the star clusters (present day mass function). It also defines the brightest star cluster luminosity, although the brightest object often is brighter than the expected value, making it difficult to understand if the brightest cluster was formed by a special mechanism or is only a size-of-sample effect (Hunter et al. 2003; Larsen 2002). In this thesis we simulate star cluster luminosity functions using

the derived α values and the brightest star cluster on each galaxy can be explained as a size-of-sample effects (see chapter 3).

- **Star clusters as merger tracers:** Massive star clusters, which survived interactions with their host galaxy, are observed in gas rich mergers (e.g. Whitmore & Schweizer 1995; Schweizer 1997). Galaxies showing signs of previous interactions show globular clusters with ages similar to the merger remanent (e.g. Schweizer & Seitzer 1998; Goudfrooij et al. 2001). Therefore merger events leave imprints in the local globular cluster systems making possible to trace back those events.

- **Globular cluster color distributions and specific frequency:** When more than one filter is available, it is possible to study the color distributions of the globular clusters. The color distributions have been mainly studied in elliptical galaxies (for a recent comprehensive study on this kind of galaxies see the ACS Virgo Cluster Survey, Côté et al. 2004). It has been found that globular clusters generally show bi-modal distributions in elliptical galaxies (showed first by Zepf & Ashman 1993). This bimodality argues in favor of different mechanisms, origins and, metallicities of the globular cluster sub-populations. The studies of globular clusters in spiral galaxies are more challenging than in ellipticals because of the dust lying in the galaxy disk causes reddening toward each object and makes its correction more difficult. Due to this, the number of spiral galaxies in which globular clusters have been seen is much smaller than elliptical galaxies. Therefore, the globular cluster studies are mostly reduced to the Milky Way, M31 and M33. An extra caveat of the colors must be pointed out: An increase of ages show the same effect than an increase of metallicities in the integrated light of the globular clusters. Effect known as the age metallicity degeneracy (e.g. Faber 1972, 1973; Rose 1985; Renzini & Buzzoni 1986; Worthey 1994). In order to break this effect at least 4 colors covering a wide range in wavelength are needed. The best way to avoid this effect is through spectroscopic studies as it is done in this thesis in chapter 4.

The specific frequency of globular clusters is a magnitude weighted quantity which allows to compare different globular cluster populations in different galaxies under the same condition. It was defined by Harris & van den Bergh (1981) as :

$$S_N = N_{GC} \times 10^{0.4 \times (M_V + 15)} \quad (1.1)$$

Where N_{GC} is the total number of globular clusters in the galaxy and M_V is the visual magnitude of the host galaxy. The specific frequency is higher for elliptical galaxies than for spiral galaxies.

1.1.3 The environments of the star clusters

In this subsection I briefly discuss where star clusters have been found. It is far from be a complete review on the subject, but at least should give to the reader an idea of what is going on; moreover, where this thesis fit in. Therefore, it is bias toward young star clusters in spiral galaxies. For more complete reviews I suggest to look at Whitmore (2003), Larsen (2004b) for young star clusters and Harris (1991), Ashman & Zepf (1998) and Brodie & Strader (2006) for globular cluster reviews.

During the last 15 years extragalactic star cluster studies has been mainly focused on massive star clusters. Early studies were done in non-merger galaxies such as NGC 1569 and NGC 1705. (O’Connell et al. 1994), M82 (O’Connell et al. 1995), and in 9 starburst galaxies (Meurer et al. 1995). However, systematic studies started with the observations of merging galaxies and whether globular clusters were being formed (Whitmore 2003). Shortly after, the studies were expanded toward young massive star clusters in starburst galaxies and later expanded toward spiral galaxies and dwarf/irregular galaxies.

Galaxy mergers

It is in this environment where the most spectacular star cluster population results have been obtained. For example, Lutz (1991) found young globular cluster candidates in the merger remnant NGC 3597. Holtzman et al. (1996) found blue objects in NGC 6052 which are likely to be comparable in mass to Milky Way globular clusters. Carlson et al. (1998) found young star clusters in NGC 1275 with colors which suggest that they are a single-age population. Whitmore et al. (1993) found “40 blue point-like objects” in NGC 7252 with colors, spatial distributions, and sizes compatible with the hypothesis that these objects formed after the collision of two spiral galaxies. Schweizer et al. (1996) found 102 star cluster candidates in NGC 3921, concluding that the star clusters or the progenitors experienced the same violent relaxation as the luminous matter of the two merging galaxies. All previous examples correspond to merger remnants, but the most spectacular due to its close distance, the text book example, is the ongoing merger of NGC 4038/39 (Whitmore & Schweizer 1995), the “Antennae” (See Fig.1.3), which confirmed the possibility for globular clusters to be formed in mergers.

Galaxy mergers have shown that in these violent environments the star cluster formation blooms and that the formation of young massive star clusters (i.e. the young counterpart of the globular clusters) is more likely, although it is not the only environment on which they form.

Starburst galaxies

Starburst galaxies show high rate of star formation. Sometimes the starburst is stimulated by small interaction with nearby galaxies, accretion of companion satellite galaxies or internally stimulated, and since star clusters trace the ongoing star formation, they have been also observed in this environment. For example, in the central region of spiral NGC 253 Watson et al. (1996) found few massive star clusters. Barth et al. (1995) found star clusters in the ring of NGC 1097 and NGC 6951. A famous example of a starburst galaxy is M82 where van den Bergh (1971) found bright knots. Later, O’Connell et al. (1995) confirmed the previous result and they found 100 star clusters. Most of the previous galaxies show some evidence of interaction with their neighbors, but starburst galaxies can also be observed without any interaction with any neighbor as it is the case of NGC 5253. In this galaxy Harris et al. (2004) concluded that the star cluster formation was not triggered by an interaction because NGC 5253 is too isolated.

Starburst galaxies are the proof that massive star cluster formation is not exclusive

of merging galaxies and a hint that massive star clusters form where strong star formation occurs. In this thesis we study an isolated starburst galaxy NGC 5236, we confirm massive star clusters previously detected by Larsen & Richtler (1999) and we add new candidates.

Dwarf and irregular galaxies

Among the irregular galaxies, young star clusters were found in one of the closest one: The Large Magellanic Cloud (e.g. Shapley & Lindsay 1963; Searle et al. 1980; van den Bergh 1981; Elson & Fall 1985). Several star clusters were found in I Zw 18 (Meurer et al. 1995). Two highly studied dwarf (starburst) galaxies are NGC 1569 (e.g. Arp & Sandage 1985; O’Connell et al. 1994; de Marchi et al. 1997; Hunter et al. 2000, and others) and NGC 1705 (e.g. Melnick et al. 1985; O’Connell et al. 1994; Maíz-Apellániz 2001; Billett et al. 2002; Vázquez et al. 2004). Conti & Vacca (1994) found blue knots in the dwarf galaxy He 2-10 which contains two starburst regions. Several star clusters in irregular galaxies were found by Billett et al. (2002).

Dwarf and Irregular galaxies also show young massive star clusters and star clusters, however most of the galaxies are starburst galaxies or they are in interaction with other galaxies.

Spiral galaxies

Spiral galaxies correspond to 60% of all galaxies in low-density region of the universe (Binney & Tremaine 1987). They are galaxies like the Milky Way and M31. They contain a prominent disk composed of stars, gas and, dust. Among the properties of the disk the most characteristic one are spiral arms. Spiral arms are filaments in which stars are continuously being formed. The spiral arms show different shapes, lengths and, prominence from one galaxy to another (Binney & Tremaine 1987).

Two of the best studied spiral galaxies are M31 and M33. M31 is known since ancient times. The first work was the identification of nebulous objects as globular clusters by Hubble (1932). Almost half a century later Hodge (1979) made a catalog of 403 star cluster candidates and later Hodge et al. (1987) found that some of these clusters were young clusters. Barmby et al. (2000) found several young star clusters from globular cluster catalogs and Beasley et al. (2004, 2005) noted that several globular clusters showed young star cluster type spectra. The latest work was done by Krienke & Hodge (2007). They found intermediate and old open clusters, also evidence of the same rate of star cluster destruction as in the Milky Way and, they extrapolate a total number of 80000 star clusters in M31. M33 has been studied for almost 50 years. Hiltner (1960) observed the colors and magnitudes of the star clusters in both galaxies. Since then, several compilations of star clusters in M33 have been published (e.g. Melnick & D’Odorico 1978; Christian & Schommer 1982, 1988; Mochejska et al. 1998; Chandar et al. 1999, 2001; Sarajedini et al. 2000, among others).

More systematic studies involving several spiral galaxies under the same observational constraints have been done by Larsen & Richtler (1999); Larsen (1999); Larsen &

Richtler (2000); Larsen (2004b, 2002) and this thesis, for the young star cluster population and by Olsen et al. (2004); Chandar et al. (2004); Rhode et al. (2007) for the globular cluster population. These studies compare the properties of the star clusters in their host galaxy as well as the properties of their host galaxies. An important result from these studies is that the luminosity function of star clusters show values $\alpha \sim 2$ (Larsen 2002), we also found similar values in this work, and the globular cluster specific frequency in spirals seems to correlate best with the Hubble type and bulge/total ration, rather with galaxy luminosity or galaxy mass (Chandar et al. 2004), however Rhode et al. (2007) conclude that the specific frequency of metal-poor globular cluster increases with the galaxy mass. But, from the spectroscopic analysis in NGC 45, the color of its globular clusters and, the derived specific frequency suggest that NGC 45 does not follow the conclusions drawn by Rhode et al. (2007)

Spiral galaxies have shown that the formation of massive star clusters may occur not only in starburst galaxies, also in “normal spiral galaxies”

Concluding remarks

Star clusters are present in almost all kind of galaxies. Regarding the young massive star clusters, their presence in several environments has been investigated and the possible limits of their formation in unperturbed galaxies and dwarf/irregular galaxies have been widely explored. However, the low mass extreme is by far not deeply investigated. Up to now Billett et al. (2002) and Eskridge et al. (2008) have investigated the star cluster population in unperturbed dwarf/irregular galaxies. A direct complement to this work is the chapter 2 of this thesis where the low luminosity unperturbed galaxy NGC 45 is shown to have similar star cluster properties, despite the fact that is a spiral galaxy.

Here is the original driving of this thesis but instead of investigating dwarf and irregular galaxies, this work investigates spiral galaxies which are unperturbed . One of the advantages presented here are that the galaxies were observed using the same instrument (HST) and the data is directly comparable without bias due to different instrumental setup and data limitations.

1.1.4 Deriving ages

Prior to finishing this introduction it is worth to explain the models and the methods used for age and mass derivations in this thesis.

Simple Stellar Population (SSP) models

If we took one of the Milky Way globular clusters with known properties (such as mass, age, and chemical composition) and we put it outside the local group, we will not see the individual stars that compose it. We will see the combined light, i.e. the integrated colors as the addition of the effects of the light from each star.

If the integrated light is the only information that we can get from this star cluster, Is it possible to recover the previously known properties? Moreover, if we could calculate how the individual properties were/are at earlier/later times we can therefore calculate how the

integrated light will change with time. This idea was originally posed by Crampin & Hoyle (1961) and it was the beginning of Simple Stellar Population models, although the first formal work was made by Tinsley (1968). The main idea behind the Simple Stellar Population models is that star clusters are composed by individual stars sharing the same chemical composition (formed from the same cloud) and age (formed at the same time). Three basic ingredients form the Simple Stellar Population models: Stellar evolutionary tracks, stellar atmosphere models and the Initial Mass Function (IMF). Stellar evolutionary tracks describe the evolution in time of the luminosity, the surface gravity, the bolometric luminosity and, magnitude (according to several pass-band definitions) of a star for a given mass and chemical composition considering “overshooting” (e.g. Fagotto et al. 1994a,b,c; Bertelli et al. 1994; Girardi et al. 2000) or not considering it (e.g. Cassisi et al. 1998; VandenBerg et al. 2000).

Simple Stellar Population models combine evolutionary tracks with either stellar atmosphere models or observed spectral libraries (e.g. Bruzual & Charlot 2003; Maraston 1998) and the Initial Mass Function describes the original distribution of stellar masses (e.g. Salpeter 1955; Miller & Scalo 1979; Kroupa et al. 1993; Chabrier 2003).

The models are computed by integrating the contribution of the individual stars. Two different techniques are used: The isochrone synthesis (e.g. Chiosi et al. 1988; Charlot & Bruzual 1991) and the fuel consumption approach (Renzini & Buzzoni 1986; Buzzoni 1989; Maraston 1998; Maraston et al. 2004). In the first one, the isochrones are computed up to the end for an instantaneous-burst stellar population and the properties of the stellar populations interpolated from a set of stellar tracks. The second method considers that the contribution of stars in any given post main sequence stage to the integrated luminosity of the simple stellar population is directly proportional to the amount of fuel burned during that stage (Renzini & Buzzoni 1986). For a discussion of both method see Renzini (1994).

In the first two chapters of this thesis we use Simple Stellar Population models for star cluster age and mass derivations. Two models are used for this purpose. GALEV Anders & Fritze-v. Alvensleben (2003) and Girardi (Private communications) models based on Girardi et al. (2000, 1996). GALEV models are based on isochrones from the Padova group and model atmosphere spectra from Lejeune et al. (1997, 1998), considering Salpeter and Scalo IMF and, including gaseous emission. Emission lines contribute to the broad band fluxes in an important way during very early evolutionary stages of star clusters in regions with strong ongoing star formation. For this reason, GALEV models are used as the main age-mass theoretical model and the Girardi models used as comparison results.

However, Simple Stellar Population models have limitations, including the Simple Stellar Population models chosen here. Stars in the star clusters are formed purely stochastic by consumption of the available amount of gas, and at the level of small (open) clusters, this effect has a direct implication of the assumption for the initial stellar mass function (i.e. modeling the number of stars and their masses which will form the cluster). Since the theoretical evolution of stars is based on a discrete grid of masses, approximations must be assumed in order to fit the gaps between the discrete mass ranges. Only systems more massive than $\sim 10^5 M_{\odot}$ show low impact of the stochasticity of the initial mass function.

3DEF-method

This method compares the energy distributions² of the observed star clusters with those predicted by the models (see Figure.1.4).

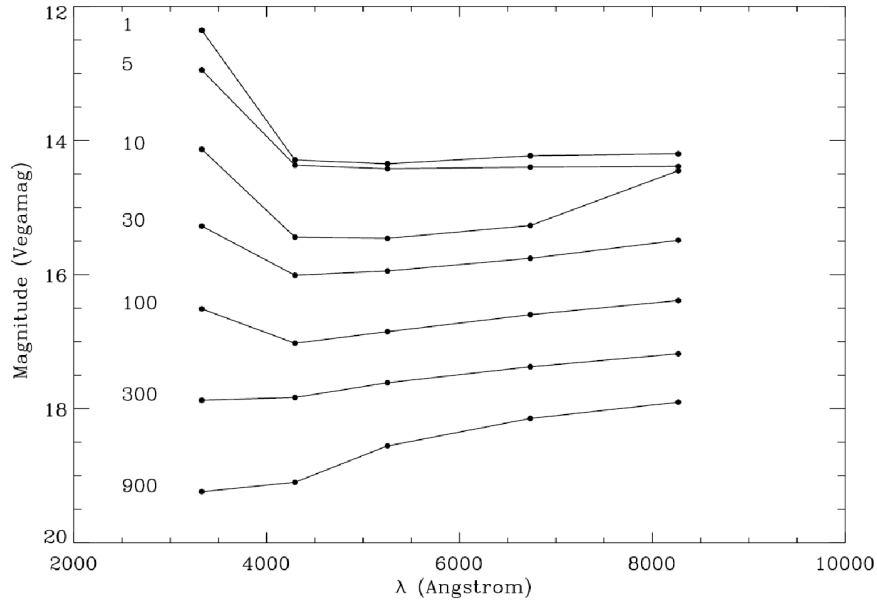


Figure 1.4: Example of theoretical Spectral Energy Distributions (SED) in magnitudes as function of wavelength for STARBURST99 models. The age of the cluster in Myr is indicated and the model corresponds to a cluster with initial mass of $10^6 M_{\odot}$ at the distance of M51. Figure from Bik et al. (2003).

Three quantities of the observed star clusters are unknown: The age, the mass and, the internal extinction towards the clusters. For this purpose those quantities are minimized using a χ^2 minimum criteria i.e. $\chi_v^2 = \chi^2/\nu$, where ν is the number of degrees of freedom. Thus, the number of observed bandpass combinations must be the same number of bandpass in the Simple Stellar Population models.

To use this method, it is necessary to know the distance to the galaxy where the clusters lie in order to correct the model magnitudes and the extinction toward the galaxy, although extinction is not extremely necessary because the method itself can calculate the extinction as a fit parameter. Nevertheless, we corrected our photometries by galactic extinction law (Schlegel et al. 1998) and we limited the internal extinction $E(B - V)$ up to 3 magnitudes.

The method creates a grid in age (which depends on the model age resolution), extinction (applied to each single point of the model between the limits i.e. 0 and 3 magnitudes) and, mass. Regarding the mass: the models are calculated for a fixed cluster initial mass which is later scaled according to the observed magnitudes. The grid is compared with

²Magnitude as function of wavelength is a distribution known as an energy distribution.

the observations using minimum χ^2 criteria and the output corresponds to the mass, age and, extinction of each individual star cluster.

The method has the limitation that it requires accurate photometry, which can be challenging when star clusters are not isolated, and their light may be contaminated by the neighbor objects leading in an overestimation/underestimation of their masses and ages. The masses derived by the method are luminous masses (i.e. derived from the photometry). Therefore, even if the model considers dark objects which are contributing to the total mass of the clusters (e.g. neutron stars) the amount of those objects in the real clusters may change and thus the mass will be underestimated or overestimated. Also a fixed metallicity shall be assumed. We note that the metallicity, in principle can be left as a free parameter and later on (from the minimum χ^2) the value can be used to derive the individual star cluster metallicities. However, this does not ensure that the output will have a physical meaning. For this reason always the metallicity is chosen to be the closest one from the literature and the individual star cluster metallicities are assumed to be the same.

An extra limitation need to be point out. The method tends to assign the same age to several star clusters at ages where the color of the models change. This is seen, for example, at 10^7 yr and 5×10^8 yr in the Fig. 3.6. This effect can lead to the misinterpretation of a burst at those ages, while in reality it is just an artifact of the method.

The Lick/IDS spectra system

The Lick/IDS system was developed with the purpose of predicting index (i.e. absorption features in the globular cluster and elliptical galaxy spectra) strengths in the integrated light of stellar populations, as function of age and metallicity. It was first developed by Burstein et al. (1984), refined by Gorgas et al. (1993), completed by Worthey (1994), expanded to four new indices by Worthey & Ottaviani (1997) and updated with new index definitions by Trager et al. (1998). It consists of 25 index definitions from the IDS database which contains absorption-line strengths of 381 galaxies, 38 globular clusters, and 460 stars based on 7417 spectra in the 4000 – 6000 Å region observed at the Lick Observatory from 1972 up to 1984. The method consists of measuring the difference of flux between the absorption feature (molecular or atomic) and the adjacent pseudo-continuum features $F_{C\lambda}$. The pseudo-continuum is defined as:

$$F_P = \int_{\lambda_1}^{\lambda_2} F_{\lambda} d\lambda / (\lambda_2 - \lambda_1) \quad (1.2)$$

where F_P is the mean flux in each continuum passband. The boundaries of the passbands are defined by λ_1 and λ_2 (indicated by the brown lines in figure 1.5), The continuum level in the feature passband is obtained by interpolation between the mean fluxes in each continuum passband (F_C in figure 1.5).

The molecular indices are expressed in magnitudes and defined as:

$$M = -2.5 \log \left[\frac{1}{\lambda_2 - \lambda_1} \int_{\lambda_1}^{\lambda_2} \frac{F_{I\lambda}}{F_{C\lambda}} d\lambda \right] \quad (1.3)$$

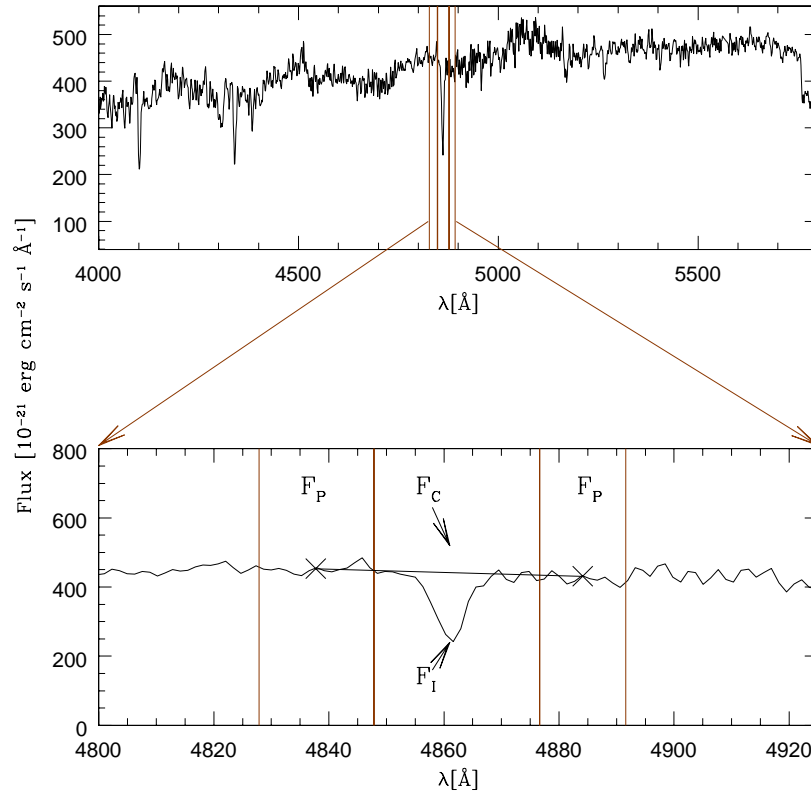


Figure 1.5: Graphical definition of an index. The top figure shows a typical spectra of a globular cluster. In the bottom a zoom of the top figure is shown in the region of the index $H\beta$. F_P are the regions where the pseudo-continua are calculated. The crosses show the two starting points on which the pseudo-continuum will be considered. The black arrows indicate where are F_I and F_C

The atomic index is expressed in Angstroms and defined as:

$$E = \int_{\lambda_1}^{\lambda_2} \left(1 - \frac{F_{I\lambda}}{F_{C\lambda}} \right) d\lambda \quad (1.4)$$

The Lick/IDS system has been widely used. However, it is a challenging task to obtain accurate measurements. The spectra must have a high signal to noise ratio, the velocity of the object must be known accurately and, the spectra must be free of artifacts from the process of the treatment of the data.

Without these considerations it is highly probable that indices ages and abundances values derived in the stellar population models will not describe the observed object indices and thus the object ages and abundances will remain unknown.

Chapter 2

Imaging of star clusters in unperturbed spiral galaxies with the Advanced Camera for Surveys: I. The low luminosity galaxy NGC 45

Astronomy & Astrophysics, 2007, 464, 495
M. D. Mora, S. S. Larsen & M. Kissler-Patig

Abstract

Star clusters are present in almost all types of galaxies. Here we investigate the star cluster population in the low-luminosity, unperturbed spiral galaxy NGC 45, which is located in the nearby Sculptor group. Both the old (globular) and young star-cluster populations are studied. Previous ground-based observations have suggested that NGC 45 has few if any “massive” young star clusters. We aim to study the population of lower-mass “open” star clusters and also identify old globular clusters that could not be distinguished from foreground stars in the ground-based data. Star clusters were identified using *UBVI* imaging from the *Advanced Camera for Surveys (ACS)* and the *Wide Field Planetary Camera 2 (WFPC2)* on board the *Hubble Space Telescope*. From broad band colors and comparison with simple stellar population (SSP) models assuming a fixed metallicity, we derived the age, mass, and extinction. We also measured the radius for each star cluster candidate. We identified 28 young star cluster candidates. While the exact values of age, mass, and extinction depend somewhat on the choice of SSP models, we find no young clusters with masses higher than a few $1000 M_{\odot}$ for any model choice. We derive the luminosity function of young star clusters and find a slope of $\alpha = -1.94 \pm 0.28$. We also identified 19 old globular clusters, which appear to have a mass distribution that is roughly consistent with what is observed in other globular cluster systems. Applying corrections for spatial incompleteness, we estimate a specific frequency of globular clusters of $S_N=1.4-1.9$, which is significantly higher than observed for other late-type galaxies (e.g. SMC, LMC, M33). Most of these globular clusters appear to belong to a metal-poor population, although they coincide spatially with the location of the bulge of NGC 45.

2.1 Introduction

Especially since the launch of the HST, young star clusters have been observed in an increasing variety of environments and galaxies. This includes interacting galaxies such as NGC 1275 (e.g. Holtzman et al. 1992), the Antennae system (e.g. Whitmore & Schweizer 1995), tidal tails (e.g. Bastian et al. 2005c), but also some normal disk galaxies (e.g. Larsen 2004a). This shows that star clusters are common objects that can form in all star-forming galaxies. It remains unclear what types of events trigger star cluster formation and the formation of “massive” clusters in particular. It has been suggested that (at least some) globular clusters may have been formed in galaxy mergers (Schweizer 1987), and the observation of young massive star clusters in the Antennae and elsewhere may be an important hint that this is indeed a viable mechanism, although not necessarily the only one. In the case of normal spiral galaxies, spiral arms may also stimulate the molecular cloud formation (Elmegreen 1994) and thus the possibility of star cluster formation.

While a large fraction of stars appear to be forming in clusters initially, many of these clusters ($\sim 90\%$) will not remain bound after gas removal and disperse after $\sim 10^7$ years (Whitmore 2003). This early cluster disruption may be further aided by mass loss due to the stellar evolution and dynamical processes (Fall 2004), so that many stars initially born in clusters eventually end up in the field.

Much attention has focused on star clusters in extreme environments such as mergers and starbursts, but little is currently known about star and star cluster formation in more quiescent galaxies, such as low-luminosity spiral galaxies. The Sculptor group is the nearest galaxy group, and it hosts a number of late-type galaxies with luminosities similar to those of SMC, LMC, and M33 (Cote et al. 1997). One of the outlying members is NGC 45, a low surface-brightness spiral galaxy with $M_B = -17.13$ and distance modulus $(m - M) = 28.42 \pm 0.41$ (Bottinelli et al. 1985). This galaxy was included in the ground-based survey of young massive clusters (YMCs) in nearby spirals of Larsen & Richtler (1999), who found only one cluster candidate. Several additional old globular cluster candidates from ground-based observations were found by Olsen et al. (2004), but none of them has been confirmed.

In this paper we aim at studying star cluster formation in this galaxy using the advantages of the HST space observations. We identify star clusters through their sizes, which are expected to be stable in the lifetime of the cluster (Spitzer 1987). Then we derive their ages and masses using broadband colors with the limitations that this method implies, such as model dependences (de Grijs et al. 2005). Also we study how the choice of model metallicities affects our results.

This chapter is structured in the following way, beginning in Sect. 2.2, we describe the observations, reductions, photometry, aperture corrections and, artificial object experiments. In Sect. 2.3, we describe the selection of our cluster candidates, the color magnitude diagram and their spatial distribution. In Sect. 2.4 we describe the properties of young star clusters. In Sect. 2.5 we comment on the globular cluster properties, and Sect. 2.6 contains the discussion and conclusions.

2.2 Data and reductions

Two different regions in NGC 45 were observed with the HST ACS Wide Field Channel on July 5, 2004. One pointing included the center of the galaxy ($\alpha_{2000} = 00^h 14^m 0^s.30$, $\delta_{2000} = -23^\circ 10' 04''$) and the other covered one of the spiral arms ($\alpha_{2000} = 00^h 14^m 14^s.90$, $\delta_{2000} = -23^\circ 12' 29''$). For each frame, two exposures of 340 seconds each were acquired through the filters F435W ($\sim B$) and F555W ($\sim V$), and a pair of 90 and 340 seconds was obtained through the filter F814W ($\sim I$). In addition, for each pointing, two F336W ($\sim U$ -band) exposures of 1200 s each were taken with the WFPC2. The ACS images are shown in Fig. 2.1, including the footprint of the WFPC2 exposures. Due to the smaller field-of-view of WFPC2, only part of the ACS frames have corresponding U -band imaging.

Following standard “on-the-fly” pipeline processing, the raw ACS images were drizzled using the MULTIDRIZZLE task (Koekemoer et al. 2002) in the STSDAS package in IRAF¹. For most of the parameters in Multidrizzle we used the default values. However, we disabled the automatic sky subtraction, because it did not work well for our data, due to the highly non-uniform background level. The WFPC2 images were combined using the CRREJ task and standard parameter settings.

2.2.1 Photometry

The source detection was carried out in the ACS $F435W$ images using SExtractor V2.4.3 (Bertin & Arnouts 1996). The object coordinates measured in the B_{F435W} frame were used as input for the SExtractor runs on the other two ACS frames. An area of 5 connected pixels, all of them are more than 4 sigma above the background, was defined as an object. From the output of SExtractor we kept the FWHM measured in each filter and the object coordinates.

Aperture photometry was done with the PHOT task in IRAF, using the SExtractor coordinates as input. This was preferred over the SExtractor magnitudes because of the greater flexibility in DAOPHOT for choosing the background subtraction windows. We used an aperture radius of 6 pixels for the ACS photometry, which matches the typical sizes of star clusters well at the well distance of NGC 45 (1 ACS/WFC pixel ~ 1.2 pc). The sky was subtracted using an annulus with inner radius of 8 pixels and a 5 pixel width.

Because the U_{F336W} exposures were not as deep as the ACS exposures, we used the ACS object coordinates transformed into the WFPC2 frame in order to maximize the number of objects for which U_{F336W} photometry was available. We defined a transformation between the ACS and WFPC2 coordinate systems using the GEOMAP task in IRAF, and transformed the ACS object lists to the WFPC2 frame with the GEOXYTRAN task. Each transformation typically had an rms of 0.5 pixels. The transformed coordinates were used as input for the WFPC2 aperture photometry. We used a 3 pixel aperture radius, which is the same physical aperture as in the ACS frames. The counts were converted

¹IRAF is distributed by the National Optical Astronomical Observatory, which is operated by the Association of Universities for Research in Astronomy, Inc, under cooperative agreement with the National Science Foundation.

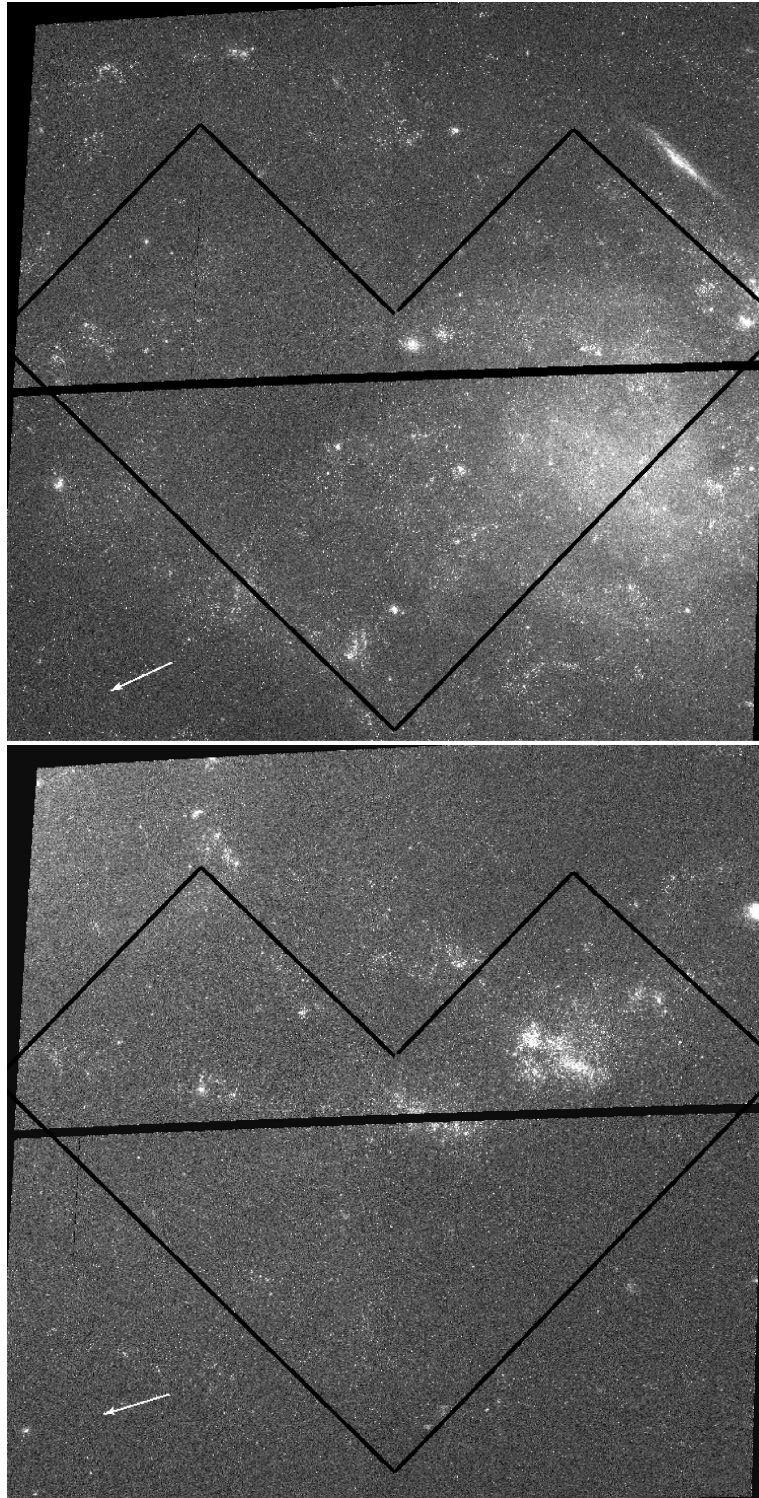


Figure 2.1: The two F435W ACS images of NGC 45 with the HST WFPC2 (F336W) pointings also indicated. The arrows indicate the north.

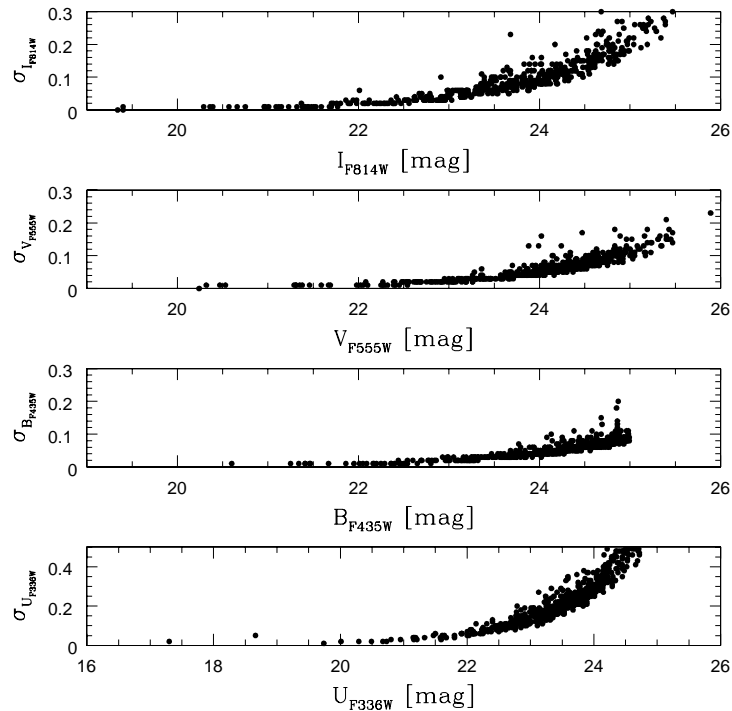


Figure 2.2: Photometry errors of the detected sources. The aperture radii used for the photometry are 6 pixels for the ACS data and 3 pixels for WFPC2.

to the Vega magnitude system using the HST zero-points taken from the HST web page² and based on the spectrophotometric calibration of Vega from Bohlin & Gilliland (2004).

We identified a total of 14 objects in common with the ACS data and the WFPC2 chips. For the Planetary Camera (PC), we were not able to find any common objects to determine the correct transformation.

2.2.2 Object sizes

Measuring object sizes is an important step in disentangling stars from extended objects. We performed size measurements on the ACS data. For this purpose we used the ISHAPE task in BAOLAB (Larsen 1999). ISHAPE models a source as an analytical function (in our case, King 1962 profiles) convolved with the PSF. For each object Ishape starts from an initial value for the FWHM, ellipticity, orientation, amplitude, and object position, which are then used in an χ^2 iterative minimization. The output includes the derived FWHM, chi-square, flux, and signal-to-noise for each object plus a residual image. A King concentration parameter of $c=30$, fitting radius of 10 pixels, and a maximum centering radius of 3 pixels were adopted as input parameters for Ishape. These results are

²<http://www.stsci.edu/hst/acs/analysis/zeropoints/>

described in Sect. 2.3.

2.2.3 Aperture corrections

Aperture corrections from our photometric apertures to a reference ($1''.45$) aperture should ideally be derived using the same objects in all the frames³. Those objects should be extended, isolated, and easily detectable. In our case this was impossible because most of the objects were not isolated, and the few isolated ones were too faint in the WFPC2 frame. For this reason, we decided to create artificial extended objects and derive the aperture corrections from them. We proceed for the ACS as follows.

First, we generated an empirical PSF for point sources in the ACS images, using the PSF task in DAOPHOT running within IRAF. Since we want to be sure that we are only selecting stars in the PSF construction, we used ACS images of the Galactic globular cluster 47 Tuc⁴. We selected 139, 84, and 79 stars through the B_{F435W} , V_{F555W} , and I_{F814W} filters with 10 sec, 150 sec, and 72 sec of exposure time, respectively. We could not use the same objects in all the filters because the ACS frames have different pointings and exposure times. The selected stars were more or less uniformly distributed over the CCD, but we avoided the core of the globular cluster because stars there were crowded and saturated. We used a PSF radius of 11 pixels and a fitting radius of 4 pixels on each image. This was the maximum possible radius for each star without being affected by the neighboring one.

Second, models of extended sources were generated using the BAOLAB *MKCMPPSF* task (Larsen 1999). This task creates a PSF by convolving a user-supplied profile (in our case the empirical ACS PSF) with an analytical profile (here a King 1962 model with concentration parameter $r_{\text{tidal}}/r_{\text{core}} = 30$) with a FWHM specified by the user. The result is a new PSF for extended objects.

Third, we used the *MKSYNTH* task in BAOLAB to create an artificial image with artificial extended sources on it.

For the WFPC2 images we proceeded in a similar way, but we used the Tiny Tim (Krist 1993) package for the PSF generation. We kept the same PSF diameter as for the ACS images. We then followed the same procedure as for the ACS PSF. Aperture corrections were done taken into account the profile used for size measurements (King30) and the size derived from it for each object. Since sizes were measured in the ACS frames, we assumed that objects in the WFPC frames have similar sizes. Aperture corrections were corrected from 6 pixels for the ACS data and 3 pixels for WFPC2 to a nominal $1''.45$ (where aperture corrections start to remain constant) reference aperture. The corrections are listed in Table 2.1

Colors do not change significantly as a function of size. From Table 2.1, we note that an error in size will be translated into a magnitude error: e.g. 0.3 pixel of error in the measured FWHM correspond to $\Delta m = 0.07$ which, translated into mass, corresponds to a 7% error. We also keep in mind that adopting an average correction over each small size

³Globular clusters' half light radii are in the range 1-10 pc; i.e. clusters will appear extended in ACS images at the distance of NGC 45

⁴Based on data obtained from the ESO/ST-ECF Science Archive Facility.

Table 2.1: Aperture corrections as a function of object size (FWHM).

(1)	(2)	(3)	(4)	(5)
$FWHM(\text{pix})$	$U_{F336W}[\text{mag}]$ WFPC2	$B_{F435W}[\text{mag}]$ ACS	$V_{F555W}[\text{mag}]$ ACS	$I_{F814W}[\text{mag}]$ ACS
0.20 – 0.75	−0.050	−0.053	−0.046	−0.054
0.75 – 1.50	−0.168	−0.167	−0.153	−0.163
1.50 – 2.15	−0.358	−0.343	−0.337	−0.345
2.15 – 2.75	−0.517	−0.506	−0.491	−0.505

range (0.20-0.75, 0.75-1.50, 1.50-2.15, 2.15-2.75) can introduce an additional uncertainty in mass of $\sim 8\%$

The other systematic effect on our measurements is that aperture correction changes for the different profiles. We adopt a King30 profile, fitting most of our objects best. For comparison we give some examples of the effect below. For an object of FWHM=0.5 pixels, the aperture correction varies from $\Delta m = -0.036$ [mag] (3% in mass) considering a KING5 profile up to $\Delta m = -0.205$ [mag] (17% in mass) considering a King100 profile. For an object of FWHM=1.2 pixels, the aperture correction varies from $\Delta m = -0.045$ [mag] using King5 (4% in mass), up to $\Delta m = -0.437$ [mag] (35% in mass) considering a King100 profile. And for an object of FWHM=2.5 pixels, the aperture correction varies from $\Delta m = -0.078$ (7% in mass) considering a King5 profile up to $\Delta m = -0.645$ [mag] (45% in mass) considering a King100 profile. Thus in general the exact size and assumed profiles will cause errors in mass.

2.2.4 Artificial object experiments

We need to estimate the limits of our sample’s reliability in magnitudes and sizes. In the following we investigate how factors such as the degree of crowding and the background level affect the detection process and size derivation. To do so, we added 100 artificial objects and repeated the analysis for 3 different sub-regions in the ACS images: “field I” was centered on the bulge of the galaxy, “field II” included a crowded region with many young stars, and “field III” covered a low-background region far from the center of the galaxy (see Fig. 2.3). Each field measured 1000 x 1000 pixels, and the artificial objects were distributed in an array of 10 by 10. A random shift between 0 and 20 pixels was added to the original object positions. In this way, the minimum separation between objects is 60 pixels.

The artificial objects were built using an artificial PSF as described in the second step of the aperture correction. Objects with a fixed magnitude were then added to a zero-background image (as in the third step of aperture correction). Finally we added this image, containing the artificial objects, to the science image using the IMARITH task in IRAF. This was done for objects with magnitudes between $m(B_{F435W})=16$ and $m(B_{F435W})=26$ and different FWHM (0.1 pixels (stars), 0.5, 0.9, 1.2, 1.5, and 1.8 pixels).

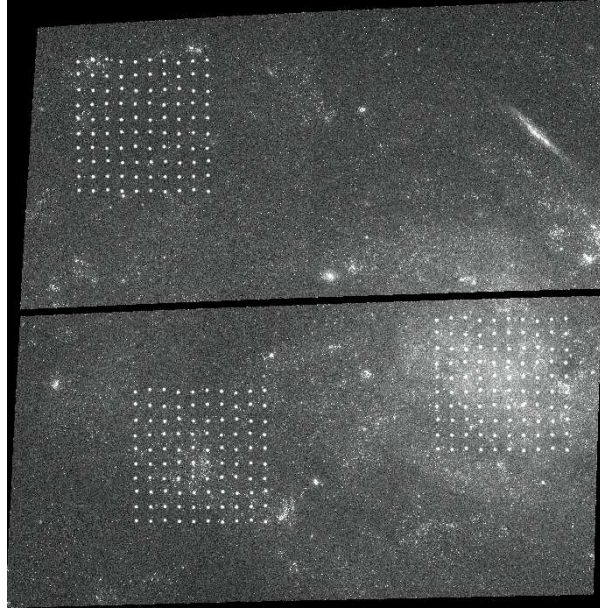


Figure 2.3: Artificial objects added to the science image. The three different test fields are shown, starting from the right and going clockwise: Field I (high background, and crowded background), Field II (young star-forming region), Field III (low background region).

The recovering process was performed in exactly the same way as for the original science object detections (SExtractor detection, aperture photometry, and Ishape run). Figure 2.4 shows the fraction of artificial objects recovered as a function of magnitude for different intrinsic object sizes and for each of the three test fields. As expected, the completeness tests show that more extended objects are more difficult to detect at a fixed magnitude. Fields II and III show very similar behavior, perhaps not surprisingly, since the crowded parts of field II cover only a small fraction of the test field. The higher background level in Field I results in a somewhat shallower detection limit, but for all the fields the 50% completeness limit is reached between $m(B_{F435W})=25$ and $m(B_{F435W})=26$.

The artificial object experiments also allow us to test the reliability of the size measurements. In Fig. 2.5 we plot the average value of the absolute difference between the input FWHM and the recovered FWHM as a function of magnitude for the three different fields. More extended clusters show bigger absolute differences between the input and output FWHM at fixed magnitude compared with the less extended. Uncertainties are generally larger in the crowded and high background regions. In Field 1, the artificial object tests give an average difference between the input FWHM and the recovered one of $\sigma=0.006$ pixels for an object with $m(B_{F435W})=20$ and $\text{FWHM}(\text{input})=0.5$ pixels. The corresponding errors at $m(B_{F435W})=23$ and $m(B_{F435W})=24$ are $\sigma=0.06$ pixels and $\sigma=0.12$ pixels, and a 50% error ($\sigma=0.25$ pixels) is reached at $m(B_{F435W})\sim 25$. The relative errors also remain roughly constant at a fixed magnitude for more extended objects;

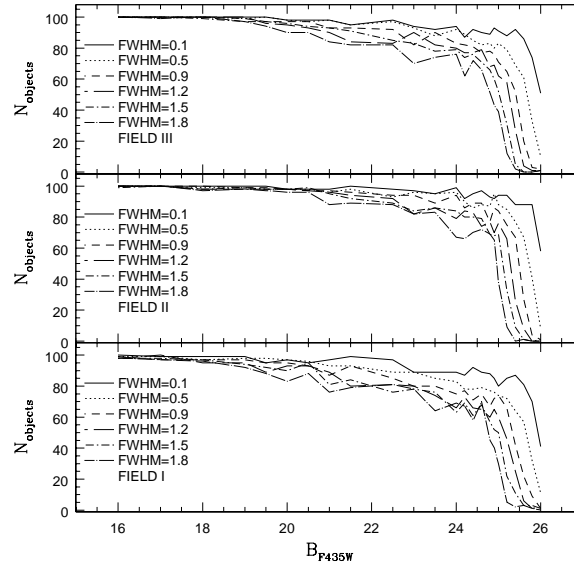


Figure 2.4: Completeness profiles for each of the test “fields” in the ACS image. The different lines represent different FWHMs.

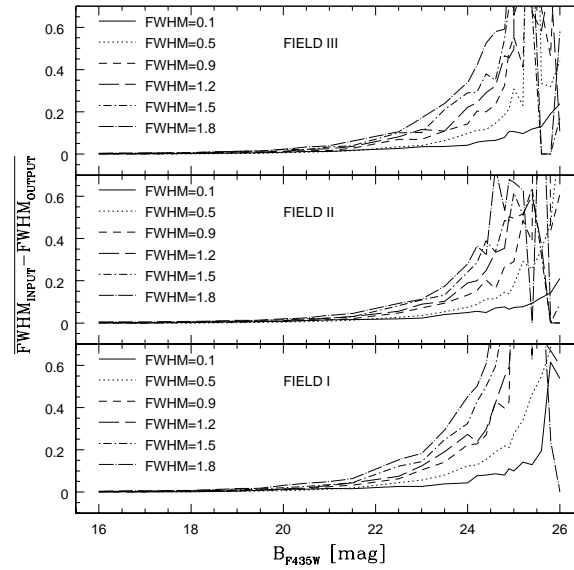


Figure 2.5: Absolute value of the average of the input FWHM and the recovered value for each magnitude on each field. Faintest magnitudes show biggest FWHMs differences. The 0σ observed in the fields II and III at $B_{F435W} \sim 25.5$ means that no objects were recovered in these bins.

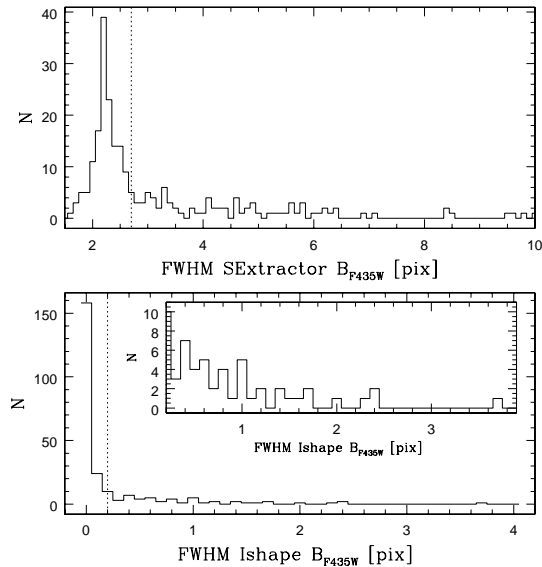


Figure 2.6: Histogram of the size distributions from ISHAPE with a zoom in to the extended objects (bottom) and SExtractor (top). The dotted line shows the size selection criteria.

for $\text{FWHM}=1.8$ pix the 50% error limit is at $m(B_{F435W})=24.6$.

2.3 Selection of cluster candidates

For the selection of star cluster candidates, we took advantage of the excellent spatial resolution of the ACS images. At the distance of NGC 45, one ACS pixel ($0''.05$) corresponds to a linear scale of about 1.2 pc. With typical half-light radii of a few pc (e.g. Larsen 2004a), young star clusters are thus expected to be easily recognizable as extended objects. However, the high spatial resolution and depth of the ACS images also add a number of complications: as discussed in the previous section, our detection limit is at $B \sim 25.5$, or $M_B \sim -3$ at the distance of NGC 45. Clusters of such low luminosities are often dominated by a few bright stars, so it can be difficult to distinguish between a true star cluster and chance alignments of individual field stars along the line-of-sight. Therefore, we limit ourselves to brighter objects for which reliable sizes can be measured. We adopt a magnitude limit of $m(B_{F435W})=23.2$, corresponding to $M_B \sim 5.5$ and to a size uncertainty of $\sim 20\%$ for objects with $\text{FWHM} \leq 2.5$ pixel. Only one object (ID=9) has a larger FWHM than this.

In an attempt to improve our object detection scheme, we use both size estimates from ISHAPE and SExtractor. In Fig. 2.6 we plot the distribution of size measurements for all the objects with $B_{F435W} \leq 23.2$.

The SExtractor sizes show a peak around $\text{FWHM} \sim 2.5$, corresponding to the PSF

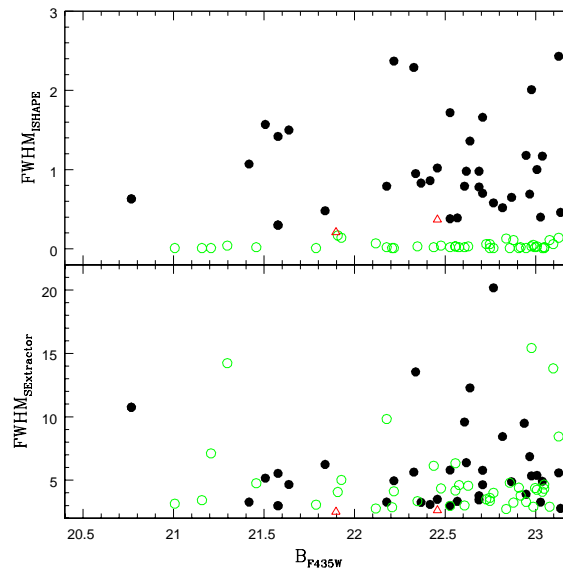


Figure 2.7: Object FWHMs as measured by ISHAPE and SExtractor. Filled circles are objects considered extended by both methods. Open circles were considered as extended objects only by SExtractor and triangles are objects considered extended only by ISHAPE.

FWHM, while the ISHAPE distribution peaks at 0 (recall that the ISHAPE sizes are corrected for the PSF). We adopt the size criteria of $FWHM_{SEX} \geq 2.7$ and $FWHM_{ISHAPE} \geq 0.2$ to select extended objects. In Fig. 2.7 we plot all objects with at least one condition fulfilled. From this figure it is evident that several objects were considered to be extended according to the SExtractor sizes, while the ISHAPE fit yield to near-zero size. Such objects might be close groupings of stars where SExtractor yields the size of the whole group, while ISHAPE fits a single star. On the other hand, there are very few objects that are classified as extended by ISHAPE but as compact according to SExtractor.

Objects that fulfill both conditions are considered to be star cluster candidates. Objects that fulfill only one condition are considered to be possible clusters. Objects that did not pass any condition were rejected (i.e. classified as stars). All the objects were visually inspected to avoid contamination by HII regions. Finally 66 objects were rated as star cluster candidates and 64 as possible clusters, while 59 of these “possible” star cluster were considered as stars by ISHAPE and 2 as stars by SExtractor. From the 66 star cluster candidates, 36 have 4-band photometry and 30 have only ACS (3-band) photometry. In the following, only star cluster candidates are considered for the analysis.

2.3.1 Young clusters vs globular clusters

In Fig. 2.8 the color magnitude diagrams are shown for star clusters candidates and possible clusters. Two populations can be distinguished: A population of blue (and prob-

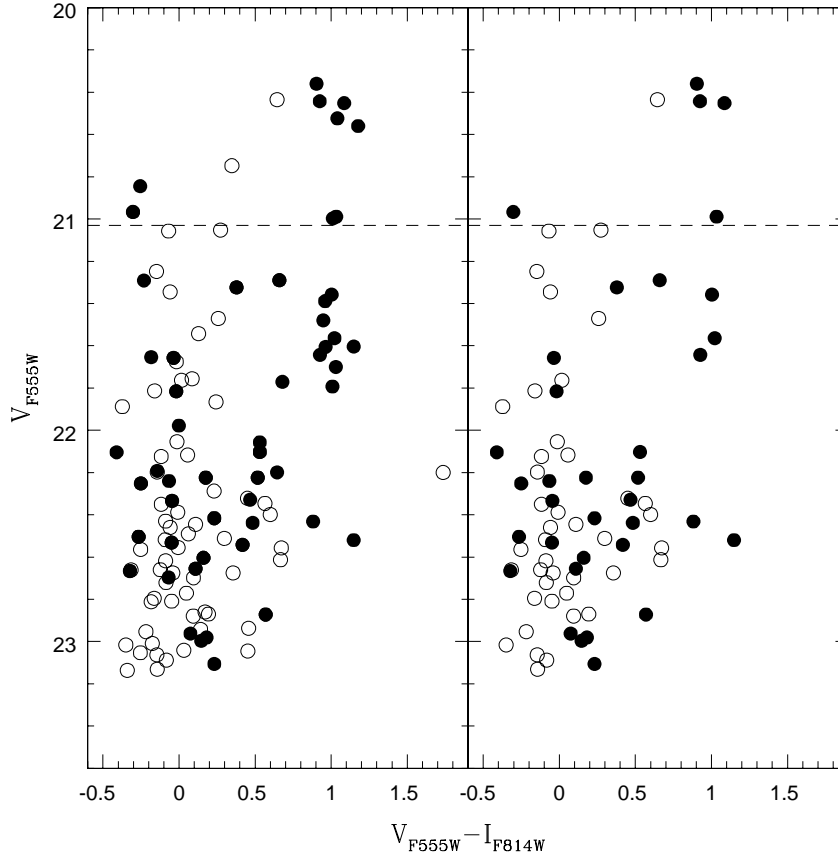


Figure 2.8: Color-magnitude diagram for objects in NGC 45. The left side corresponds to all objects with B_{F435W} , V_{F555W} and, I_{F814W} ACS photometry and the right side correspond to objects with 4-band photometry (ACS filters plus U_{F336W} from WFPC2). Filled circles are extended objects (i.e. star clusters) selected by SExtractor and Ishape, while open circles are objects that did not pass one of the size selection criteria. The dashed line is the TO of the old MW globular clusters system $M_{V,TO} \sim -7.4$.

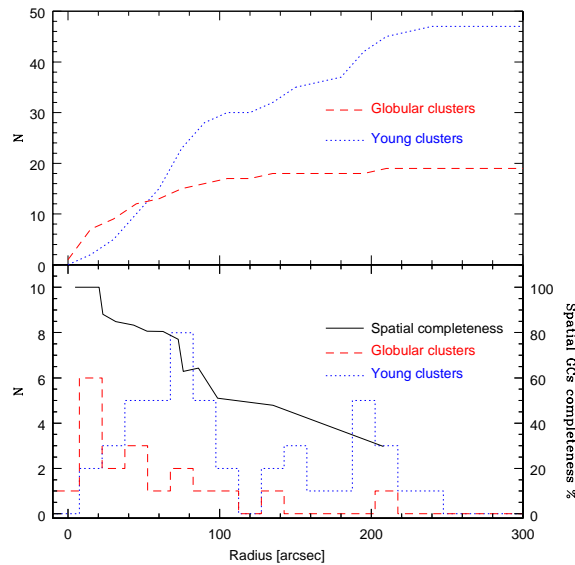


Figure 2.9: Star cluster spatial distribution from the center of the galaxy at different radius. Top: Cumulative distribution with radius. Bottom: Number of objects per radius and globular cluster spatial completeness.

ably young) objects with $V_{F555W} - I_{F814W} \leq 0.8$ (with a main concentration around $V_{F555W} - I_{F814W} \sim 0$), and a red population $V_{F555W} - I_{F814W} \geq 0.8$, concentrated around $V_{F555W} - I_{F814W} \sim 1$ (globular clusters). Two blue clusters brighter than $V_{F555W} = 21$ ($M_V \sim -7.5$) are found. The red objects have colors consistent with those expected for old globular clusters and are all extended according to both the SExtractor and ISHAPE size criteria.

The spatial distribution is shown in Fig. 2.9 for all the clusters with 3-band photometry (ACS field of view). Globular clusters are concentrated towards the center of the galaxy, and their number decreases with their distance. In contrast, young clusters are distributed in the outer part of the galaxy showing 2 major concentrations at 78 arcsec and 190 arcsec. Young clusters are associated with star forming regions, therefore it is more likely to find them in spiral arms like the first concentration rather than in the center. The second concentration corresponds mainly to the clusters detected in the second pointing covering one of the spirals arms and young regions.

Spatial completeness is 100% up to 20 arcsec radius. Beyond 20 arcsec, the completeness drops down to 20% at 200 arcsec radius. For all completeness corrections, we assume the non-covered areas to be similar to the covered area in all respects.

The detection of young and globular star clusters do not vary differentially with radius. Therefore the central concentration of the globular clusters is not an artifact of detection completion.

Assuming that the covered area is representative of the non-covered area and that the number and distribution of star clusters are similar in the non-covered area, we expect

that the observed tendency of globular clusters being located towards the center of the galaxy and the young ones toward the outer parts will remain.

In the following we discuss the young clusters and globular clusters separately. Our sample includes 36 star clusters with UBVI data (28 young star clusters and 8 globular clusters) and 11 globular clusters with BVI data. We will not discuss further the ages nor masses derived for the globular clusters since they are unreliable due to their faint U_{F336W} band magnitudes. Only for completeness we show their derived ages and masses in the table 2.3.

2.4 Young star clusters

In this section, we discuss the properties of young clusters in more detail.

2.4.1 Colors

The $U_{F336W} - B_{F435W}$ vs. $V_{F555W} - I_{F814W}$ two-color diagram of NGC 45 young star cluster candidates (not reddening corrected) is shown in Fig. 2.10. Also shown in the figure are GALEV (Anders & Fritze-v. Alvensleben 2003) SSP models for different metallicities. Age increases along the tracks from blue towards redder colors. The “hook” at $V_{F555W} - I_{F814W} \sim 0.5$ and $U_{F336W} - B_{F435W} \sim -1$ corresponds to the appearance of red supergiant stars at $\sim 10^7$ years and is strongly metallicity dependent. Many of the clusters have colors consistent with very young ages ($< 10^7$ years), and some older cluster candidates are spread along the theoretical tracks.

The cluster colors show a considerable scatter compared with the model predictions, significantly larger than the photometric errors. For younger objects, the scatter may be due to random fluctuations in the number and magnitude of red supergiant stars present in each cluster (Girardi et al. 1995). Reddening variations can also contribute to the scatter, and for the older clusters ($\gtrsim 1$ Gyr), metallicity effects may also play a role since the models in each panel follow a fixed metallicity.

Generally, the cluster colors seem to be better described by models of sub-solar metallicity ($Z=0.004$ and $Z=0.008$). Considering that the luminosity of NGC 45 is intermediate between those of the small and large Magellanic clouds, we might indeed expect young clusters to have intermediate metallicities between those typical of young stellar populations in the Magellanic clouds.

2.4.2 Ages and masses

One of main problems in deriving ages, metallicities, and masses for star clusters in spirals is that we do not know the extinction towards the individual objects. Bik et al. (2003) propose a method known as the “3D fitting” method to solve this problem. This method estimates the extinction, age, and mass by assuming a fixed metallicity for each single cluster. The method relies on a SSP model (in our case GALEV assuming a Salpeter IMF, Anders & Fritze-v. Alvensleben 2003), which provides the broad-band colors as a

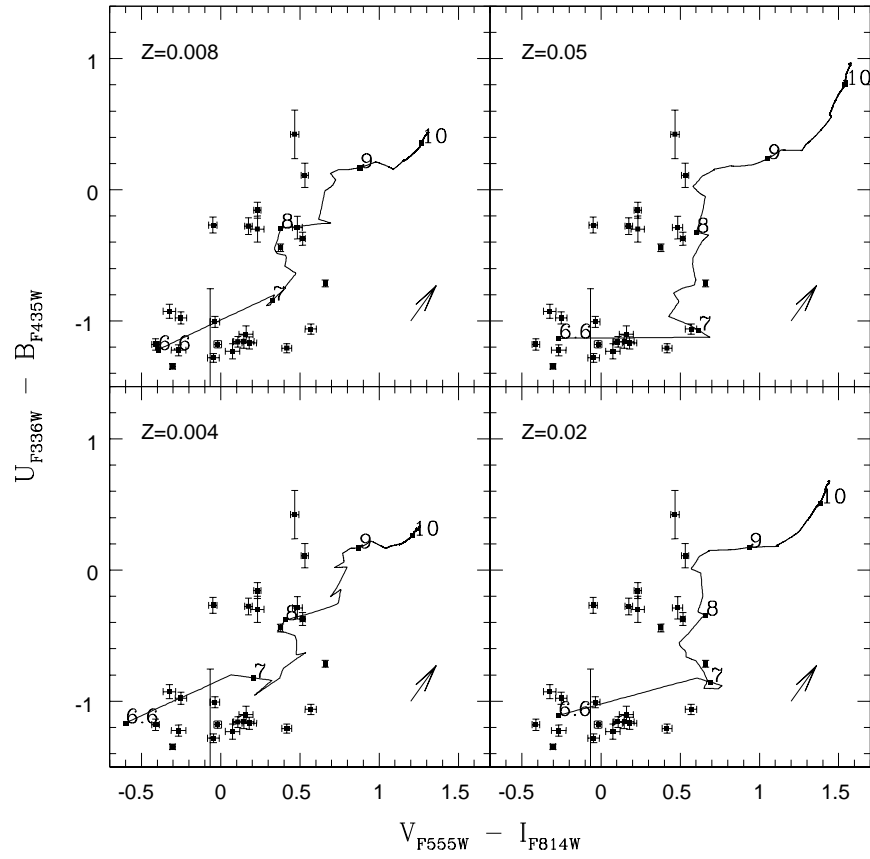


Figure 2.10: Color-color diagram of NGC 45 star cluster candidates, uncorrected for reddening. Each line corresponds to SSP GALEV models of different metallicities for a Salpeter IMF and ages from 1 Myr up to 10 Gyr. The arrow corresponds to an extinction of 1 mag.

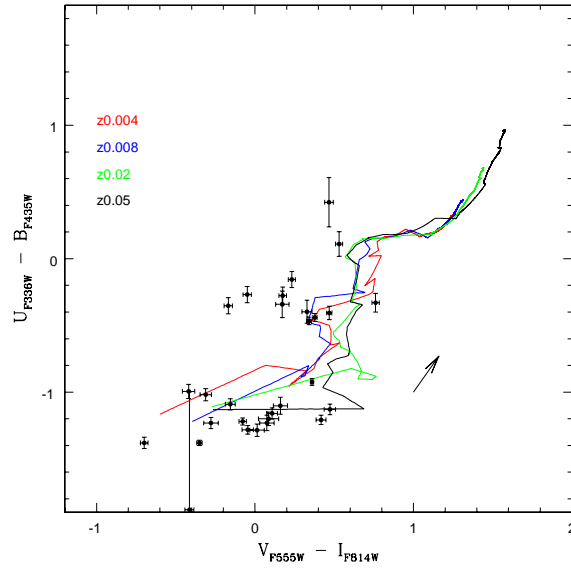


Figure 2.11: Reddening-corrected color-color diagram of NGC 45 star clusters. Each cluster was corrected according to the lowest χ^2 metallicity-fitted model. All the theoretical tracks are plotted for 4 different metallicities. See Tables 2.2 and 2.3 for the derived values.

function of age and metallicity. The algorithm compares the model colors with the observed ones and searches for the best-fitting extinction (using a step of 0.01 in $E(B - V)$) and age for each cluster, using a minimum χ^2 criterion. Finally the mass is estimated by comparing the mass-to-light ratios predicted by the models (for a fixed metallicity) with the observed magnitudes.

In Fig. 2.11 we plot the model tracks for 4 metallicities, together with the cluster colors corrected for reddening, according to the best χ^2 fitting for the different metallicities. The 3D fitting method will move the clusters in the opposite direction with respect to the reddening arrow in Fig. 2.11, finding the closest matching model.

From Hyperleđa (Patuřel et al. 2003), the internal extinction in B-band for NGC 45 is $A_B = 0.34$, based on the inclination and the morphological galaxy type taken from Bottinelli et al. (1995). Assuming $A_B = 1.324 * A_V$ from Rieke & Lebofsky (1985), we expect $E(B - V) \sim 0.08$. The mean derived extinction for the clusters is $E(B - V) = 0.04$ for $Z = 0.008$ and $Z = 0.004$, $E(B - V) = 0.05$ for $Z = 0.02$, and $E(B - V) = 0.1$ for $Z = 0.05$. These values agree well with our derived value. Considering that some clusters lie in the foreground and some in the background, the extinction value from the literature agrees well with the extinctions we derive for our star clusters.

The 3D fitting method was applied for all clusters with 4-band photometry assuming in turn for different metallicities ($Z=0.004$, $Z=0.008$, $Z=0.02$, and $Z=0.05$). To explore how the assumed metallicity affects the derived parameters, we plot the cluster masses in Fig. 2.12 against cluster ages for all the models. In a general overview of each plot

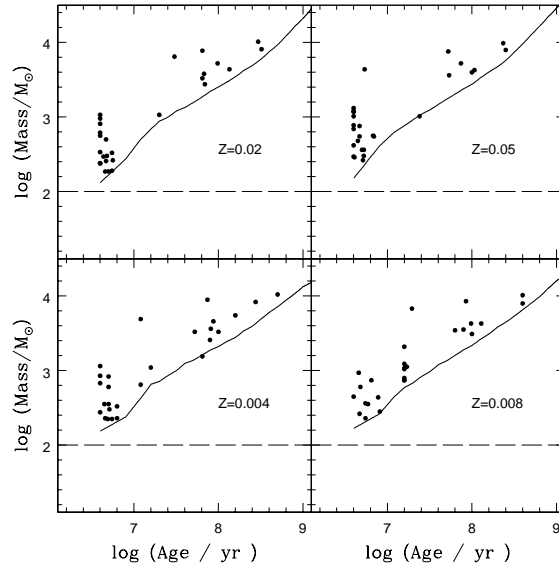


Figure 2.12: Mass as a function of cluster age. All star cluster candidates with masses greater than $100 M_{\odot}$ are plotted here. Filled circles are young clusters. The lines represent a cluster of $F435W = 23.1$ at different ages and masses for each metallicity.

we see concentrations of clusters around particular ages, e.g. near $\log(\text{Age}/\text{yr}) \sim 7.2$ and ~ 8 in the $Z=0.008$ plot. These concentrations are not physical, but instead artifacts due to the model fitting (see Bik et al. 2003). In particular, the concentration around $\log(\text{Age}/\text{yr}) \sim 7$ is due to the rapid change in the integrated cluster colors at that age (corresponding to the “hook” in Fig. 2.10). The figure again illustrates that the exact age at which this feature appears is metallicity dependent.

Independent of metallicity, Fig. 2.12 shows a concentration of young and not very massive clusters ($M \lesssim 10^3 M_{\odot}$) around $10^{6.8}$ yr. At older ages, the number of detected cluster candidates per age bin (note the logarithmic age scale) decreases rapidly. This is a result of fading due to stellar evolution (as indicated by the solid lines), as well as cluster disruption (see Sect. 2.4.4).

2.4.3 Sizes

The young cluster candidates detected in NGC 45 are generally low-mass, compact objects. The average size (from ISHAPE) is $\text{FWHM} = 1.16 \pm 0.2$ pixel, equivalent to a half-light radius of $R_{\text{eff}} = 2.0 \pm 0.2$ pc (errors are the standard error of the mean). These mean sizes are somewhat smaller than those derived by Larsen (2004a) for clusters in a sample of normal spiral galaxies, which typically range from 3–5 pc. Previous work on star clusters has shown that there is at most a shallow correlation between cluster sizes and masses. For example, young star clusters found in NGC 3256 by Zepf et al. (1999) and by Larsen (2004a) in a sample of nearby spiral galaxies show a slight correlation

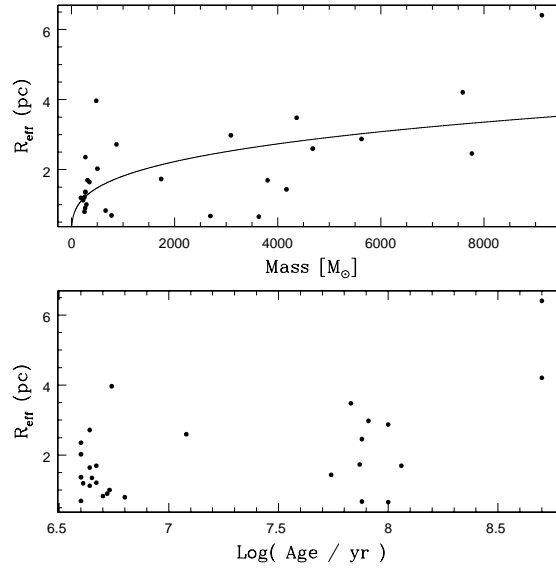


Figure 2.13: Effective radius vs mass (top) and age (bottom). The curve on top is the fitting of a power-law $R_{eff} = a * M^b$

between their radii and masses, although Bastian et al. (2005a) do not find any apparent relation between radii and masses in M51. Larsen (2004a) derived the following relation between cluster mass and size: $R_{eff} = 1.12 \times (M/M_{\odot})^{0.10}$ pc. For a cluster mass of $10^3 M_{\odot}$, which is more typical of the young clusters observed here, this corresponds to a mean size of 2.2 pc. Thus, the difference between the cluster sizes derived by other studies of extragalactic star clusters and those found for NGC 45 here may be at least partly due to the lower cluster masses encountered in NGC 45. Of course, biases in the literature studies also need to be carefully considered. For example, Larsen (2004a) excludes the most compact objects, which might cause the mean sizes to be systematically overestimated in that study.

Figure 2.13 shows the effective radius versus mass and age for the cluster candidates in NGC 45 (mass estimates are for $Z=0.008$). The plotted line is the best-fitting relation of the form :

$$R_{eff} = a * M^b \quad (2.1)$$

where $a = 0.24 \pm 0.16$ and $b = 0.29 \pm 0.08$ are the best-fitting values. As in previous studies, there is a slight tendency for the more massive clusters to have larger sizes, but our fit has a large scatter and the constants are not tightly constrained. Therefore we suggest that the NGC 45 sample cannot be taken as strong evidence of a size-mass relation, but it does not contradict the general shallow trends found in other studies.

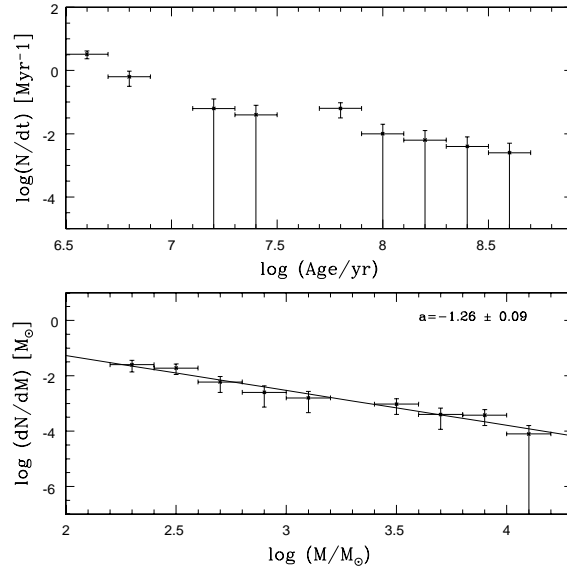


Figure 2.14: Age distribution (top) and mass distribution of clusters (bottom). The line is the fitting line of slope $a = -1.26 \pm 0.09$.

2.4.4 Cluster disruption time

Boutloukos & Lamers (2003) defined the disruption time as

$$t_{dis}(M) = t_4^{dis} (M/10^4 M_{\odot})^{\gamma}, \quad (2.2)$$

where t_4^{dis} is the disruption time of a cluster with an initial mass of $10^4 M_{\odot}$. The constant γ has been found empirically to have a value of about $\gamma = 0.6$ (Boutloukos & Lamers 2003). If a constant number of clusters are formed per unit time (constant cluster formation rate) and clusters are formed in a certain mass range with a fixed cluster initial mass function (CIMF), which can be written as a power law

$$N(M) \sim M^{-\alpha}, \quad (2.3)$$

then the number of clusters (per age interval) detected above a certain fixed magnitude limit depends only on fading due to stellar evolution, as long as there is no cluster disruption. When cluster disruption becomes significant, this behavior is broken and the number of clusters decreases more rapidly with time. In this simple scenario, no distinction is made between cluster disruption due to various effects (interaction with the interstellar medium, bulge/disk shocks, internal events such as two-body relaxation), and it is assumed that a single “disruption time-scale” applies (with the mass dependency given above).

Under these assumptions, the timescale on which cluster disruption is important can be derived from the cluster age- and mass distributions, which are both expected to show

a break:

$$\log\left(\frac{t_{\text{cross}}}{10^8}\right) = \frac{1}{1-\gamma\zeta} \left[\log\left(\frac{t_4^{\text{dis}}}{10^8}\right) + 0.4\gamma(m_{\text{ref}} - V_{\text{lim}}) \right] \quad (2.4)$$

$$\log\left(\frac{M_{\text{cross}}}{10^4}\right) = \frac{1}{1-\gamma\zeta} \left[\zeta \log\left(\frac{t_4^{\text{dis}}}{10^8}\right) + 0.4(m_{\text{ref}} - V_{\text{lim}}) \right] \quad (2.5)$$

(Eqs. 15 and 16 in [Boutloukos & Lamers 2003](#)). In these equations, V_{lim} is the detection limit, and m_{ref} is the apparent magnitude of a cluster with an initial mass of $10^4 M_{\odot}$ at an age of 10^8 years, the subscript ‘‘cross’’ is the breaking point between the cluster fading and the cluster disruption and ζ gives the rate of fading due to stellar evolution.

Figure 2.14 shows the age- and mass distributions for young cluster candidates in NGC 45. Figure 2.14 shows no obvious break in either the mass- or age distributions. In order to see a hint of a break, it would be necessary to include the lowest-mass and/or youngest bins, but as discussed above, the age determinations are highly uncertain below 10^7 yr, as is the identification of cluster candidates with masses of only $\sim 100 M_{\odot}$. Considering that the sample is $\sim 80\%$ complete at $m(F435W) = 23.2$, it is unlikely that completeness effects can be responsible for the lack of a break in the mass- and age distributions. Furthermore, many of the objects with ages below $\sim 10^7$ years may be unbound and not ‘‘real’’ star clusters. We may thus consider 10^7 years as an upper limit for any break and therefore $t_{\text{cross}} \lesssim 10^7$ years. Similarly, we may put an upper limit of $\log M_{\text{cross}} \lesssim 2.5$ on any break in the mass function. Nevertheless, considering the slope value and assuming $\alpha = 2.0$, we derived $\gamma = 0.73 \pm 0.09$ that agrees with the γ value found in other studies.

In Fig. 2.15 we plot the detection limit (in mass) vs. age for $B_{\text{lim}} = 23.1$. From this we derived $\zeta = 0.97$ and $0.4(m_{\text{ref}} - B_{\text{lim}}) = -0.782$. Fixing $\gamma = 0.6$ and using Eq. 15 from [Boutloukos & Lamers \(2003\)](#), we get $\log(t_4/10^8) \lesssim 0.05$ and finally :

$$\log t_{\text{dis}} \lesssim 8 + 0.6 \log M_{\text{cl}}/10^4 \quad (2.6)$$

where t_{dis} is in years and mass is in M_{\odot} . Since the young clusters in NGC 45 generally have masses below $10^4 M_{\odot}$, the disruption times will accordingly be less than 10^8 years, and it is therefore not surprising that no large number of older clusters are observed (apart from the old globular clusters).

2.4.5 Luminosity function

Figure 2.16 shows the luminosity function of young star clusters in NGC 45, the luminosity function without correction for incompleteness, i.e. for all the clusters with $B_{F435W} < 23.2$, and the completeness-corrected luminosity function for a source with FWHM=1.2 pixels. The histogram was fitted using χ^2 with a relation of the form

$$\log N = aM_B + b, \quad (2.7)$$

which yield $a = 0.37 \pm 0.11$, $b = -7.9 \pm 2.5$. This can be converted to the more common representation of the luminosity function as a power-law $dN(L_B)/dL_B = \beta L_B^{\alpha}$, using Eq.

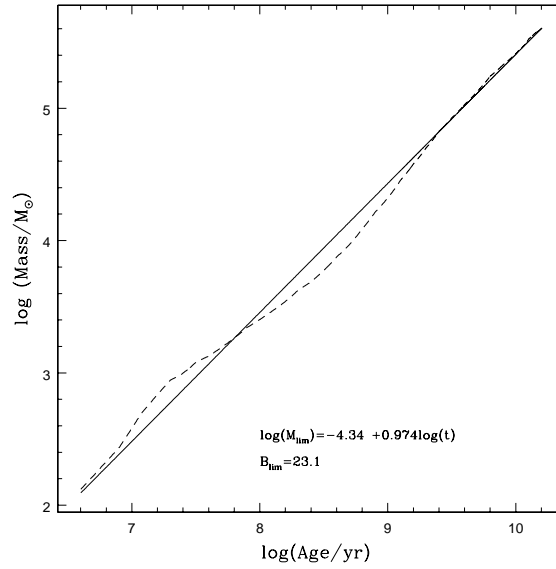


Figure 2.15: Detection limit for all ages and masses for a cluster of $B_{F435W} = 23.1$ represented by the dashed line. The solid line is a linear fit to this relation.

4 from Larsen (2002):

$$\alpha = -(2.5a + 1), \quad (2.8)$$

which yields $\alpha = -1.94 \pm 0.28$.

This value is in agreement (within the errors) with slopes found in Larsen (2002) and other studies of $-2.4 \leq \alpha \leq -2.0$ for a variety of galaxies. It is also consistent with the LMC value $\alpha = -2.01 \pm 0.08$ from Table 5 in Larsen (2002).

Alternatively, the slope of the luminosity function may be estimated by carrying out a maximum-likelihood fit directly to the data points, thus avoiding binning effects. Such a fit is sensitive to the luminosity range over which the power law is normalized, however. A fit restricted to the luminosity range of the clusters included in our sample ($21.17 < B_{F435W} < 23.08$) yields $\alpha = -1.99 \pm 0.40$, in good agreement with the fit in Fig. 2.16. If we restrict the fitting range to objects brighter than $B_{F435W} = 22.5$ we get a steeper slope, but with a larger error: $\alpha = -3.2 \pm 0.8$. Likewise, allowing for a higher maximum luminosity in the normalization of the power-law and including a correction for completeness also leads to a steeper slope. In conclusion, the luminosity function is probably consistent with earlier studies, but the small number of clusters makes it difficult to provide tight constraints on the LF slope in NGC 45.

2.5 Globular clusters

In this section we comment briefly on the globular clusters in NGC 45.

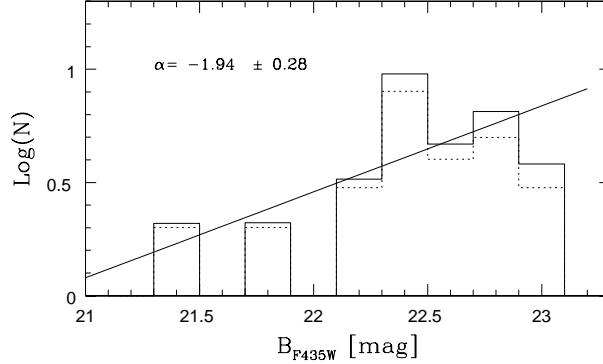


Figure 2.16: B_{F435W} band luminosity function of the cluster candidates. The dashed histogram is the uncorrected luminosity function, while the solid histogram is the completeness-corrected one. The solid line represents the power-law fit of the form $dN(L)/dL \propto L^\alpha$ to the corrected LF for a cluster $FWHM=1.2$ pixels.

2.5.1 Sizes and color distribution

For all extended objects with observed colors $0.8 < (V_{F555W} - I_{F814W}) < 1.2$ (i.e. globular clusters), we measured an average $FWHM = 1.7 \pm 0.4$ pixels from ISHAPE, which is equivalent to a half-light radius of $R_{eff} = 2.9 \pm 0.7$ pc (errors are the standard error of the mean). These sizes well agree with the average half-light radius found by Jordán et al. (2005) in the ACS Virgo Cluster Survey ($R_{eff} = 2.7 \pm 0.35$ pc).

Due to the age-metallicity degeneracy in optical broad-band colors (e.g. Worthey 1994), we cannot independently estimate the ages and metallicities of the globular clusters. It is still interesting to compare the color distribution of the globular cluster candidates in NGC 45 with those observed in other galaxies, (e.g. Gebhardt & Kissler-Patig 1999; Kundu & Whitmore 2001; Larsen et al. 2001). To do this we transformed the ACS magnitudes to standard Bessel magnitudes, following the Sirianni et al. (2005) recipe.

In Fig. 2.17 the color ($V - I$) histogram of the NGC 45 GCs is shown. Most of the objects have $V - I \leq 1.0$, with a mean color of $V - I = 0.90 \pm 0.01$. Three objects have redder colors ($(V - I) \geq 1$), with a mean color of $V - I = 1.05 \pm 0.02$. Thus the majority of objects in NGC 45 fall around the blue peak seen in galaxies where globular clusters exhibit a bimodal color distribution. e.g. globular clusters of NGC 45 are very likely metal-poor “halo” objects (e.g. Kissler-Patig 2000b).

2.5.2 Globular-cluster specific frequency

Harris & van den Bergh (1981) defined the specific frequency S_N as

$$S_N = N_{GC} 10^{0.4*(M_V+15)} \quad (2.9)$$

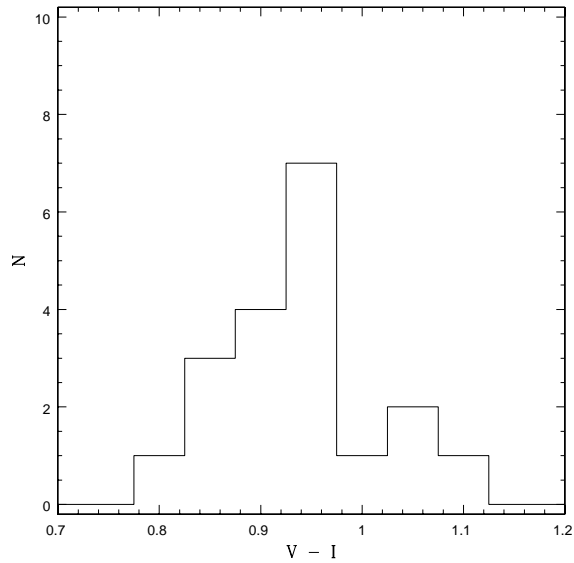


Figure 2.17: Histogram of the $V - I$ color distribution for globular clusters in NGC 45.

where N_{GC} is the total number of globular clusters that belong to the galaxy and M_V is the absolute visual magnitude of the galaxy. The 19 globular cluster candidates detected in NGC 45 provide a lower limit on the globular cluster specific frequency of $S_N = 1.4 \pm 0.15$, using for NGC 45 $V_{TOT} = 10.66 \pm 0.11$ from the HyperLeda⁵ database (Patrel et al. 2003) and applying a correction for foreground reddening of $A_V = 0.07$ mag (using $A_B = 0.09$ from Schlegel et al. 1998 and assuming $A_B/A_V = 1.324$; Rieke & Lebofsky 1985).

A more accurate estimate needs to take the detection completeness and incomplete spatial coverage into account. The globular cluster luminosity function (GCLF) generally appears to be fit well by a Gaussian function, and the total number of clusters can therefore be estimated by counting the number of clusters brighter than the turn-over and multiplying by 2. This reduces the effect of uncertain corrections at the faint end of the GCLF (but of course introduces the assumption that the GCLF does indeed follow a Gaussian shape). Here we adopted the mean turnover of disk galaxies from Table 14 in Carney (2001) at $M_{TO} = -7.46 \pm 0.08$, i.e. $V = 21.03$. This is indicated by the horizontal line in Fig. 2.8.

With these assumptions we calculated $N_{GCLF} = 13^{+7}_{-2}$ in the observed field of view. An inspection of Fig. 2.8 suggests that our estimate of the GCLF turn-over magnitude may be too bright, with only 6 (one third) of the detected objects falling above the line representing the turn-over. This could mean that the distance is underestimated (note the large uncertainty of ± 0.41 mag on the distance modulus), or that the GCLF does not follow the canonical shape.

⁵<http://leda.univ-lyon1.fr>

In any case, since our ACS frames cover only part of NGC 45, these numbers need to be corrected for spatial incompleteness. For this purpose, we drew a circle centered in the galaxy through each globular cluster, and we counted that globular cluster as $1/fc$, where fc is the fraction of that circle falling within the ACS field of view. In this way we estimated that at least $N_{expected} = 7 \pm 3$ more globular clusters would be expected outside the area covered by the ACS pointings. Finally, the total estimated number of globular clusters ($N_{GC} = N_{GCLF} + N_{expected}$) in NGC 45 is $N_{GC} = 20_{-3}^{+8}$ and the specific frequency is $S_N = 1.5_{-0.6}^{+0.8}$. If instead the 19 clusters are corrected for spatial incompleteness directly, we estimate a total of 26 globular clusters and $S_N = 1.9 \pm 0.7$.

In marked contrast to the relatively modest population of young star clusters, NGC 45 shows a remarkably large population of old globular clusters for its luminosity. We derived specific frequencies of $S_N = 1.9 \pm 0.7$ and $S_N = 1.5_{-0.6}^{+0.8}$, depending on how the total number of globular clusters is estimated. This is significantly higher than in other late-type galaxies, e.g., Ashman & Zepf (1998) quote the following values for late-type galaxies in the Local Group: LMC ($S_N = 0.6 \pm 0.2$), M33 ($S_N = 0.5 \pm 0.2$), SMC ($S_N = 0.2$), and M31 ($S_N = 0.9 \pm 0.2$). Does this make NGC 45 a special galaxy? Did something happen in the distant past of the galaxy? Globular clusters are distributed in a similar way to the Milky Way halo globular clusters (i.e. concentrated toward the center). The globular cluster color distribution (Fig. 2.17) suggests that most of them share the same metallicity, except three that might represent a “metal-rich peak”. Thus, most of the globular clusters in NGC 45 may be analogues of the “halo globular clusters” in the Milky Way or, more generally, the metal-poor globular cluster population generally observed in all major galaxies (e.g. Kissler-Patig 2000b).

2.6 Discussion and conclusions

We have analyzed the star cluster population of the nearby, late-type spiral galaxy NGC 45. Cluster candidates were identified using a size criterion, taking advantage of the excellent spatial resolution of the Advanced Camera for Surveys on board HST. In fact, the high resolution and sensitivity, combined with the modest distance of NGC 45, mean that the identification of star clusters is no longer limited by our ability to resolve them as extended objects. Instead, as we are probing farther down the cluster mass- and luminosity distributions, the challenge is to disentangle real physical clusters from the random line-of-sight alignments of field stars. The high resolution also means that the ISHAPE code may fit individual bright stars in some clusters instead of the total cluster profile, which can be quite irregular for low-mass objects. Thus, we rely on a combination of ISHAPE and SExtractor size estimates for the cluster detection. The detection criteria are conservative, and it is possible that we may have missed some clusters. The ages and masses were then estimated from the broad-band colors, by comparison with GALEV SSP models.

Our ACS data have revealed two main groups of star clusters in NGC 45. We found a number of relatively low-mass ($< 10^4 M_{\odot}$) objects that have most probably formed more or less continuously over the lifetime of NGC 45 in its disk, similar to the open

clusters observed in the Milky Way. We see a high concentration of objects with ages $< 10^7$ years, many of which may not survive as systems of total negative energy. The mass distribution of these objects (Fig. 2.14) is consistent with random sampling from a power-law. The lack of very massive (young) clusters in NGC 45 may then be explained simply as a size-of-sample effect. We do not see a clear break in the mass- or age- distributions, and therefore cannot obtain reliable estimates of cluster disruption times as prescribed by Boutloukos & Lamers (2003). However, we have tentatively estimated an upper limit of about 100 Myr on the disruption time (t_4) of a $10^4 M_\odot$ cluster. Also, we do not see any evidence of past episodes of enhanced cluster formation activity in the age distribution of the star clusters, suggesting that NGC 45 has not been involved in major interactions in the (recent) past. Thus, star cluster formation in this galaxy is most likely triggered/stimulated by internal effects, such as spiral density waves.

Small number statistics, uncertain age estimates, and the difficulty of reliably identifying low-mass clusters prevent us from determining accurate cluster disruption time-scales. If our estimate of the disruption time is correct, then it is somewhat puzzling that a large population of old globular clusters are also observed, since a $10^5 M_\odot$ cluster should have a disruption time of only ~ 400 Myrs. Given that the globular cluster candidates are usually located closer to the center than the young clusters, one might expect an even shorter disruption time unless disruption of young clusters is dominated by mechanisms that are not active in the center, such as spiral density waves or encounters with giant molecular clouds. We note that more accurate metallicity and age measurements for the globular clusters will require follow-up spectroscopy.

Acknowledgements:

We would like to thank Nate Bastian for his useful comments and H.J.G.L.M. Lamers for providing the 3D code program. Also we would like to thank the referee Dr. Uta Fritze-von Alvensleben for insightful comments that helped in improving this paper.

(1)	(2)	(3)	(4)	(5)	(6)	(7)	(8)	(9)
ID	RA	DEC	B	σ	V	σ	I	σ
	2000	2000	F435W	F435W	F555W	F555W	F814W	F814W
(10)	(11)	(12)	(13)	(14)	(15)	(16)	(17)	(18)
U	σ	FWHMB	FWHMB	FWHMV	FWHMI	$E(B - V)$	$E(B - V)$	$E(B - V)$
F336W	F336W	(pix)	(pix)	(pix)	(pix)	Z=0.008	Z=0.004	Z=0.02
(19)	(20)	(21)	(22)	(23)	(24)	(25)	(26)	(27)
$E(B - V)$	$\log(\text{Age}/\text{yr})$	$\log(\text{Age}/\text{yr})$	$\log(\text{Age}/\text{yr})$	$\log(\text{Age}/\text{yr})$	$\log(M/M_{\odot})$	$\log(M/M_{\odot})$	$\log(M/M_{\odot})$	$\log(M/M_{\odot})$
Z=0.05	Z=0.008	Z=0.004	Z=0.02	Z=0.05	Z=0.008	Z=0.004	Z=0.02	Z=0.05
1	0:14:15.46	-23:12:48.11	21.442	0.007	21.290	0.007	20.630	0.007
20.728	0.024	4.660	1.500	1.430	0.890	0.25	0.21	0.07
0.41	7.08	7.29	7.48	6.73	3.69	3.83	3.81	3.64
2	0:14:14.95	-23:13:17.73	22.518	0.013	22.532	0.013	22.581	0.023
22.249	0.059	3.330	0.390	0.450	0.280	0.00	0.10	0.33
0.35	7.90	6.89	6.60	6.60	3.41	2.64	2.75	2.84
3	0:14:14.92	-23:13:23.83	22.816	0.024	22.962	0.024	22.887	0.038
21.585	0.053	4.880	0.650	0.720	1.290	0.00	0.00	0.00
0.00	6.69	7.20	6.66	6.71	2.35	2.90	2.27	2.42
4	0:14:14.70	-23:13:20.37	22.652	0.018	22.666	0.021	22.989	0.033
21.725	0.050	5.780	0.700	0.780	0.650	0.00	0.00	0.08
0.10	6.66	6.74	6.60	6.60	2.36	2.36	2.38	2.47
5	0:14:15.40	-23:13:55.51	22.174	0.011	22.224	0.011	21.707	0.012
21.801	0.049	3.250	0.830	0.750	0.570	0.04	0.02	0.00
0.00	7.72	7.80	7.83	7.73	3.52	3.54	3.58	3.56

Table 2.2: Young star clusters.

Table 2.2 cont.

(1)	(2)	(3)	(4)	(5)	(6)	(7)	(8)	(9)
ID	RA	DEC	B	σ	V	σ	I	σ
	2000	2000	F435W	F435W	F555W	F555W	F814W	F814W
(10)	(11)	(12)	(13)	(14)	(15)	(16)	(17)	(18)
U	σ	FWHMB	FWHMB	FWHMV	FWHMI	$E(B - V)$	$E(B - V)$	$E(B - V)$
F336W	F336W	(pix)	(pix)	(pix)	(pix)	Z=0.008	Z=0.004	Z=0.02
(19)	(20)	(21)	(22)	(23)	(24)	(25)	(26)	(27)
$E(B - V)$	$\log(\text{Age}/\text{yr})$	$\log(\text{Age}/\text{yr})$	$\log(\text{Age}/\text{yr})$	$\log(\text{Age}/\text{yr})$	$\log(M/M_{\odot})$	$\log(M/M_{\odot})$	$\log(M/M_{\odot})$	$\log(M/M_{\odot})$
Z=0.05	Z=0.008	Z=0.004	Z=0.02	Z=0.05	Z=0.008	Z=0.004	Z=0.02	Z=0.05
6	0:14:15.00	-23:13:50.93	22.183	0.012	22.224	0.014	22.049	0.020
21.906	0.063	5.800	1.720	1.890	1.940	0.00	0.00	0.00
0.41	7.91	7.90	7.81	6.60	3.56	3.55	3.52	3.08
7	0:14:14.17	-23:13:20.00	22.814	0.022	23.106	0.024	22.874	0.035
22.514	0.097	5.370	1.000	0.720	1.120	0.00	0.05	0.21
0.00	7.81	6.91	6.64	7.38	3.19	2.45	2.47	3.01
8	0:14:11.63	-23:12:18.28	22.837	0.016	22.240	0.013	22.306	0.025
21.199	0.883	4.910	1.170	1.780	2.260	0.37	0.29	0.41
0.43	6.60	6.68	6.60	6.60	2.93	2.78	2.91	3.01
9	0:14:02.07	-23:07:58.54	22.340	0.017	22.061	0.017	21.547	0.019
24.114	0.486	9.490	3.700	4.080	3.880	0.00	0.00	0.02
0.01	8.70	8.60	8.51	8.40	4.13	4.02	4.05	4.02
10	0:14:94.67	-23:09:22.27	22.718	0.018	22.604	0.020	22.444	0.040
21.616	0.061	20.170	0.580	0.960	1.670	0.02	0.04	0.00
0.19	6.80	7.20	6.75	6.67	2.52	3.03	2.42	2.74

Table 2.2 cont.

(1)	(2)	(3)	(4)	(5)	(6)	(7)	(8)	(9)
ID	RA	DEC	B	σ	V	σ	I	σ
	2000	2000	F435W	F435W	F555W	F555W	F814W	F814W
(10)	(11)	(12)	(13)	(14)	(15)	(16)	(17)	(18)
U	σ	FWHMB	FWHMB	FWHMV	FWHMI	$E(B - V)$	$E(B - V)$	$E(B - V)$
F336W	F336W	(pix)	(pix)	(pix)	(pix)	Z=0.008	Z=0.004	Z=0.02
(19)	(20)	(21)	(22)	(23)	(24)	(25)	(26)	(27)
$E(B - V)$	$\log(\text{Age}/\text{yr})$	$\log(\text{Age}/\text{yr})$	$\log(\text{Age}/\text{yr})$	$\log(\text{Age}/\text{yr})$	$\log(M/M_{\odot})$	$\log(M/M_{\odot})$	$\log(M/M_{\odot})$	$\log(M/M_{\odot})$
Z=0.05	Z=0.008	Z=0.004	Z=0.02	Z=0.05	Z=0.008	Z=0.004	Z=0.02	Z=0.05
11	0:14:02.66	-23:09:33.45	22.971	0.016	22.104	0.010	22.515	0.022
21.792	0.040	3.260	0.400	0.350	0.670	0.31	0.24	0.33
0.35	6.60	6.60	6.60	6.60	2.83	2.65	2.79	2.89
12	0:14:14.03	-23:10:00.62	21.823	0.013	21.657	0.016	21.693	0.026
20.816	0.040	5.630	2.290	3.930	2.890	0.10	0.03	0.22
0.24	6.70	6.81	6.60	6.60	2.92	2.87	2.98	3.07
13	0:14:02.55	-23:10:32.22	22.917	0.015	22.997	0.022	22.851	0.060
21.759	0.048	6.860	0.690	0.940	2.660	0.00	0.00	0.00
0.05	6.74	7.20	6.70	6.72	2.35	2.87	2.27	2.48
14	0:14:01.45	-23:10:05.05	22.491	0.014	22.655	0.017	22.547	0.029
21.332	0.039	3.440	0.780	0.910	1.870	0.00	0.00	0.00
0.00	6.71	7.20	6.67	6.72	2.48	3.02	2.41	2.56
15	0:14:01.45	-23:10:04.85	22.416	0.013	22.542	0.016	22.125	0.027
21.208	0.033	6.380	0.980	0.950	3.040	0.00	0.00	0.00
0.00	7.20	7.20	6.74	6.83	3.04	3.09	2.52	2.75

Table 2.2 cont.

(1)	(2)	(3)	(4)	(5)	(6)	(7)	(8)	(9)
ID	RA	DEC	B	σ	V	σ	I	σ
	2000	2000	F435W	F435W	F555W	F555W	F814W	F814W
(10)	(11)	(12)	(13)	(14)	(15)	(16)	(17)	(18)
U	σ	FWHMB	FWHMB	FWHMV	FWHMI	$E(B - V)$	$E(B - V)$	$E(B - V)$
F336W	F336W	(pix)	(pix)	(pix)	(pix)	Z=0.008	Z=0.004	Z=0.02
(19)	(20)	(21)	(22)	(23)	(24)	(25)	(26)	(27)
$E(B - V)$	$\log(\text{Age}/\text{yr})$	$\log(\text{Age}/\text{yr})$	$\log(\text{Age}/\text{yr})$	$\log(\text{Age}/\text{yr})$	$\log(M/M_{\odot})$	$\log(M/M_{\odot})$	$\log(M/M_{\odot})$	$\log(M/M_{\odot})$
Z=0.05	Z=0.008	Z=0.004	Z=0.02	Z=0.05	Z=0.008	Z=0.004	Z=0.02	Z=0.05
16	0:14:01.15	-23:10:21.52	22.362	0.014	22.103	0.013	21.572	0.018
22.472	0.091	4.640	1.660	1.820	2.270	0.00	0.00	0.00
0.00	8.44	8.60	8.47	8.37	3.92	4.01	4.01	3.99
17	0:14:02.37	-23:10:59.48	23.081	0.020	22.981	0.024	22.800	0.039
21.913	0.042	2.770	0.460	0.620	0.750	0.00	0.02	0.00
0.14	6.80	7.20	6.74	6.70	2.36	2.87	2.28	2.56
18	0:14:02.83	-23:11:10.11	22.638	0.019	22.438	0.020	21.954	0.025
22.350	0.084	5.340	2.010	1.680	1.430	0.13	0.10	0.00
0.00	7.94	7.99	8.13	8.03	3.66	3.63	3.64	3.63
19	0:14:01.65	-23:10:58.16	21.781	0.011	21.816	0.013	21.834	0.020
20.603	0.024	6.240	0.480	0.730	0.550	0.00	0.00	0.00
0.05	6.70	7.20	6.67	6.67	2.78	3.32	2.70	2.88
20	0:13:56.63	-23:08:48.94	22.624	0.020	22.329	0.018	21.862	0.020
23.047	0.183	5.570	2.430	2.470	2.670	0.00	0.00	0.00
0.00	8.70	8.60	8.51	8.40	4.02	3.90	3.91	3.90

Table 2.2 cont.

(1)	(2)	(3)	(4)	(5)	(6)	(7)	(8)	(9)
ID	RA	DEC	B	σ	V	σ	I	σ
	2000	2000	F435W	F435W	F555W	F555W	F814W	F814W
(10)	(11)	(12)	(13)	(14)	(15)	(16)	(17)	(18)
U	σ	FWHMB	FWHMB	FWHMV	FWHMI	$E(B - V)$	$E(B - V)$	$E(B - V)$
F336W	F336W	(pix)	(pix)	(pix)	(pix)	Z=0.008	Z=0.004	Z=0.02
(19)	(20)	(21)	(22)	(23)	(24)	(25)	(26)	(27)
$E(B - V)$	$\log(\text{Age}/\text{yr})$	$\log(\text{Age}/\text{yr})$	$\log(\text{Age}/\text{yr})$	$\log(\text{Age}/\text{yr})$	$\log(M/M_{\odot})$	$\log(M/M_{\odot})$	$\log(M/M_{\odot})$	$\log(M/M_{\odot})$
Z=0.05	Z=0.008	Z=0.004	Z=0.02	Z=0.05	Z=0.008	Z=0.004	Z=0.02	Z=0.05
21	0:13:57.52	-23:09:15.97	22.441	0.014	22.334	0.017	22.380	0.032
21.159	0.029	12.280	1.360	1.820	2.780	0.00	0.00	0.00
0.09	6.70	6.77	6.68	6.65	2.55	2.55	2.48	2.68
22	0:13:56.78	-23:08:58.02	22.761	0.015	22.872	0.018	22.303	0.031
21.699	0.036	8.440	0.520	0.680	3.980	0.02	0.06	0.00
0.08	7.08	7.23	7.30	6.84	2.81	3.05	3.03	2.74
23	0:13:59.86	-23:10:22.19	22.409	0.018	22.504	0.020	22.770	0.041
21.186	0.038	9.580	0.790	0.970	1.490	0.00	0.00	0.00
0.01	6.60	6.67	6.60	6.61	2.44	2.42	2.38	2.46
24	0:13:59.88	-23:10:23.29	22.140	0.015	22.252	0.016	22.503	0.032
21.163	0.043	13.540	0.950	0.990	1.080	0.00	0.00	0.05
0.07	6.65	6.74	6.60	6.60	2.55	2.56	2.53	2.62
25	0:13:59.72	-23:10:23.64	22.494	0.014	22.432	0.015	21.551	0.018
22.248	0.069	3.770	0.980	1.260	2.200	0.03	0.02	0.08
0.10	8.20	8.11	7.99	7.87	3.74	3.63	3.72	3.72

Table 2.2 cont.

(1)	(2)	(3)	(4)	(5)	(6)	(7)	(8)	(9)
ID	RA	DEC	B	σ	V	σ	I	σ
	2000	2000	F435W	F435W	F555W	F555W	F814W	F814W
(10)	(11)	(12)	(13)	(14)	(15)	(16)	(17)	(18)
U	σ	FWHMB	FWHMB	FWHMV	FWHMI	$E(B - V)$	$E(B - V)$	$E(B - V)$
F336W	F336W	(pix)	(pix)	(pix)	(pix)	Z=0.008	Z=0.004	Z=0.02
(19)	(20)	(21)	(22)	(23)	(24)	(25)	(26)	(27)
$E(B - V)$	$\log(\text{Age}/\text{yr})$	$\log(\text{Age}/\text{yr})$	$\log(\text{Age}/\text{yr})$	$\log(\text{Age}/\text{yr})$	$\log(M/M_{\odot})$	$\log(M/M_{\odot})$	$\log(M/M_{\odot})$	$\log(M/M_{\odot})$
Z=0.05	Z=0.008	Z=0.004	Z=0.02	Z=0.05	Z=0.008	Z=0.004	Z=0.02	Z=0.05
26	0:14:01.90	-23:11:30.50	21.165	0.008	20.967	0.009	21.270	0.014
19.818	0.018	5.160	1.570	2.430	2.040	0.04	0.00	0.06
0.08	6.60	6.66	6.60	6.60	3.06	2.97	3.03	3.12
27	0:14:00.38	-23:10:51.70	22.476	0.012	22.416	0.013	22.184	0.018
22.320	0.059	2.990	0.380	0.410	0.460	0.00	0.00	0.00
0.00	8.00	8.00	7.84	8.00	3.52	3.49	3.44	3.60
28	0:13:59.37	-23:10:32.15	21.385	0.008	21.324	0.008	20.946	0.011
20.944	0.028	5.530	1.420	1.440	1.510	0.03	0.00	0.00
0.00	7.87	7.93	7.81	7.72	3.95	3.93	3.89	3.88

(1): Cluster ID; (2): RA; (3): DEC; (4), (5), (6), (7), (8), (9), (10), (11): Photometry and the error in magnitude units; (12): FWHM derived using SExtractor for the F435W band in pixels; (13), (14), (15): FWHM derived using ISHAPE in pixels for each band.; (16), (17), (18), (19): Extinction derived for each metallicity model.; (20), (21), (22), (23): Cluster Ages derived for each metallicity model in Log(yrs).; (24), (25), (26), (27): Cluster masses derived for each metallicity model in solar masses. All the values in **bold** correspond to the best fit value for each cluster.

(1)	(2)	(3)	(4)	(5)	(6)	(7)	(8)	(9)
ID	RA	DEC	B	σ	V	σ	I	σ
	2000	2000	F435W	F435W	F555W	F555W	F814W	F814W
(10)	(11)	(12)	(13)	(14)	(15)	(16)	(17)	(18)
U	σ	FWHMB	FWHMB	FWHMV	FWHMI	$E(B - V)$	$E(B - V)$	$E(B - V)$
F336W	F336W	(pix)	(pix)	(pix)	(pix)	Z=0.008	Z=0.004	Z=0.02
(19)	(20)	(21)	(22)	(23)	(24)	(25)	(26)	(27)
$E(B - V)$	$\log(\text{Age}/\text{yr})$	$\log(\text{Age}/\text{yr})$	$\log(\text{Age}/\text{yr})$	$\log(\text{Age}/\text{yr})$	$\log(M/M_{\odot})$	$\log(M/M_{\odot})$	$\log(M/M_{\odot})$	$\log(M/M_{\odot})$
Z=0.05	Z=0.008	Z=0.004	Z=0.02	Z=0.05	Z=0.008	Z=0.004	Z=0.02	Z=0.05
29	0:14:12.89	-23:11:46.79	21.528	0.007	20.360	0.004	19.456	0.004
22.727	0.078	2.980	0.300	0.240	0.350	0.65	0.57	0.00
0.61	8.71	8.90	10.18	8.60	5.52	5.50	6.10	5.52
30	0:14:14.82	-23:13:21.23	20.714	0.005	20.443	0.005	19.518	0.004
19.861	0.014	10.750	0.630	0.560	0.580	0.34	0.39	0.14
0.40	7.08	7.21	7.07	6.83	4.18	4.42	3.85	4.10
31	0:14:04.22	-23:09:49.63	22.749	0.016	22.520	0.015	21.372	0.012
21.999	0.054	3.890	1.180	1.200	1.360	0.43	0.38	0.26
0.42	7.08	7.30	7.19	6.96	3.49	3.61	3.36	3.46
32	0:14:01.28	-23:09:38.08	21.707	0.011	20.989	0.008	19.955	0.007
21.871	0.056	4.950	2.370	2.410	2.670	0.00	0.00	0.02
0.00	9.20	9.35	9.05	8.96	4.97	5.05	4.95	4.93
33	0:14:03.64	-23:10:44.86	21.981	0.011	21.358	0.009	20.355	0.009
22.250	0.059	3.270	0.790	0.790	0.890	0.13	0.07	0.14
0.11	8.95	9.06	8.86	8.76	4.77	4.68	4.80	4.75

Table 2.3: Globular clusters with 4 band photometry.

Table 2.3 cont.

(1)	(2)	(3)	(4)	(5)	(6)	(7)	(8)	(9)
ID	RA	DEC	B	σ	V	σ	I	σ
	2000	2000	F435W	F435W	F555W	F555W	F814W	F814W
(10)	(11)	(12)	(13)	(14)	(15)	(16)	(17)	(18)
U	σ	FWHMB	FWHMB	FWHMV	FWHMI	$E(B - V)$	$E(B - V)$	$E(B - V)$
F336W	F336W	(pix)	(pix)	(pix)	(pix)	Z=0.008	Z=0.004	Z=0.02
(19)	(20)	(21)	(22)	(23)	(24)	(25)	(26)	(27)
$E(B - V)$	$\log(\text{Age}/\text{yr})$	$\log(\text{Age}/\text{yr})$	$\log(\text{Age}/\text{yr})$	$\log(\text{Age}/\text{yr})$	$\log(M/M_{\odot})$	$\log(M/M_{\odot})$	$\log(M/M_{\odot})$	$\log(M/M_{\odot})$
Z=0.05	Z=0.008	Z=0.004	Z=0.02	Z=0.05	Z=0.008	Z=0.004	Z=0.02	Z=0.05
34	0:14:03.91	-23:10:54.72	21.225	0.007	20.452	0.005	19.367	0.005
21.585	0.035	3.270	1.070	1.060	1.040	0.24	0.15	0.25
0.23	8.95	9.10	8.86	8.73	5.26	5.14	5.29	5.23
35	0:14:03.53	-23:10:48.80	22.263	0.012	21.643	0.009	20.716	0.010
22.087	0.061	3.490	1.020	1.030	1.040	0.49	0.68	0.45
0.94	7.75	6.91	7.81	6.60	4.29	3.79	4.32	3.99
36	0:14:01.52	-23:10:06.25	22.226	0.012	21.564	0.009	20.542	0.008
22.367	0.078	3.080	0.860	0.960	0.960	0.56	0.00	0.00
0.00	7.99	9.26	9.05	8.92	4.57	4.75	4.70	4.68

For column descriptions see Table 2.2

Table 2.4: Globular clusters with 3 band photometry.

(1)	(2)	(3)	(4)	(5)	(6)	(7)	(8)	(9)	(10)	(11)	(12)	(13)
ID	RA	DEC	B	σ	V	σ	I	σ	FWHMB	FWHMB	FWHMV	FWHMI
	2000	2000	F435W	F435W	F555W	F555W	F814W	F814W	SExtractor (pix)	ISHAPE (pix)	ISHAPE (pix)	ISHAPE (pix)
37	0:14:08.84	-23:11:58.16	22.244	0.013	21.604	0.009	20.455	0.008	4.120	1.750	1.840	2.270
38	0:14:07.07	-23:10:33.77	22.456	0.017	22.199	0.015	21.554	0.016	5.730	3.150	2.690	2.140
39	0:14:05.77	-23:10:06.71	21.996	0.013	21.389	0.010	20.429	0.010	5.450	2.760	2.890	2.870
40	0:14:06.93	-23:10:47.15	20.602	0.006	19.978	0.005	19.035	0.005	5.120	1.530	1.580	1.600
41	0:14:04.97	-23:10:15.83	22.290	0.014	21.605	0.010	20.641	0.010	4.530	1.790	1.870	1.890
42	0:14:04.18	-23:10:34.09	21.671	0.008	20.997	0.007	19.985	0.006	3.640	1.040	1.120	1.280
43	0:14:04.94	-23:10:54.28	21.267	0.007	20.524	0.005	19.483	0.005	3.650	1.170	1.220	1.260
44	0:14:04.17	-23:10:53.98	21.295	0.008	20.560	0.006	19.383	0.005	3.970	1.610	1.550	1.540
45	0:14:04.67	-23:11:18.17	22.388	0.013	21.480	0.009	20.532	0.008	4.450	1.410	1.510	1.500
46	0:14:04.01	-23:11:06.07	22.566	0.012	21.793	0.010	20.784	0.010	3.200	0.750	0.940	0.930
47	0:14:04.40	-23:11:16.11	22.453	0.020	21.700	0.015	20.669	0.015	9.680	7.250	7.570	7.170

Column (1): Globular cluster ID. Column (2): RA. Column (3): DEC. Columns (4), (5), (6), (7), (8), (9): Photometry and the error in magnitude units. Column (10): FWHM derived using SExtractor for the F435W band in pixels. Columns (11), (12), (13): FWHM derived using ISHAPE in pixels for each band.

Chapter **3**

ACS Imaging of Star clusters in
unperturbed spiral galaxies: II. The
relative properties of star clusters in
five late type spirals

Submitted to Astronomy & Astrophysics

M. D. Mora, S. S. Larsen, M. Kissler-Patig, J. P. Brodie & T. Richtler

Abstract

Our goal is to investigate the formation of star clusters in relatively unperturbed environments. To do this, we studied the five nearby spiral galaxies: NGC 45, NGC 1313, NGC 4395, NGC 5236, and NGC 7793. We obtained images of the galaxies and their star cluster systems in *UBVI* using the *Advanced Camera for Surveys (ACS)* and the *Wide Field Planetary Camera 2 (WFPC2)* on board the *Hubble Space Telescope*. From a comparison of the broad-band colours with simple stellar population (SSP) models, we derived for each galaxy individual properties for the clusters such as masses, ages, and sizes, as well as global star cluster systems properties such as the age distribution, luminosity function, and disruption time for clusters. We identified about 600 star cluster candidates in the five galaxies, spanning typically ages from 3.9 Myr up to 1 Gyr and masses from $10^2 M_{\odot}$ up to $10^5 M_{\odot}$. We used the cluster age distribution to reconstruct the recent star formation history of each galaxy, and observed significant variations from galaxy to galaxy. We further derived the luminosity function of the young star clusters, and found slopes around $\alpha \sim -2$ (similar to the ones found in previous studies) and the brightest star cluster magnitudes consistent with a random sampling of the luminosity function without involving an upper mass cut-off. Finally, the sample includes only a handful of old globular clusters in each galaxy from which we derive low globular cluster specific frequencies.

3.1 Introduction

The formation of star clusters accompanies the formation of stars in the evolution of a galaxy. Yet, the final ratio of stars to clusters is observed to vary considerably (Harris 1991) and it remains unclear which factors influence this ratio. Understanding this aspect is, however, important to progress in our general understanding of star formation in galaxy and the formation mechanisms of star clusters.

A particular aspect is the influence of environment and how much the latter affects the star cluster formation. We have evidence that violent star forming events, such as galaxy mergers and starbursts, greatly stimulate star cluster formation (e.g. Holtzman et al. 1992; Whitmore & Schweizer 1995; Harris et al. 2004; Bastian et al. 2005c). But such events are not a necessary conditions for the formation of star clusters, since it is also observed in dwarf galaxies (e.g. Elson & Fall 1985; Conti & Vacca 1994; Billett et al. 2002) and spirals (Larsen & Richtler 1999). Does the ratio of stars to clusters depend on the star formation intensity? Will it be high in galaxies that formed stars at low rates?

But the ratio of stars to clusters is not only dictated by the formation mechanism, it is also a function of the destruction processes, in particular the ones that affect young star clusters at early stages of their evolution. Disruption times of young star clusters as a function of their properties (e.g. Boutloukos & Lamers 2003; Fall 2004, 2006), or as a function of the interactions between them and their surrounding media such as spiral arms and molecular clouds (e.g. Gieles et al. 2006b, 2007a) have attracted considerable interest in the last years. Are destruction processes the main drivers for the varying star to cluster ratios observed in galaxies?

In this paper, we investigate both the formation and disruption history of star clusters in relatively unperturbed environments: normal, non-interacting disk galaxies. We build on our first example NGC 45 (Mora et al. 2007), and extend the analysis to four more spiral galaxies: NGC 1313, NGC 4395, NGC 5236, and NGC 7793. Our sample includes late-type galaxies with both grand-design and flocculent spiral structure, spanning a large range in area-normalized star formation rate (Larsen & Richtler 2000) and cluster surface density as determined from ground-based observations. To minimize the extinction, all galaxies are close to face-on orientation and all have a similar distance modulus of $(m-M) \sim 28$.

The five galaxies of our sample have been previously studied from the ground by Larsen & Richtler (1999); Larsen (1999); Larsen & Richtler (2000). Massive star cluster candidates were found, supporting the fact that they can form as an ongoing process, as well as in a star formation bursts. The authors found that ratio of stars to clusters correlates with the star formation rate, and that the formation of young massive star clusters is favoured in environments with active star formation. The formation of massive young star clusters in starburst or mergers may be the extreme case of a more general phenomenon.

Taking advantage of the excellent spatial resolution of the Advanced Camera for Surveys (ACS) on board of HST, we investigate in this work how the star cluster properties such as sizes, ages, masses, disruption time-scales, etc, compare between the galaxies of the sample. The work is structured as follows: the observations, data reduction, photometry and completeness analysis are described in Sect. 3.2 In Sect. 3.3, we detail our

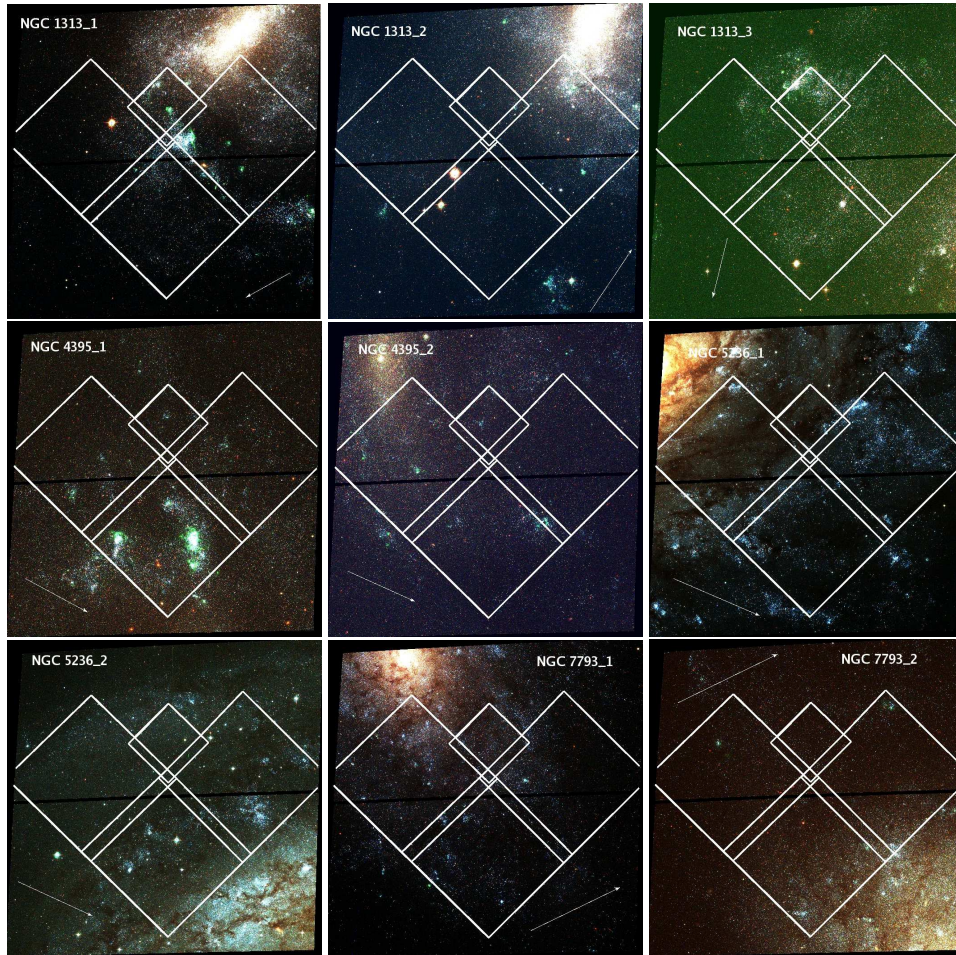


Figure 3.1: ACS colour images for all pointings of our galaxy sample, with over-layed WFPC2 field-of-view. The arrows indicate North.

star cluster selection criteria, before showing the colour–colour and colour–magnitude diagrams for the star clusters in Sect. 3.4. In Sect. 3.5, we discuss the properties of individual clusters, such as masses, ages, extinctions, measured sizes. In Sect. 3.6 and 3.7, we turn to global properties of the systems and present the star cluster luminosity functions, and star cluster age distributions, respectively. In Sect. 3.8 and 3.9, we briefly get back to extended objects, and old globular clusters. Finally, in Sect. 3.10, we discuss our results and draw some conclusions.

Throughout this work, we frequently followed procedures tested and outlined in our pilot study of NGC 45 (Mora et al. 2007) and refer to this paper for details.

Table 3.1: Pointing coordinates and exposure times for the galaxies in our sample. For NGC 45 see Mora et al. (2007)

Galaxy	RA (J2000)	DEC (J2000)	F336W sec	F435W sec	F555W sec	F814W sec	Date D.M.Y
NGC 1313_1	03 : 18 : 24	-66 : 28 : 22	2800	680	680	676	19.07.05
NGC 1313_2	03 : 18 : 17	-66 : 31 : 49	2800	680	680	676	20.12.05
NGC 1313_3	03 : 17 : 42	-66 : 30 : 40	2800	680	680	676	27.05.05
NGC 4395_1	12 : 26 : 00	+33 : 31 : 02	2400	680	680	430	12.06.05
NGC 4395_2	12 : 25 : 45	+33 : 34 : 26	2400	680	680	430	13.06.05
NGC 5236_1	13 : 37 : 00	-29 : 49 : 40	2400	680	680	430	30.07.05
NGC 5236_2	13 : 37 : 06	-29 : 55 : 30	2400	680	680	430	09.08.05
NGC 7793_1	23 : 57 : 41	-32 : 35 : 20	2400	680	680	430	10.12.04
NGC 7793_2	23 : 58 : 04	-32 : 36 : 10	2400	680	680	430	10.12.04

Table 3.2: Summary of galaxy properties.

	NGC 45	NGC 1313	NGC 4395	NGC 5236	NGC 7793
type ^a	SA(s)dm	SB(s)d	SA(s)m	SAB(s)c	SA(s)d
B [†]	11.37 ± 0.11	9.66 ± 0.41	10.84 ± 0.26	7.82 ± 0.21	9.71 ± 0.15
B-V [†]	0.71	0.49	0.46	0.66	0.54
A _B [‡]	0.09	0.47	0.08	0.29	0.08
(m-M) ₀	28.42 ± 0.41 ¹	28.2 ²	28.1 ³	27.84 ± 0.15 ⁴	27.6 ± 0.2 ⁵
[Fe/H]	-	-	-	-	-1.22 ⁶
[12 + log(O/H)]	-	-	8.48 ± 0.13 ⁷	8.9 - 9.1 ⁸	-
Z	-	0.008 ⁹	-	-	-
T _N ¹⁰	0.28	1.12	0.21	1.77	1.21
T _{L(U)} ¹¹	0.24	1.47	0.07	2.23	1.15

^a Retrieved from the NASA/IPAC Extragalactic Database (NED); [†] Patrel et al. (2003) retrieved from Hyperleda; [‡] Schlegel et al. (1998) retrieved from NED; ¹Bottinelli et al. (1985); ²de Vaucouleurs (1963); ³Karachentsev & Drozdovsky (1998); ⁴de Vaucouleurs (1979); ⁵Carignan (1985); ⁶Karachentsev et al. (2003); ⁷van Zee et al. (1998); ⁸Bresolin & Kennicutt (2002); ⁹Larsen et al. (2007). ¹⁰Larsen & Richtler (1999). ¹¹Larsen & Richtler (2000).

3.2 Observation and reductions

The galaxies were observed with the HST ACS Wide Field Channel and the WFPC2. The pixel scales are 0.05'' and 0.1'' for the ACS and the WFPC2, respectively. For each galaxy two different regions were observed, with the exception of NGC 1313 for which three pointings were obtained. All ACS pointings together with the WFPC2 footprint are shown in Figure 3.1. Exposure times and pointing coordinates are listed in Table 3.1.

The ACS images, after the standard ‘‘on-the-fly’’ pipeline reduction, were drizzled using the task MULTIDRIZZLE task (Koekemoer et al. 2002) in the STSDAS / PyRAF package. We used default parameter values but disabling the automatic sky subtraction due to the highly non-uniform background level. The WFPC2 images were combined using the CRREJ task with standard parameter settings.

3.2.1 Photometry

Sources were detected in the deepest ACS band (V_{F555W}) using the SExtractor (Bertin & Arnouts 1996) package and setting the detection threshold to 5 connected pixels 4 sigma over the background. The coordinates of the detected objects were used as input for the SExtractor runs in the other two ACS bands.

The aperture photometry in BVI was performed with the PHOT task (using the SExtractor coordinates as input) in IRAF¹. At the distance of our galaxies (~ 5 Mpc), the ACS pixel size corresponds to ~ 1 pc, while typical star cluster sizes are a few pc. As a compromise between the object size and crowding, we used for the photometry an aperture radius of 6 pix (with the sky determined in an annulus 5 pix wide at 8 pix radius).

The U_{F336W} -band photometry was performed on the WFPC2 images. Here also, we used the ACS object coordinates, transformed (using ~ 20 common objects and the task GEOMAP) into the WFPC2 frames, to identify the objects. The transformed coordinates were accurate to ~ 0.5 pix rms, and were used as input for the WFPC2 aperture photometry. The aperture photometry and sky determination in the WFPC2 images were done using the same physical sizes as used for the ACS images: 3 pix aperture radius (sky annulus at 4 pix, 2.5 pix wide) for the WFPC2; and 6 pix aperture radius (sky annulus at 8 pix, 5 pix wide) for the Planetary Camera (PC).

The counts were converted to the Vega magnitude system using the HST zero points taken from the HST web page² based on the spectrophotometric calibration of Vega from Bohlin & Gilliland (2004). Also Charge Transfer Efficiency corrections were applied to the U_{F336W} band following the updated version of Dolphin (2000).³

The aperture corrections were performed in the same way as in Mora et al. (2007): we created 6 artificial source types with different FWHMs: 0.2, 0.5, 0.9, 1.2, 1.5, and 1.8 pixels. On each of them, we performed the aperture correction from 6 pixels up to a nominal $1.''45$ reference aperture for the ACS and the WFPC2, and thus derived an empirical relation between the object sizes and their aperture correction. In this way, we corrected the photometry of each object according to its size. Because the object sizes were only measured in the ACS band (and not in the WFPC2 frames), we assumed that objects have the same size in the U -band as on the F435W images. The aperture corrections that we derive as a function of FWHM (in pix) are:

$$\begin{aligned}
 \Delta M_{F336W} &= -0.234 \times FWHM_B + 0.069 \\
 \Delta M_{F435W} &= -0.226 \times FWHM_B + 0.059 \\
 \Delta M_{F555W} &= -0.225 \times FWHM_V + 0.067 \\
 \Delta M_{F814W} &= -0.226 \times FWHM_I + 0.060
 \end{aligned}
 \tag{3.1}$$

For an object size $FWHM \geq 1.8$ pix, we extrapolated the aperture correction from the equation 3.1.

¹IRAF is distributed by the National Optical Astronomical Observatory, which is operated by the Association of Universities for Research in Astronomy, Inc, under cooperative agreement with the National Science Foundation.

²<http://www.stsci.edu/hst/acs/analysis/zeropoints/>

³http://www-int.stsci.edu/instruments/wfpc2/Wfpc2_cte/dolphin_cte.html

Finally, for each galaxy, we adopted the galactic foreground extinction according to Schlegel et al. (1998) (values listed in Table 3.2).

3.2.2 Size measurements

As a next step, we disentangled extended objects from point-like sources by measuring their physical sizes (as opposed to FWHM on the images). This was performed using the ISHAPE task in BAOLAB (Larsen 1999): each source was modelled using a King (1962) profile with a concentration parameter $c = 30$, convolved with the instrument PSF (as derived from images of the globular cluster 47 Tuc, see Mora et al. (2007) for details). For each object the output of ISHAPE included the physical FWHM, chi-square of the fitting, flux, signal to noise, and a residual image. These sizes are discussed below in section 3.5.4 and 3.9.1.

3.2.3 Completeness tests

We quantify the reliability of the derived magnitudes and sizes using a series on completeness tests.

For these tests, we selected the most crowded field for each galaxy (pointing 1 in all cases) and added 300 artificial objects in three different regions: 100 objects were added at random position in each of a low-/intermediate-/high-background region. We followed the process describe in more details in Mora et al. (2007) and finally compared the number of added and recovered stars in each field.

For each galaxy, the limiting magnitude as a function of size, as well as the uncertainty on the size as a function of magnitude are shown in Fig. 3.2. As expected, extended objects are more difficult to detect than less extended ones. For objects with FWHM= 1.8 pix, we computed a 50% completeness between $V_{F555W} \sim 24.5$ and 25.3 mag.

As for the sizes, we show the average value of the absolute difference between the input and recovered FWHM. We notice that extended objects in more crowded galaxies (NGC 7793 and NGC 5236) have greater uncertainties than the same extended objects in less crowded galaxies at the same magnitude. On average, sizes can be measured with an accuracy of ~ 0.2 pix down to about one magnitude above the 50% completion limit.

3.3 Star cluster selection

3.3.1 Sample selection by size and brightness limit

We based the selection of star clusters on the object size, both as measured by ISHAPE and by SExtractor. Similar to the procedure in Mora et al. (2007), we exclude all point sources and consider as star cluster candidates all extended objects.

The ISHAPE and SExtractor size distributions display narrow peaks, with the vast majority of objects at $\text{FWHM} < 0.2$ pixels and $\text{FWHM} < 2.7$ pixels, respectively (see Fig. 3.3). These are considered to be point sources, and we define the above thresholds as our cut-on for star cluster candidates. This corresponds to physical sizes of roughly 0.3 pc

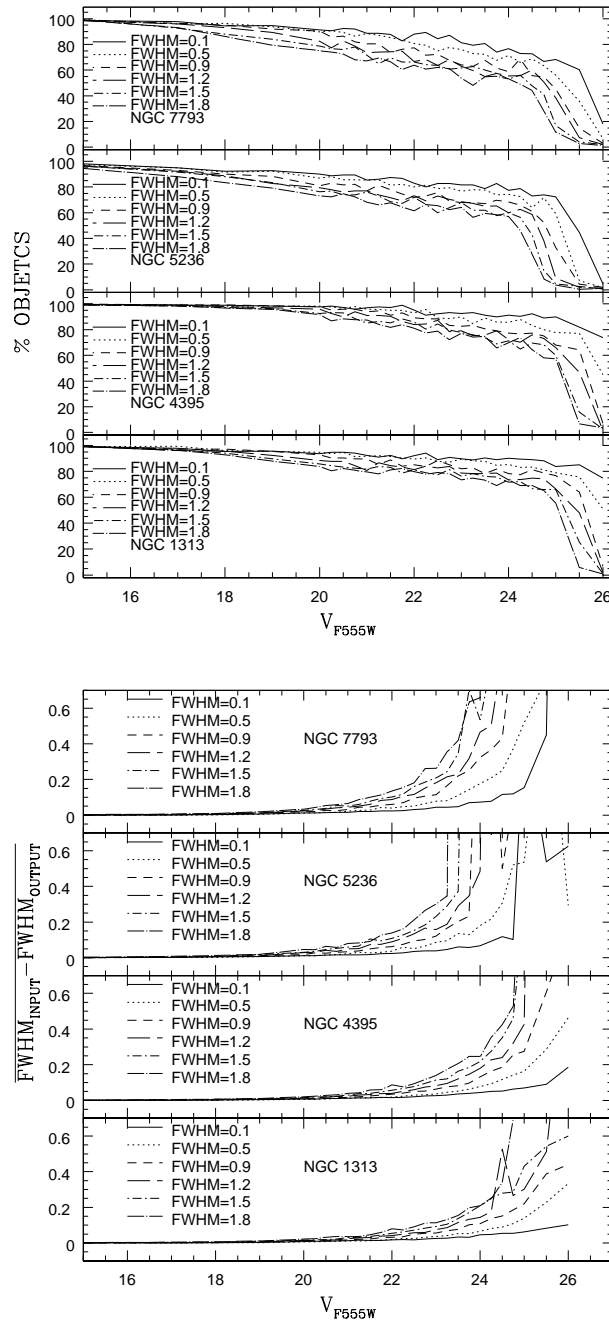


Figure 3.2: Top: Completeness in object finding as a function of magnitude for our four galaxies. Bottom: Average absolute difference between the input and recovered FWHM as a function of object magnitude.

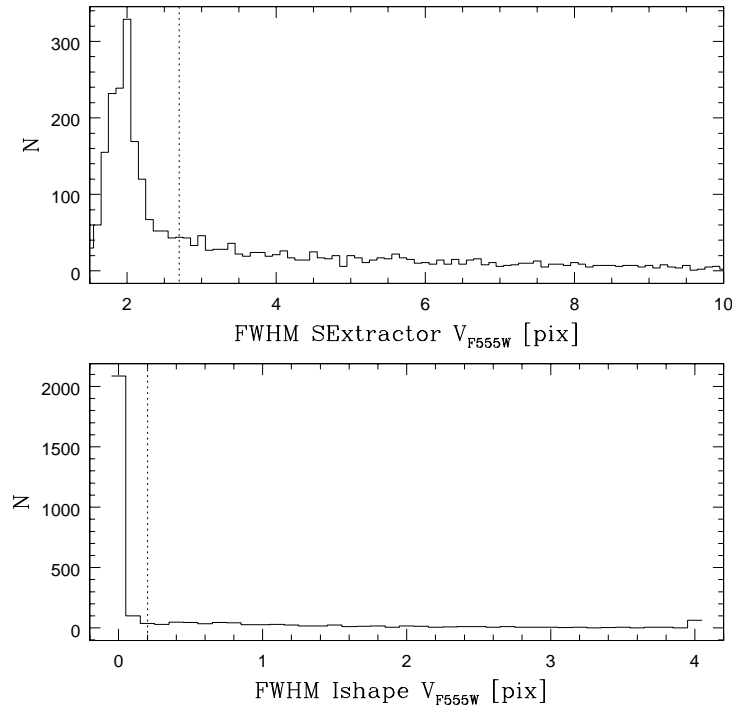


Figure 3.3: Histogram of the objects sizes in the full sample, as measured using ISHAPE (bottom) and SExtractor (top). The dotted line shows our size selection criteria.

and greater at the distance of our sample, which should not exclude any star cluster. The largest objects have sizes up to 10 pc, similar to the largest clusters observed in the Milky Way.

In a second step, we apply an absolute magnitude cut-off to the complete sample. In order to do so, we determined the limiting magnitude (at 60% completeness) for the worst case (extended objects in NGC 7793) to be $V_{F555W} = 22.5$. This corresponds to an absolute magnitude $M_{F555W} \sim -5.1$ at the distance of our sample and we apply it to the rest of the galaxies.

In summary, we selected for our further analysis objects more extended than ~ 0.3 pc in size, and brighter than -5 mag in M_V as star cluster candidates. The number of objects detected in the ACS fields and the sub-group included in the WFPC2 fields are listed in Table 3.3.

3.3.2 Selection of old star cluster in the colour–magnitude diagrams

We focussed in this work on young stellar clusters, but will discuss the population of old globular clusters further below.

In order to identify the population of old globular clusters in our sample galaxies, we used the colour–magnitude diagrams, shown in Fig. 3.4. In the case of face-on spiral-

Table 3.3: Number of selected star clusters in the ACS and WFPC2 field-of-views.

Galaxy	in ACS fields	in the WFPC2 fields
NGC 1313	703	246
NGC 4395	78	44
NGC 5236	880	219
NGC 7793	167	79

galaxies, disentangling the old from young star cluster population is a challenging task, as young *reddened* star cluster might exhibit similar colours to old globular clusters. Reddening will, however, make the star clusters appear fainter, so that by imposing both a colour and magnitude cut, we can recover the bright fraction of the old globular cluster population.

In order to do so, we have chosen the $B_{F435W} - V_{F555W}$ colour–magnitude diagrams, most capable of separating the two populations. The clearest separation between young and old cluster candidates is seen in NGC 5236, where the young star cluster population is seen at $B_{F435W} - V_{F555W} \sim 0$ and the globular cluster candidates have $B_{F435W} - V_{F555W} \sim 0.7$. As expected, below the turn-over magnitude of the globular cluster luminosity function (GCLF, marked as dashed line in Fig. 3.4) reddened young cluster increasingly scatter into the globular cluster colours .

For further analysis (see Sect. 3.9), we use the case of NGC 5236, the clearest case, to adopted the selection criteria for globular cluster candidates: $B_{F435W} - V_{F555W} > 0.5$ and $V_{F555W} < (m - M)_0 + V_{F555W}^{TO} - 0.2$ where $V_{TO} = -7.46 \pm 0.08$ from Carney (2001). I.e. we restrict ourselves to candidates brighter the the luminosity function turn-over.

These criteria yield 4 globular cluster candidates in NGC 1313 and NGC 7793, 8 globular cluster candidates in NGC 5236, and none in NGC 4395.

3.4 Colour–colour distributions

The determination of ages, masses and internal extinction towards our candidate clusters relies on colour–colour diagrams that we briefly present in this section.

In Fig. 3.5 the colour–colour diagrams (corrected for foreground extinction but not for internal extinction) are shown for all the galaxies. Simple Stellar Population (SSP) models from GALEV (Anders & Fritze-v. Alvensleben 2003) and Girardi (private communication)⁴ for different metallicities are overplotted.

Ages are increasing along the tracks from blue towards redder colours . The feature around $V_{F555W} - I_{F814W} \sim 0.5$ and $U_{F336W} - B_{F555W} \sim -1$ is strongly metallicity dependent and corresponds to the appearance of the red supergiant stars at 10^7 yr. In general star clusters have colours which are in agreement with the theoretical tracks. Some prominent features are:

⁴http://pleiadi.pd.astro.it/isoc_photsys.02/isoc_acs_hrc/index.html

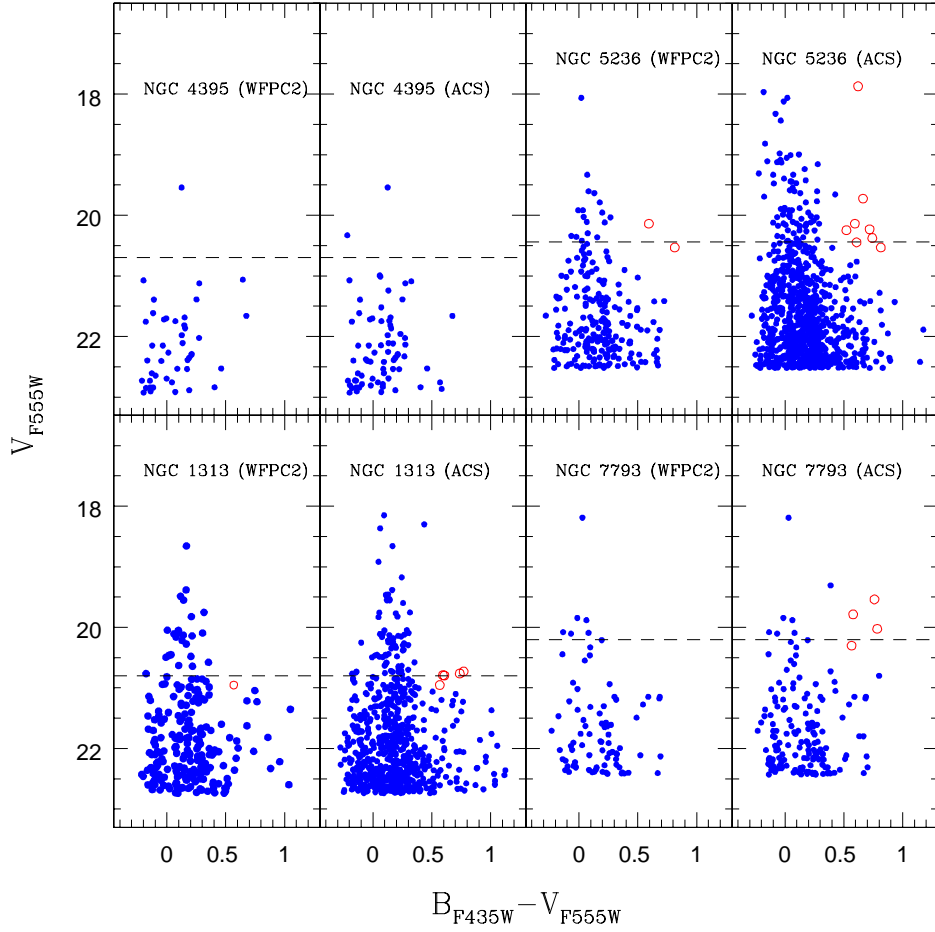


Figure 3.4: $B_{F435W} - V_{F555W}$ colour–magnitude diagrams for star cluster candidates in the ACS and WFPC2 field-of-view. Blue dots are young star cluster candidates while the red open circles marked our globular cluster candidates. Dashed lines shown the GCLF turn-over magnitude of the Milky Way GCLF: $M_{VTO} \sim -7.4$. The different limiting magnitudes correspond to the absolute magnitude $V_{cut} = -5.1$ cut adapted to the distance of each galaxy.

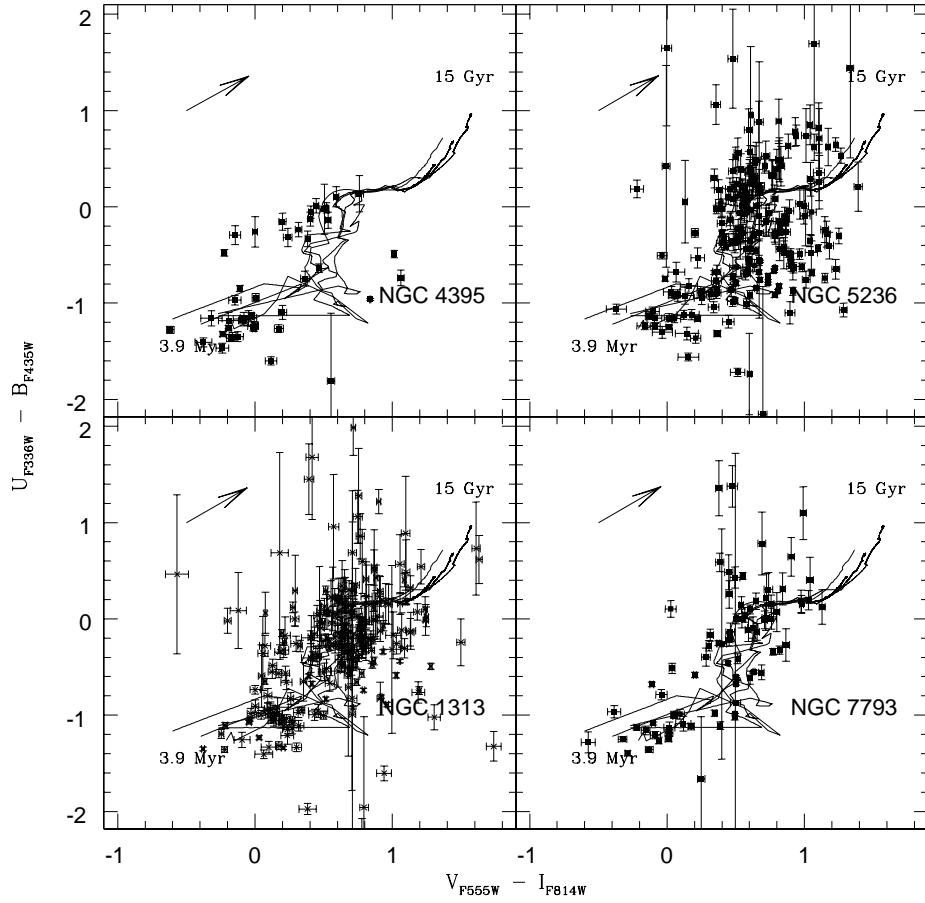


Figure 3.5: colour–colour diagrams of the young star cluster candidates in NGC 1313, NGC 4395, NGC 5236, and NGC 7793. The arrow in each plot represents the extinction correction of $A_V = 1.0$. The plotted tracks correspond to GALEV and Girardi Simple Stellar Population models for ages from 3.9 Myr up to 15 Gyr. Objects above the tracks are objects with large error in the U_{F336W} band. Also objects with small sizes and small masses (see the last paragraph of section 3.5.4).

- In the case of NGC 4395 star clusters are seen in two groups, one at $U_{F336W} - B_{F435W} \sim -1$ (corresponding to $\sim 3.9 - 10$ Myr) and the other at $U_{F336W} - B_{F435W} = 0$ (corresponding to $\sim 3 \times 10^8$ yr). According to the position of the clusters and the model track there are no clusters older than 10^9 yr.

- In the case of NGC 7793, star clusters are seen along the model tracks uniformly distributed. NGC 7793 does not show clusters redder than $V_{F555W} - I_{F814W} > 1.2$.

- NGC 5236, as well as NGC 1313, show star clusters concentrated at intermediate ages, mostly around 100 Myr ($V_{F555W} - I_{F814W} \sim 0.6$). Several star clusters are seen

below the model tracks (at $V_{F555W} - I_{F814W} > 1.0$), consistent with being reddened, very young star clusters.

- NGC 1313 shows a minor concentration of intermediate age clusters at $V_{F555W} - I_{F814W} \sim 0.2$ and $U_{F336W} - B_{F435W} \sim -1.0$.

3.5 Ages, masses and sizes

3.5.1 Fitting ages, masses and internal extinction simultaneously

In this section, we discuss in more details the ages, masses, the process of deriving them, and the sizes of the star clusters.

One of the main problems in deriving ages and masses is the uncertainty of the internal extinction toward the individual star clusters. This makes it impossible to compare directly observed star cluster colours and magnitudes with SSP models. This can be solved using a method known as “3D fitting” (Bik et al. 2003). The method relies on Simple Stellar Populations (SSP) models (broad band colours as a function of age for fixed metallicities) and compares model colours with the observed ones, searching for the best fitting extinction and age for each star cluster, using a minimum χ^2 criteria. Masses are derived using the mass-to-light ratios predicted by the models in combination with the reddening-corrected observed magnitudes and an assumed distance modulus. The extinction toward individual clusters was fitted in steps of $E(B - V) = 0.01$ introducing some discretisation in the ages and masses.

Two different SSP models were used for comparison: the GALEV (Anders & Fritzev. Alvensleben 2003) and the Girardi (private communication) models.⁵ The GALEV models are based on the SSP models of Schulz et al. (2002) including gaseous continuum and line emission assuming a Salpeter or Scalo IMF (in this work we used only the Salpeter IMF). The models have an age range from 3.98 Myr up to 15.9 Gyr for all the metallicities ranging from $Z=0.0004$ to $Z=0.05$. The Girardi SSP models are based on a combination of stellar evolutionary tracks from Girardi et al. (2000) (low and intermediate-mass stars), Bertelli et al. (1994) and Girardi et al. (1996), all including convective overshooting and assuming radiative opacities from Iglesias et al. (1992). Girardi models have an age range from 3.98 Myr up to 17.7 Gyr for the metallicities $Z=0.004$ and $Z=0.019$; and an age range from 63 Myr up to 17.7 Gyr for the metallicities $Z=0.001$ and $Z=0.03$.

In Fig. 3.6 we plot the derived cluster masses against cluster ages for our five galaxies, as function of four different metallicities from the GALEV and the Girardi models, respectively. The discrete extinction and age grids create stripes and gaps at fixed ages (see also Bik et al. 2003; Bastian et al. 2005a; Gieles et al. 2005; Fall et al. 2005; Whitmore et al. 2007, and others).

In the case of the Girardi models with $Z=0.001$ and $Z=0.03$ a concentration of clusters in one or two bins around 63 Myr is seen in all galaxies. This artifact is due to the fact that most of these piled clusters have ages younger than the ages provided by the model

⁵http://pleiadi.pd.astro.it/isoc_photsys.02/isoc_acs_hrc/index.html

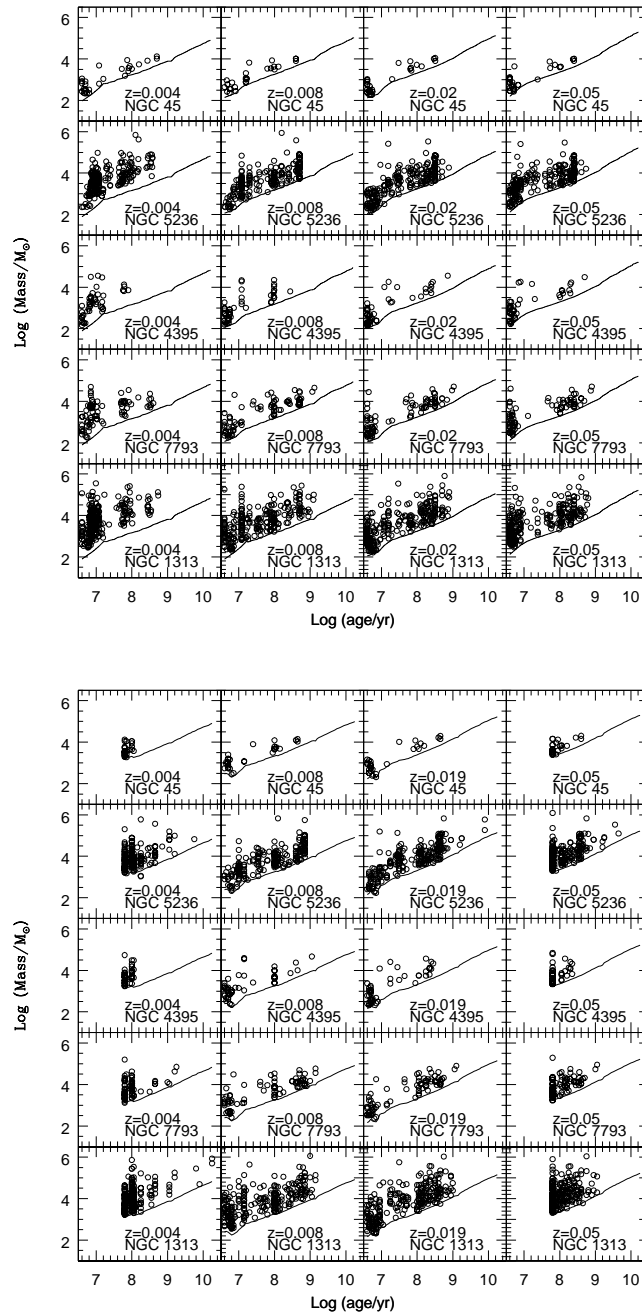


Figure 3.6: Mass as a function of cluster age as derived using four fixed metallicities. Top: GALEV models. Bottom: Girardi models. See text for details.

and the method assigned the youngest available age on the model. Star clusters with ages older than 1 Gyr are not seen in any metallicities except for $Z=0.019$ from Girardi

Table 3.4: Median internal extinction $E(B-V)$ towards the star clusters.

Galaxy	E(B-V)	E(B-V)	E(B-V)	E(B-V)
	pointing 1	pointing 2	pointing 3	all fields
NGC 1313	0.15	0.15	0.14	0.15
NGC 4395	0.00	0.00	-	0.00
NGC 5236	0.10	0.08	-	0.08
NGC 7793	0.00	0.00	-	0.00

where two clusters are seen at almost 10 Gyr. Excluding Girardi models for $Z=0.001$ and $Z=0.03$, we observe in NGC 5236 and NGC 1313 that the star clusters are distributed more uniformly across the ages with respect to the three other galaxies.

The Girardi and GALEV SSP models have two metallicities in common: $Z=0.004$ and $Z=0.02/0.019$. A comparison of the results from these show that they agree well in age and mass derivations. The main difference are the gap sizes which are wider for the Girardi than for the GALEV models, and the older clusters found in NGC 5236 for $Z=0.019$ which are not seen for $Z=0.02$ GALEV.

We found 6 star clusters with masses greater than $10^5 M_{\odot}$: 4 in NGC 1313 and 2 in NGC 5236. Among the 4 star clusters in NGC 1313, three are in common with Larsen (1999): ID: n1313-379, n1313-275 and, n1313-780 which correspond in this work to the object ID= NGC1313_3_7, NGC1313_2_50 and, NGC1313_1_4 respectively. The other object is ID=NGC1313_2_39. One of the two massive star clusters in NGC 5236, (the object ID= NGC5236_1_4) is probably contaminated by a neighbour and might not be as massive as derived, nevertheless, and for completeness, this object is listed in the Table 3.11. The other object is the object ID=NGC5236_2_82.

3.5.2 Internal extinction

As mentioned above, the 3D fit code returns the extinction internal to the galaxy toward the individual clusters. In Table 3.4 we show the median internal extinction for the star clusters for each pointing and the total median extinction in a given galaxy.

Clearly, towards the detected clusters, the internal extinction is low with very little variations between pointings in a galaxy: median $E(B - V) = 0$ for NGC 4395 and NGC 7793, and median $E(B - V) = 0.1 - 0.15$ for NGC 1313 and NGC 5236.

These median extinction values explain why in NGC 4395 and NGC 7793 no objects are located below the model tracks in the colour-colour diagrams, while in NGC 1313 and NGC 5236 some objects are (see Fig.3.5).

We note that far less clusters are detected in NGC 4395 and NGC 7793 than in the two other galaxies. If this was due to extinction, the median extinction would be at least as high as in the two other galaxies. Thus, we rather interpret this as a physical effect: the small number of clusters may be due to low overall star-formation rates and gas densities in these galaxies, which in turn implies a low amount of dust, i.e. extinction.

3.5.3 Cumulative age distributions

We compare the star-cluster age distributions in the different galaxies by comparing their cumulative age distributions. We summed the clusters from old to young, the ages for a single case being derived using a fixed metallicity and given model.

First, we examine whether the star-cluster formation history is a local process or can be averaged over an entire galaxy. In Fig. 3.7, we show for each galaxy the cumulative distribution for each pointing, and note that the cluster formation history varies more from galaxy to galaxy than spatially inside a given galaxy. Keeping in mind that some variations exist inside a given galaxy, we nevertheless feel confident to average over an entire galaxy and compare the star-cluster formation histories between galaxies.

Second, we examine the influence of our assumed fixed metallicity on the formation histories as represented by our cumulative age distributions. From literature work (see Table 3.2) we know the galaxies *not* to share the same metallicity. In Fig. 3.8, we assume the same metallicity for each galaxy, derive the ages (using a GALEV model in that case) and compare the cumulative distribution. Clearly, the assumed metallicity influences the shape of the cumulative distribution but does not remove any general trend that might be present (e.g. NGC 4395 shows for all assumed metallicity a sharp rise at young ages, NGC 5236 shows a much steadier increase in all cases).

Finally, we verify that the model used to derive the ages does not significantly affect the shape of the cumulative age distribution (see Fig. 3.9 top panels) and show the overall comparison between the cumulative age distributions of the five galaxy in Fig. 3.9, bottom panel. Indeed, the cumulative distributions using ages derived from the Girardi model do not significantly differ from the ones using ages derived by the GALEV models.

For the final comparison (Fig. 3.9, bottom panel) we assigned to each galaxy the metallicity as found in the literature. The cumulative age distributions clearly differ. We quantified this by running Kolmogorov-Smyrnov tests (K-S tests) between the distributions (testing for single maximal deviations). All K-S tests returned D values greater than 0.2 and P values near 0, indicating that the distributions differ significantly.

Qualitatively, NGC 1313 and NGC 5326 show a steadier rise of the cumulative distribution, indicating a more continuous cluster formation history. Taken together with the significantly higher number of young star clusters found in these two galaxy when compared to the three others, indicates that they maintained a steadily high star-cluster formation over the last few hundred Myr. This in turn could explain the higher median extinction (due to the presence of more gas and dust).

The three other galaxies (NGC 45, NGC 4395 and NGC 7793) are characterised by shallower distributions, with a clear rise at very young ages (tens of Myr). Together with the lower number of clusters detected, this lead to the interpretation that the young star-cluster population in these galaxies is dominated by a recent increase in the star-formation activity. However, we note that the age distributions will also be affected by possibly different disruption time-scales in the different galaxies (see Sect. 3.7).

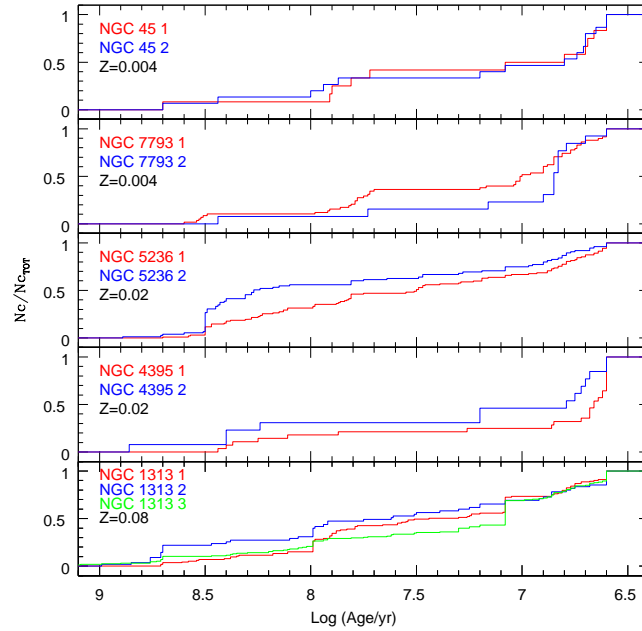


Figure 3.7: Normalized cumulative star-cluster age distributions for each pointing in each galaxy. Ages were derived here using the GALEV models and a fixed metallicity per galaxy. Variations in the cumulative distribution are larger from galaxy to galaxy than inside a given galaxy.

3.5.4 Sizes

The size distributions for the young star cluster candidates were derived in Sect. 3.2.2 and the median sizes for each galaxy are shown in Table 3.5.

We note that sizes derived in this work are slightly smaller than in Larsen (2004a). The reason for this is likely the fact that in our sample we include star clusters with masses lower than $1000 M_{\odot}$, while in Larsen (2004a) the mean sizes were derived for star clusters with masses greater than $1000 M_{\odot}$.

Also, the size distribution might be partly influenced by the completeness criteria, as the most extended objects are rejected and the size distribution gets slightly biased towards smaller sizes. For example: of the artificial star clusters created in NGC 7793 with a magnitude $V_{F555W} = 20 \sim 30\%$ with FWHM=1.8 pixels were not recovered, while only $\sim 5\%$ of the objects with FWHM=0.5 pixels were not detected.

Yet, the slight biases do not prevent the investigation of any relation between size and mass. In similar previous studies (e.g. Bastian et al. 2005b; Larsen 2004a), the relation between sizes and masses for young star clusters was already investigated, and a slight trend for more massive star cluster to be more extended was found. We considered the masses derived assuming the metallicities from Table 3.2.

Figure 3.10 shows the young star cluster candidate sizes plotted against the masses.

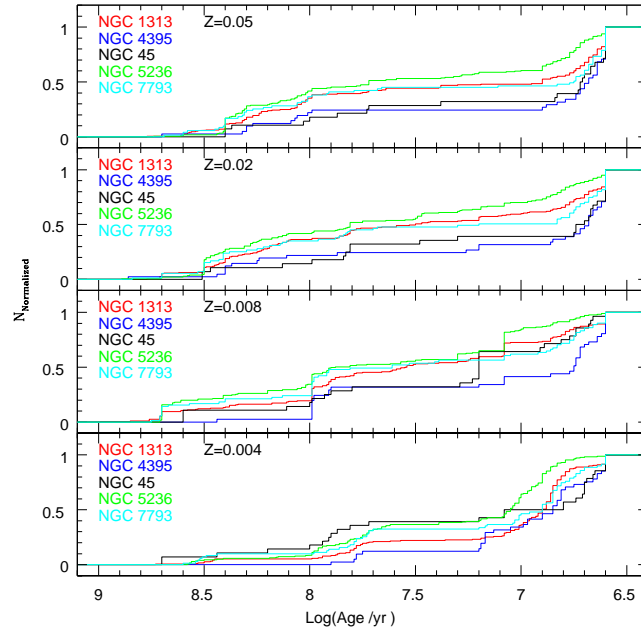


Figure 3.8: Left: Normalized cumulative cluster distributions according to GALEV. Right: The top and the middle panel correspond to the normalized cumulative cluster distribution for Girardi models. In the bottom, the normalized distributions for all the galaxies considering the closest metallicities from the literature.

A function of the form:

$$R_{eff} = a \times (M/M_{\odot})^b \quad (3.2)$$

was applied for each galaxy and the values obtained from the minimum χ^2 fitting are shown in Table 3.6.

Table 3.5: Young star cluster median effective radii.

(1) Galaxy	(2) $R_{eff}V$ <i>pc</i>	(3) $R_{eff}B$ <i>pc</i>	(4) $R_{eff}I$ <i>pc</i>	(5) < R_{eff} > <i>pc</i>
NGC 45 ¹	2.0	1.7	2.9	2.2 ± 0.4
NGC 1313	2.71	2.48	2.70	2.63 ± 0.07
NGC 4395	1.85	1.52	2.07	1.81 ± 0.15
NGC 5236	1.94	1.63	2.09	1.88 ± 0.13
NGC 7793	1.97	1.62	2.18	1.92 ± 0.16

¹ Mora et al. (2007)

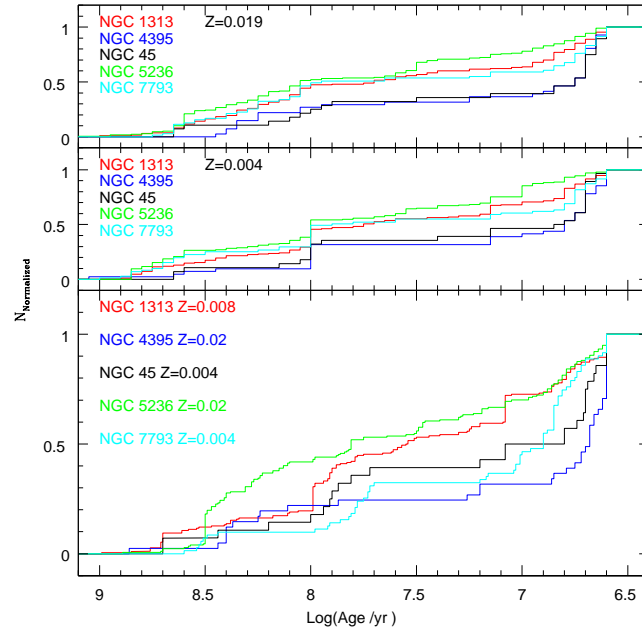


Figure 3.9: Left: Normalized cumulative cluster distributions according to GALEV. Right: The top and the middle panel correspond to the normalized cumulative cluster distribution for Girardi models. In the bottom, the normalized distributions for all the galaxies considering the closest metallicities from the literature.

Table 3.6: Size coefficients.

(1) Galaxy name. (2),(3) “a” and “b” are the derived values from Eq. 3.2. (4) Metallicity used for the derived mass in the Eq. 3.2.

(1) Galaxy	(2) a	(3) b	(4) Z
NGC 45	0.17 ± 0.13	0.34 ± 0.09	0.004
NGC 1313	0.4 ± 0.1	0.25 ± 0.03	0.008
NGC 4395	0.23 ± 0.16	0.29 ± 0.07	0.02
NGC 5236	0.33 ± 0.05	0.21 ± 0.01	0.02
NGC 7793	0.54 ± 0.07	0.16 ± 0.01	0.004

As in previous studies, we observe in all galaxies a slight trend for the more massive objects to be more extended in all galaxies. A physical interpretation could be that massive star clusters form in higher pressure environment than the lower mass ones, which also form less bound and, therefore are more affected by the disruption than higher-mass

counterparts.

From Table 3.5 all galaxies share similar mean effective radii of the star clusters, except NGC 1313 where the mean effective radius is higher (see also Fig. 3.10), due to the fact that above $1000 M_{\odot}$ the range of sizes at a given mass is significantly broader than in the other galaxies.

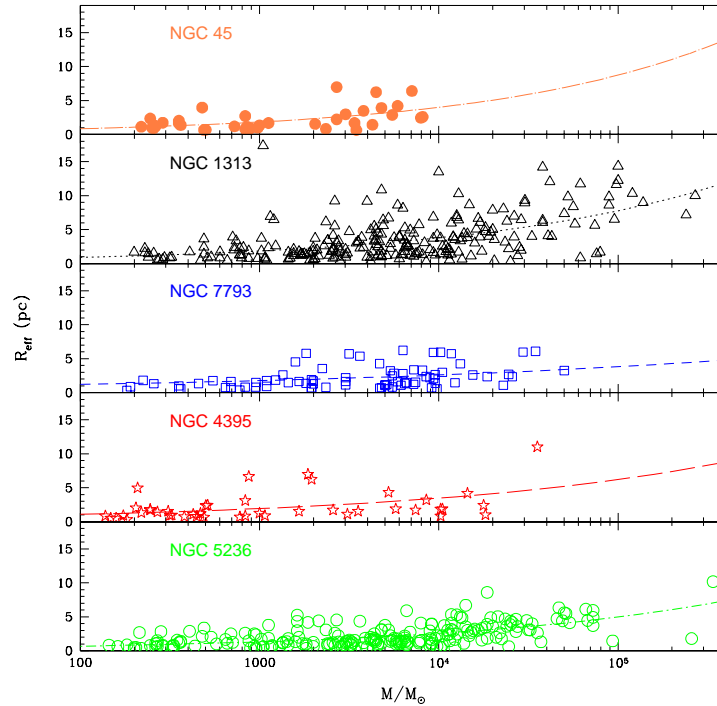


Figure 3.10: Effective radius versus mass of young star clusters. The lines correspond to fits of the form $R_{eff} = a \times M/M_{\odot}^b$.

We note also that the slopes of the power-law fits are significantly steeper than the values (~ 0.10) reported in previous studies. This might be partly due to the different mass range probed here. However, we caution that the reliability of the size measurements may be questionable for the lowest-mass clusters, whose luminosity profiles tend to be dominated by a few individual stars. Therefore, the importance of stochastic effects on the size determinations at low mass needs to be taken into account and further investigated.

3.6 Luminosity functions

The star cluster luminosity functions for four of our five galaxies are shown in Fig. 3.11. The one for NGC 45 was presented in Mora et al. (2007). Data were corrected with the completeness function calculated for an object of $\text{FWHM} = 1.2$ pixels. Each histogram was fitted by minimum χ^2 with a relation of the form:

Table 3.7: Luminosity function coefficients. (1) Galaxy name, (2), (3) a and b coefficient from Eq. 3.3, (4) α slope of the luminosity function, (5) expected V_{F555W} magnitude of the brightest star cluster from the extrapolation of the luminosity function, (6),(7),(8) V mean, V median, and σ of the brightest star cluster from the simulated luminosity functions. (9) Observed V_{F555W} magnitude of the brightest cluster. (10),(11) Mass and age of the observed brightest star cluster in M_{\odot} and yr respectively. (12) Metallicity used for mass and age derivations.

(1) Galaxy	(2) a	(3) b	(4) α	(5) V_{exp}	(6) M_v^{mean}	(7) M_v^{median}	(8) σ_{stoch}	(9) V_{obs}	(10) log Mass	(11) log Age	(12) Z
NGC 45 ¹	0.37±0.11	-7.89 ±0.37	-1.93±0.3	20.79±2.29	18.63	18.93	1.57	20.697	2.97	6.66	0.004
NGC 1313	0.43±0.04	-8.28 ±0.87	-2.08±0.1	19.13±1.14	17.08	17.26	1.15	15.856	5.22	6.60	0.008
NGC 4395	0.29±0.01	-5.69 ±1.7	-1.72±0.2	19.59±5.28	16.43	16.74	1.93	19.541	3.97	7.08	0.02
NGC 5236	0.55±0.04	-10.61±0.92	-2.38±0.11	19.22±1.06	18.02	18.21	1.01	18.062	4.72	7.39	0.02
NGC 7793	0.40±0.05	-7.60 ±1.25	-1.99±0.13	19.41±2.13	17.01	17.24	1.49	18.190	4.66	7.64	0.004

¹ from Mora et al. (2007)

$$\log N = aM_B + b \quad (3.3)$$

The slope a was then converted to the slope of the luminosity function, represented as a power-law $dN(L_B)/dL_B = \beta L_B^\alpha$, using $\alpha = -(2.5a+1)$. All fitting results are summarised in Table 3.7.

The luminosity slopes derived for NGC 1313 and NGC 5236 are in agreement with the values derived in Larsen (2002): $\alpha_{1313} = -2.01 \pm 0.12$ and $\alpha_{5236} = 2.25 \pm 0.12$; the slightly steeper slope in NGC 5236 seems to be confirmed by our study. Overall, we find luminosity slopes compatible with $\alpha \sim -2$, in agreement with the values reported in the literature for the young star cluster systems.

We further compared the expected magnitude of the brightest clusters as predicted from the luminosity functions with the actual observed values. Such a comparison indicates whether a special physical mechanism is required for the formation of the brightest clusters, or whether they can be explained simply by the size of the sample.

We simulated 1000 times each galaxy luminosity function considering the observed number of star clusters with magnitudes randomly selected up to $M_v = -5.1$, the observational cut-off magnitude of the sample. The results are summarised in Table 3.7.

For all galaxies we found a good agreement within the errors between the observed and the expected brightest cluster. NGC 1313 presents an exception, as the observed value is ~ 3 magnitudes ($\sim 3\sigma$) brighter than the prediction. We conclude that generally the brightest star clusters in the luminosity function are dictated by size-of-sample effects (Hunter et al. 2003) and correspond to a stochastic sampling of the luminosity function (see Larsen 2002). However, some galaxies seem to produce brighter star clusters – in that respect we note that NGC 1313 also showed clusters of larger average sizes. Although a connection is not demonstrated here, it might be an interesting aspect to investigate further. It should be noted that a physical truncation of the cluster *mass* function might still exist, even if the luminosity function is limited by size-of-sample effects. One signature

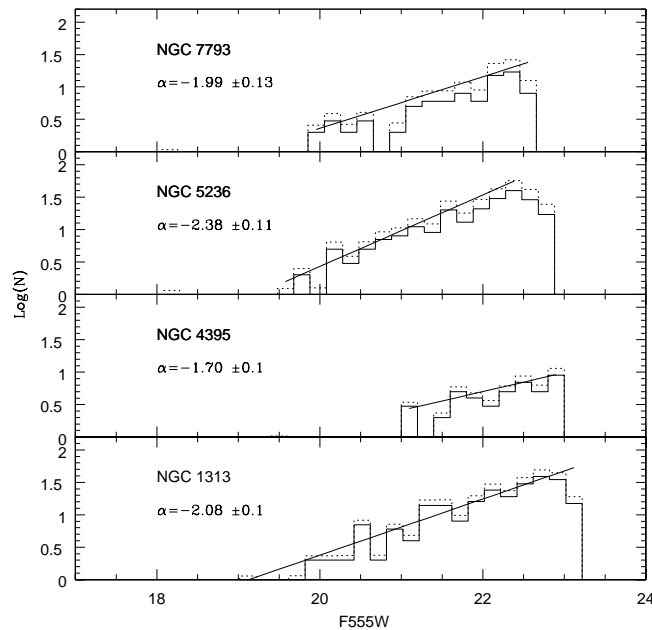


Figure 3.11: Luminosity functions for our galaxy sample. Solid histograms are the uncorrected luminosity functions while the dashed histograms are the completeness corrected luminosity functions. Straight lines represent the power-law fit of the form $dN(L)/dL \propto L^\alpha$ to the corrected histograms.

of such a physical limit to the MF is a steepening of the LF at the bright end (Gieles et al. 2006a), as hinted at in the case of NGC 5236.

3.7 Cluster disruption

In following section, we investigate the disruption time scales of the clusters. We adopt the simplified description of cluster disruption developed by Boutloukos & Lamers (2003), and thus assume that the “disruption time scale” t_{dis} of a cluster with initial mass M can be parametrized as

$$t_{\text{dis}}(M) = t_4^{\text{dis}} (M/10^4 M_\odot)^\gamma, \quad (3.4)$$

where t_4^{dis} is the disruption time of a $10^4 M_\odot$ cluster. The constant γ was found by Boutloukos & Lamers (2003) to have a value close to 0.6 (see also Lamers et al. (2004, 2005a,b)).

Boutloukos & Lamers (2003) defined this in an empirical way, assuming that clusters are formed in a constant number per unit time within a certain mass range, and with a fixed cluster initial mass function in the form of a power-law. Under these assumptions, the number of clusters per age interval, which are detected above a certain fixed magnitude

limit, will depend only on the fading due to stellar evolution, as long as there is no cluster disruption. As soon as cluster disruption becomes significant, this behavior is broken and the number of clusters decreases more rapidly with time.

Considering Eqs. 15 and 16 from [Boutloukos & Lamers \(2003\)](#) the time scale on which cluster disruption is important can be derived from either the cluster age or mass distributions:

$$\log\left(\frac{t_{\text{cross}}}{10^8}\right) = \frac{1}{1 - \gamma\zeta} \left[\log\left(\frac{t_4^{\text{dis}}}{10^8}\right) + 0.4\gamma(m_{\text{ref}} - V_{\text{lim}}) \right] \quad (3.5)$$

$$\log\left(\frac{M_{\text{cross}}}{10^4}\right) = \frac{1}{1 - \gamma\zeta} \left[\zeta \log\left(\frac{t_4^{\text{dis}}}{10^8}\right) + 0.4(m_{\text{ref}} - V_{\text{lim}}) \right] \quad (3.6)$$

In these equations, V_{lim} is the cluster detection limit and m_{ref} is the apparent magnitude of a cluster with an initial mass of $10^4 M_{\odot}$ at an age of 10^8 years, the subscript ‘‘cross’’ denotes the breaking point between the cluster fading and the cluster disruption and ζ gives the rate of fading due to stellar evolution. These quantities are related each other by the following equation:

$$\log(M_{\text{cross}}/10^4) = 0.4(m_{\text{ref}} - V_{\text{lim}}) + \zeta \log(t_{\text{cross}}/10^8) \quad (3.7)$$

The scenario described above makes no distinction between cluster disruption due to interaction with the interstellar medium, bulge/disk shocks, internal events such as two-body relaxation, and assumes that a single ‘‘disruption time-scale’’ applies. Furthermore, this formulation does not account for the apparently mass-independent loss of very young objects, sometimes dubbed ‘‘infant mortality’’ (e.g. [Fall et al. 2005](#)). This process is believed to operate mostly within the first few 10^7 years.

In [Fig. 3.12](#) we plot the age distributions for the star clusters in our galaxy sample limited by a magnitude cut of $V_{F555W} = -5.1$. Several bin widths were tried but none revealed any obvious breaks in the age distributions. Thus, we selected an intermediate bin width of $\Delta \log t = 0.35$. We then fitted straight lines of the form $\log\left(\frac{dN}{dt}\right) = a \times \log t + b$, and found slopes in the range $-1.22 > a > -1.43$.

The derived values are inconsistent with the expected slope value (~ -0.7) for a cluster age distribution which assumes no star cluster dissolution and limited by a V-band magnitude (see [Gieles et al. 2007b](#)). For U-band limited magnitude samples the slopes are expected to be ~ -1 . Also, in the above described scenario, and assuming $\gamma = 0.62$ and $\alpha = -2$, the values are somewhat shallower than the disruption slope for a V-band limited sample, which is expected to be ~ -1.6 .

As it was shown in [Lamers et al. \(2005a\)](#), the process of fading and star cluster disruption is not a process on which the break between this two stages suddenly occurs, it is a continuous process which gradually goes from the fading of the cluster regime up to the cluster disruption regime, and an approximation of straight lines (one for each regime) is valid when these two regimes are well defined. Therefore, it is not surprising that the derived values are in between these two regimes because the disruption regime may be present, but it is impossible to disentangle it from the fading regime, probably as consequence of using a magnitude-limited sample, as well as of the fact that older objects

(which are more likely to be affected by disruption) get redder and end up below our limit detection.

An additional disruption mechanism has been discussed by Whitmore et al. (2007). From observations of young star clusters in the Antennae galaxy, these authors find evidence for a constant fraction (about 90%) of the clusters being lost per unit logarithmic age interval up to at least 10^8 years. This mass-independent disruption has been named “infant mortality”. For a *mass-limited* sample, this results in an age distribution with a logarithmic slope of $a = \log(1 - \text{IMR})$, i.e. $a = -1$ for an “infant mortality” rate of 90%. However, for a *magnitude-limited* sample we would expect a slope of $a = -1.65$ (for $\text{IMR} = 90\%$ and a V-band limited sample), significantly steeper than our observed values. Our observed slopes of -1.22 to -1.44 would require infant mortality rates of less than 75% – 85% for ages up to 1 Gyr.

In summary, the slopes of our cluster age distributions are too steep to be explained by fading alone, but our data do not allow us to clearly distinguish between the relative importance of mass-dependent and mass-independent disruption.

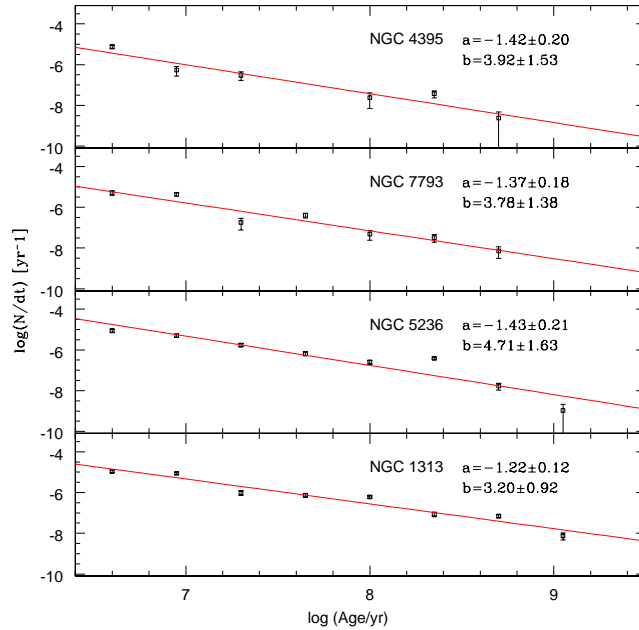


Figure 3.12: The age distributions for our galaxy sample. Lines correspond to the best fitting of the form $\log\left(\frac{dN}{dt}\right) = a \times \log t + b$.

3.8 Radial distributions

In the following section, we discuss the radial distribution of the young star clusters in four galaxies (NGC 45 being presented in Mora et al. (2007)). Since our images do cover

the galaxies asymmetrically, a spatial completeness correction first needed to be computed.

3.8.1 Spatial completeness correction

We evaluated the spatial completeness as a function of radius by using concentric circles (centred on the galaxy) with increasing radius in steps of $50''$ until the entire ACS FOV was enclosed the largest circle. For each ring, we computed the fraction covered by the ACS field of view. Each star cluster was assigned to a ring and to the corresponding spatial completeness correction.

3.8.2 Radial distribution of the surface density

In Fig. 3.13 we plot the completeness-corrected surface density of star clusters as a function of radius, as well as the completeness as function of the radius (solid lines).

For three galaxies the centre was covered by the ACS images (i.e. a 100% completeness was reached in the center of the galaxy). For NGC 5236 the pointing did not cover the central part of the galaxy. Further, note that the bumpy shapes of the completeness lines are due to the different ACS orientations for each pointing. For each galaxy, we evaluated the completeness-corrected radial surface densities profile over nine bins. The bins were defined from the centre outwards to the most distant cluster in our sample.

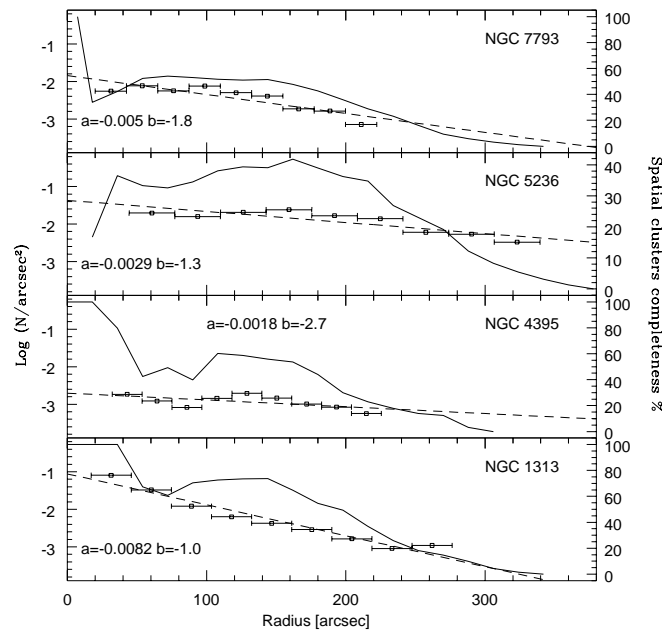


Figure 3.13: Radial surface density profiles of the star clusters, corrected for completeness. Solid lines show the spatial completeness correction (in percent) described in sec. 3.8.1. Dashed lines show the power-law fits to the profiles.

Table 3.8: Derived values from Eq. 3.8

(1) Galaxy names. (2), (3) “a” and “b” are the derived constant values, (4) e-folding distance in arcsecond

(1) Galaxy	(2) a	(3) b	(4) e – folding
NGC 1313	-0.0082 ± 0.0007	-1.0 ± 0.1	53 ± 5
NGC 4395	-0.0018 ± 0.0009	-2.7 ± 0.1	241 ± 120
NGC 5236	-0.0029 ± 0.0006	-1.3 ± 0.1	150 ± 31
NGC 7793	-0.005 ± 0.001	-1.8 ± 0.1	87 ± 17

For a qualitative comparison between the galaxies, we fitted to each completeness-corrected radial surface density profile (distance being linear, surface density being logarithmic) a line of the form:

$$\log N = aR + b \quad (3.8)$$

The results of the fits are listed in Table 3.8.2. We notice that the surface density profiles for young star cluster span a very wide range in our sampled galaxies: from almost no radial dependence in NGC 5236 and NGC 4395 (i.e. homogeneous formation of star clusters with radius), to very concentrated distribution in NGC 7793 and in particular in NGC 1313. In the latter, the surface density increases by two orders of magnitude towards the centre over the inner ~ 5 kpc.

3.9 Globular clusters

We discussed above the more prominent young star clusters, but briefly described in this section the old globular clusters found in the sample galaxies.

As mentioned in Sec.3.3.2, we considered globular cluster candidates to be objects with $V < V_{TO} - 0.2$ and colours $(B_{F435W} - V_{F555W})_0 > 0.5$.

3.9.1 Total number of globular clusters

In order to derive the total number of globular clusters in our covered area (inner 6-8 kpc), we took into account the detection completeness affecting our sample as well as the spatial incompleteness. For the detection completeness, we used the values derived in section 3.2.3. For the spatial completeness correction we used the method described in section 3.8.1.

We then extrapolated the total number of globular clusters over the full globular cluster luminosity function. We assumed that the globular cluster luminosity function in our galaxies follows the “universal” Gaussian shape and, following Jordán et al. (2006), that the Gaussian dispersion is described by the following relation:

$$\sigma = (1.12 \pm 0.01) - (0.093 \pm 0.006)(M_{B,gal} + 20) \quad (3.9)$$

Given the small number of observed objects (0 to 8) the extrapolation is necessarily uncertain. The evaluated approximate uncertainties take into account the errors in the dispersion, the magnitude of faintest globular cluster candidate with respect to the luminosity function turnover (indicating the fraction of the total area of the Gaussian that we observed), as well as the error in the globular cluster luminosity function turnover given the known distance. We maximised and minimised these (1σ) errors to derive the uncertain span in our evaluation. Our expected total numbers of globular clusters are tabulated in Table 3.9.

Specific frequencies

Harris & van den Bergh (1981) defined the specific frequency as

$$S = N_{GC} 10^{0.4 \times (M_V + 15)} \quad (3.10)$$

where N_{GC} is the total number of globular clusters that belong to the galaxy and M_V is the absolute visual magnitude of the galaxy.

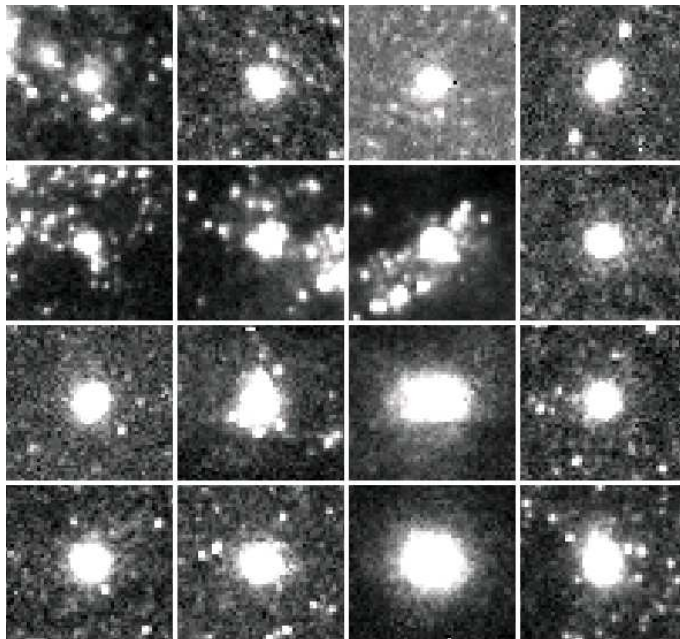


Figure 3.14: Stamps of all the globular cluster candidates detected in our sample. First row: NGC 1313, second and third row: NGC 5236, and fourth row: NGC 7793.

As mentioned above for the total number of globular clusters: due to the small number of candidates detected, the specific frequencies are inevitably subject to large uncertainties. Our derived values are given in Table 3.9.

Table 3.9: Total numbers of globular clusters and specific frequencies in the observed region

(1) Galaxy name. (2) The observed number of globular clusters candidates (for stamps of the globular cluster candidates see Fig. 3.14), (3) σ derived from Eq.3.9, (4,5) Maximum, minimum number of globular clusters derived by maximising/minimizing all assumption, (6) Average of the faintest and the brightest globular cluster luminosity turnover, the error reproduces the minimum of maximum number of clusters. (7) Derived specific frequency. *Note that all values are given for the observed regions, i.e. the inner 6-8 kpc of the galaxies.*

(1) <i>Galaxy</i>	(2) n_{GC}	(3) σ	(4) N_{GC}^{bright}	(5) N_{GC}^{faint}	(6) N_{TOT}	(7) S_N
NGC 1313	4	1.03 ± 0.04	3	11	7 ± 4	0.1 ± 0.1
NGC 5236	8	1.15 ± 0.02	31	55	43 ± 12	0.27 ± 0.14
NGC 7793	4	0.93 ± 0.02	12	22	17 ± 5	0.63 ± 0.36

In order to compare these values with *global* values as found in the literature (e.g. Harris 1991), we would need to estimate the total number of globular clusters not only in the observed region but over the whole galaxy. In principle, we could use the surface density profiles and extrapolate them to large radii, but have no indication out to which radii these would hold. Instead, as a rough estimate, we consider the Milky Way, a late-type galaxy in the luminosity range of our sample, that hosts about a third to half of its globular clusters in the inner 6 to 8 kpc. Thus, global specific frequencies for our galaxies might be two to three times larger than derived for the inner regions.

The specific frequencies listed Table 3.9 lie well below 1, i.e. in the range of low specific frequencies. Even if these were doubled or tripled to reflect global values, they would be in the range 0.5 to 1 as expected for late-type galaxies (see Harris 1991). For NGC 5236, Chandar et al. (2004) derived in a previous study S_N of 0.6 ± 0.1 , about twice our inner value, in good agreement with our estimate for the global value.

We conclude that the (low) number of globular clusters observed lies within the expectations for the type of galaxies in our sample.

Globular cluster sizes

From ISHAPE measurements (see Sect. 3.2.2) we calculated the mean effective radii of the globular cluster candidates. The values are shown in Table 3.10. Our values are slighter larger than the average half-light radius found in the ACS Virgo Cluster Survey (Jordán et al. 2005), but in good agreement with the median size (~ 3.2 pc) of the Milky Way globular clusters.

Note that within the errors, the globular cluster (as opposed to the young star clusters) in NGC 1313 do not display abnormal sizes.

Table 3.10: Red star cluster mean effective radii.

(1)	(2)	(3)	(4)	(5)
Galaxy	$R_{\text{eff}} B$	$R_{\text{eff}} V$	$R_{\text{eff}} I$	$\langle R_{\text{eff}} \rangle$
	pc	pc	pc	pc
NGC 1313	3.03	3.39	3.56	3.32 ± 0.15
NGC 5236	3.15	2.99	2.88	3.01 ± 0.08
NGC 7793	2.98	3.07	2.98	3.01 ± 0.03

3.10 Summary and discussion

We have analysed the star cluster populations in five nearby spiral galaxies. Candidates were selected applying a size criterion. Ages and masses were derived from broad band colours and compared with SSP models. Thanks to the excellent ACS resolution we were able to observe compact young star clusters down to masses of the order of $200 M_{\odot}$.

The properties of the young star clusters show considerable diversity. The star cluster formation history shows galaxies forming young star clusters rather homogeneously over the last Gyr, as well as galaxies with increased cluster formation activity on short periods. The galaxies with a rather continuous star cluster formation show a higher number of young star clusters (by almost an order of magnitude) than the ones forming star clusters in bursts. The specific frequency of old globular clusters appear to be normal (i.e. low) for these late-type spirals in our sample. In this respect, the four galaxies studied here contrast with the case of NGC 45 (Mora et al. 2007), in which we found an unusually high S_N for a late-type galaxy of 1.4 - 1.9.

We have tried to investigate the star cluster disruption. Fading alone is clearly ruled out, but we were not able to distinguish between mass-dependent and mass-independent disruption, i.e. characterise the exact disruption law.

The spatial distribution of star clusters also varies greatly in our galaxies. Some galaxies appear to form star clusters homogeneously over the 6-8 kpc probed in our study, while other show the young star cluster density to be (very) peak towards the galaxy centre.

The star cluster luminosity functions support earlier findings in the literature and are compatible with power-law distributions with a slope of around -2 . The brightest clusters are compatible with a random sampling of the luminosity function given the size of the samples. NGC 1313 presents an exception with the brightest star clusters being about three magnitudes brighter than expected.

In this regard, it is worth noticing that NGC 1313 also displays slightly large size (or a larger scatter in sizes) for its young star clusters, and has by far the most concentrated spatial distribution of star clusters. Potentially, another or additional star cluster formation process is at work in this galaxy.

Finally, we analysed the (small) population of globular cluster candidates in our galaxies and found it to be normal both in terms of number of objects and specific fre-

quencies, as well as in the sizes.

Acknowledgements:

We would like to thank H.J.G.L.M. Lamers for providing us the 3D code program and useful feedback. Nate Bastian and Mark Gieles for interesting comments about this work during the 12 Questions on Star and Massive Star Cluster Formation workshop, as well as B. Whitmore for his help on the CTE corrections.

Table 3. 11: Derived star cluster properties for all the galaxies (Sample).

ID	RA J2000	DEC J2000	x Pix	y Pix	B F435W	σ F435W	V F555W	σ F555W	I F814W	σ F814W	U F335W
σ F336W	FWHMB pix	FWHMB pix	FWHMV pix	FWHMI pix	$E(B-V)$ Z=0.004	$E(B-V)$ Z=0.008	$E(B-V)$ Z=0.02	$E(B-V)$ Z=0.05	$E(B-V)$ Z=0.004	$E(B-V)$ Z=0.019	$\log(\text{Age/yr})$ Z=0.004
$\log(\text{Age/yr})$ Z=0.008	$\log(\text{Age/yr})$ Z=0.02	$\log(\text{Age/yr})$ Z=0.05	$\log(\text{Age/yr})$ Z=0.004	$\log(\text{Age/yr})$ Z=0.019	$\log(M/M_{\odot})$ Z=0.004	$\log(M/M_{\odot})$ Z=0.008	$\log(M/M_{\odot})$ Z=0.02	$\log(M/M_{\odot})$ Z=0.05	$\log(M/M_{\odot})$ Z=0.004	$\log(M/M_{\odot})$ Z=0.019	
NGC1313_1_1	3:18:35.8632	-66:28:03.459	2429.980	757.311	21.418	0.010	21.405	0.011	21.364	0.012	20.258
0.032	19.080	1.300	1.210	1.430	0.000	0.000	0.000	0.180	0.300	0.120	6.950
6.850	6.770	6.700	6.700	6.750	3.410	2.860	2.770	3.100	3.400	3.010	
NGC1313_1_2	3:18:33.6487	-66:27:43.434	1951.000	794.048	21.362	0.009	21.093	0.008	20.307	0.006	21.168
0.053	5.080	2.030	1.780	1.320	0.000	0.150	0.170	0.190	0.120	0.210	6.900
8.280	8.160	8.020	8.400	8.150	4.290	4.370	4.350	4.340	4.450	4.500	
NGC1313_1_3	3:18:32.4677	-66:27:32.069	1683.567	807.000	22.647	0.023	22.439	0.020	21.890	0.017	22.209
0.107	5.690	1.590	1.230	1.100	0.000	0.200	0.140	0.090	0.220	0.090	6.860
7.660	7.830	7.990	7.800	8.100	3.390	3.440	3.510	3.600	3.650	3.710	
NGC1313_1_4	3:18:33.4053	-66:27:32.911	1752.953	717.063	21.153	0.013	20.853	0.010	20.279	0.011	21.333
0.060	13.750	6.660	6.410	7.220	0.000	0.130	0.210	0.220	0.070	0.280	7.940
8.610	8.340	8.230	8.850	8.350	5.110	5.080	5.040	5.030	5.230	5.260	
NGC1313_1_5	3:18:33.7834	-66:27:47.653	2032.560	821.021	21.407	0.013	21.159	0.011	20.542	0.010	21.244
0.053	11.010	4.170	3.850	4.550	0.000	0.160	0.210	0.230	0.130	0.240	7.570
8.180	8.090	7.990	8.300	8.100	4.360	4.460	4.530	4.550	4.550	4.670	
NGC1313_1_6	3:18:30.8600	-66:27:33.740	1619.000	991.545	22.467	0.021	22.168	0.018	21.229	0.011	22.039
0.099	14.570	4.570	4.500	6.480	0.440	0.650	0.490	0.630	0.600	0.530	7.050
7.080	7.200	6.970	7.000	7.250	4.240	4.100	4.000	4.090	3.980	4.210	
NGC1313_1_7	3:18:31.0300	-66:27:55.795	2014.263	1188.420	22.574	0.021	22.346	0.017	21.878	0.015	22.530
0.133	5.780	2.060	1.930	1.130	0.000	0.170	0.000	0.000	0.210	0.000	7.780
7.990	8.440	8.320	8.000	8.550	3.650	3.670	3.780	3.760	3.800	3.990	
NGC1313_1_8	3:18:31.8406	-66:28:10.642	2320.923	1248.120	22.161	0.016	22.078	0.015	21.969	0.017	21.212
0.059	3.270	0.540	0.730	0.730	0.000	0.170	0.240	0.350	0.320	0.350	6.770
6.770	6.680	6.620	6.750	6.650	2.730	2.710	2.710	2.910	3.020	2.970	
NGC1313_1_9	3:18:30.9189	-66:28:00.003	2081.302	1241.000	22.454	0.019	22.195	0.016	21.556	0.012	22.051
0.090	7.640	3.170	3.130	1.850	0.000	0.190	0.580	0.590	0.180	0.140	6.790
7.910	6.600	6.600	8.000	8.050	3.190	3.840	3.300	3.380	3.950	3.980	
NGC1313_1_10	3:18:34.0503	-66:28:42.311	3003.000	1325.275	22.000	0.017	22.100	0.016	22.076	0.019	20.562
0.035	3.500	0.760	0.460	5.220	0.060	0.160	0.020	0.160	0.220	0.020	7.080
7.080	7.200	6.900	7.150	6.950	3.330	3.190	3.110	3.120	3.450	2.950	

First row: 1.- Galaxy ID: Name_Field_N. 2.- RA (J2000). 3.- DEC (J2000). 4.- X (pix). 5.- Y (pix). 6.- B_{F435W} . 7.- Error of B_{F435W} photometry. 8.- Same as 6 but for V_{F555W} . 9.- Same as 7 but for V_{F555W} . 10.- Same as 6 but for I_{F814W} . 11 Same as 7 but for I_{F814W} . 12.- Same as 6 but for U_{F336W} . Second row: 1.- Error of U_{F336W} photometry. 2.- $FWHM_B$ according to SExtractor. 3.- $FWHM_B$ according to Ishape. 4.- $FWHM_V$ according to Ishape. 5.- $FWHM_I$ according to Ishape. 6.- Extinction derived using GALEV considering $Z = 0.004$. 7.- Same as 6 but for $Z = 0.008$. 8.- Same as 6 but for $Z = 0.02$. 9.- Same as 6 but for $Z = 0.05$. 10.- Extinction derived using Girardi considering $Z = 0.004$. 11.- Same as 10 but for $Z = 0.019$. 12.- Log of the star cluster age derived from GALEV for $Z = 0.004$. Third row: 1.- Log of the star cluster age derived from GALEV for $Z = 0.008$. 2.- Same as 1 but for $Z = 0.02$. 3.- Same as 1 but for $Z = 0.05$. 4.- Log of the star cluster age derived from Girardi for $Z = 0.004$. 5.- Same as 4 but for $Z = 0.019$. 6.- Log of the mass derived from GALEV for $Z = 0.004$. 7.- Same as 6 but for $Z = 0.008$. 8.- Same as 6 but for $Z = 0.002$. 9.- Same as 6 but for $Z = 0.005$. 10.- Log of the mass derived from Girardi for $Z = 0.004$.

Chapter **4**

Spectroscopy of globular clusters in
the low luminosity spiral galaxy
NGC 45

Astronomy & Astrophysics 2008, 489, 1065
M. D. Mora, S. S. Larsen & M. Kissler-Patig

Abstract

Extragalactic globular clusters have been studied in elliptical galaxies and in a few luminous spiral galaxies, but little is known about globular clusters in low luminosity spirals. Past observations with the ACS have shown that NGC 45 hosts an important population of globular clusters (19) as well as several young star clusters. In this work we aim to confirm the bona fide globular cluster status for 8 of 19 globular cluster candidates and to derive metallicities, ages and velocities. VLT/FORS2 multislit spectroscopy in combination with the Lick/IDS system was used to derive velocities, constrain metallicities and $[\alpha/\text{Fe}]$ element ratio of the globular clusters. We confirm the 8 globular clusters as bona fide globular clusters. Their velocities indicate halo or bulge like kinematics, with little or no overall rotation. From absorption indices such as $\text{H}\beta$, $\text{H}\gamma$ and $\text{H}\delta$ and the combined $[\text{MgFe}]'$ index we found that the globular clusters are metal-poor $[\text{Z}/\text{H}] \leq -0.33$ dex and $[\alpha/\text{Fe}] \leq 0.0$ element ratio. These results argue in favor of a population of globular clusters formed during the assembling of the galaxy.

4.1 Introduction

Globular clusters are present in almost all kinds of galaxies. Observations of extragalactic globular cluster systems have shown that globular cluster systems can often be divided into (at least) two sub-populations, although the origin of these remains unclear. In the Milky Way and M31, the metal-poor globular cluster sub-populations display halo-like kinematics and spatial distributions (e.g. Zinn 1985; Ashman & Zepf 1998; Barmby et al. 2000; Perrett et al. 2002), while the metal-rich globular clusters may be associated with the bulge and/or thick disk (e.g. Minniti 1995; Barbuy et al. 1998; Côté 1999; Bica et al. 2006). The globular cluster sub-populations in elliptical galaxies show many similarities to those in spirals, and some of the metal-rich clusters may have formed in galaxy mergers (e.g. Ashman & Zepf 1992). Some of the metal-poor (“halo”) clusters may have been accreted from dwarf galaxies (Da Costa & Armandroff 1995) or in proto-galactic fragments from which the halo assembled (Searle & Zinn 1978). A major challenge is to establish how each one of these mechanisms may fit into the paradigm of hierarchical structure formation (e.g. Santos 2003).

One important step towards understanding the roles of merging and accretion processes is to extend our knowledge about globular clusters to many different galaxy types, such as dwarf galaxies and late-type spirals, in a range of environments. Studies of globular clusters in spiral galaxies are more difficult than in early-type galaxies because the globular cluster systems are generally poorer and appear superposed on an irregular background. Consequently, most studies of extragalactic globular clusters have focused on elliptical galaxies.

In spite of the similarities, there are also important differences between globular cluster systems of large ellipticals and those of spirals like the Milky Way. Elliptical galaxies generally have many more globular clusters per unit host galaxy luminosity (i.e., higher globular cluster *specific frequencies* Harris & van den Bergh (1981) than spirals), and on average the globular cluster systems of ellipticals are more metal-rich (Kissler-Patig et al. 1999). The best studied globular cluster systems in spiral galaxies are those associated with the Milky Way and M31. Globular clusters in M31 appear similar to those in the Milky Way in terms of their luminosity functions, metallicities and, size distributions (Crampton et al. 1985; Perrett et al. 2002; Barmby et al. 2002). M33 has a large number of star clusters (Christian & Schommer 1982, 1988; Chandar et al. 2001) but many of them have young ages and there may be only a dozen or so truly “halo” globular clusters (Sarajedini et al. 2000). The Magellanic Clouds are also well-known for their rich cluster systems, but again only few of these are truly old globular clusters. The Large Magellanic Cloud has about 13 old globular clusters (Johnson et al. 1999), which however show disk-like kinematics. The Small Magellanic Cloud has only one old globular cluster, NGC 121.

The globular cluster populations in low luminosity spirals are almost unknown. The question of how these clusters formed (and their host galaxy) remain unanswered. Considering that those kind of galaxies remain almost unperturbed during their life, it is probable that we are observing their first population of globular clusters and therefore, we can approach to the conditions in which the host galaxies were formed.

The nearby Sculptor group hosts several late-type galaxies whose globular cluster systems are potentially within reach of spectroscopic observations with 8 m telescopes in a few hours of integration time. A previous study of the star cluster population in the Sculptor group was done by Olsen et al. (2004). They observed several globular cluster candidates, finding 19 globular clusters in four galaxies, most of them metal-poor with $[\alpha/\text{Fe}]$ lower than the Milky Way globular clusters.

In this paper we concentrate on the late-type, low luminosity spiral galaxy NGC 45 in Sculptor, in which we have previously identified a surprisingly rich population of old globular cluster candidates in HST/ACS imaging. NGC 45 is classified as a low luminosity spiral galaxy with $B = 11.37 \pm 0.11$ and $B - V = 0.71$ (Paturel et al. 2003). It is located at ~ 5 Mpc from us, $(m - M)_0 = 28.42 \pm 0.41$ (Bottinelli et al. 1985), in the periphery of the Sculptor group. In chapter 2 (Mora et al. 2007) we found 19 globular clusters located in projection with the galaxy bulge, which appear to belong to the metal-poor population. Those 19 globular clusters yield a S_N of 1.4 – 1.9, which is high for a late-type galaxy.

In this paper we focus on 8 of those 19 globular clusters. We analyze them through spectroscopy to confirm or reject their globular cluster status and to constrain ages and metallicities.

4.2 Candidates selection, observation and, reductions

4.2.1 Globular cluster selection

In Mora et al. (2007) we identified cluster candidates as extended objects, using a variety of size selection criteria based on the BAOLAB/ISHAPE (Larsen 1999) and SExtractor (Bertin & Arnouts 1996) packages. We found 19 extended objects fulfilling the color criteria $0.8 < V - I < 1.2$, with magnitudes $V = 19.5$ up to $V = 22.5$ that were interpreted as globular clusters. The detected globular cluster candidates had a mean color of $V - I = 0.90$, consistent with a metal-poor, old population. The mean half-light radius of the globular cluster candidates was $R_{\text{eff}} = 2.9 \pm 0.7$ pc (error is the standard error of the mean), similar to that of globular clusters in other galaxies.

4.2.2 Observations and reductions

The spectra were acquired in service mode on the ESO period 77 using the ESO Focal Reducer/low dispersion Spectrograph (FORs2) through the Multi-object spectroscopy mask exchange unit (MXU), which is mounted in Kueyen/UT2 VLT telescope at Cerro Paranal Chile. We used the GRIS_600B+22 which has a wavelength range from 3330 Å up to 6210 Å with a dispersion at the central wavelength (4650 Å) of 0.75 Å/pixel. Because of the globular cluster positions, we were only able to place 8 globular clusters on the MXU. Extra 16 filler slits were placed on young star regions, the galaxy bulge, the sky and one star. On each object a slit of 1.0'' width was placed and MXU observations were done in 7 Observing Blocks (OBs). A sample of these spectra are shown in Fig. 4.1. For the calibration, we acquired 6 Lick/IDS standard stars from Worthey et al. (1994) in long slit spectra mode using the same configuration of the globular cluster observations (for a

log of the observations see Table 4.1). The six standard stars were selected according to their spectral type (i.e. K3III, G0V, G5IV, F5VI, K3IIIIV and, A3V), covering the range of spectral types expected in a globular cluster. Each standard was observed in 3 exposure sets with a small offset in the direction of the slit in order to avoid bad pixels in the final combined spectra.

Table 4.1: Log of the observations. The second column indicates the observed mode: Multi-object spectroscopy mask exchange unit (MXU) and Long slit spectroscopy (LSS).

Object	Mode	N of exposures \times time	Obs type
NGC 45	MXU	$17 \times (3 \times 1200s)$	Science
NGC 45	MXU	$2 \times 1095s$	Science
HD180928	LSS	$3 \times 1.00s$	Lick std
HD195633	LSS	$3 \times 1.00s$	Lick std
HD165195	LSS	$2 \times (3 \times 3.00s)$	Lick std
HD003567	LSS	$3 \times 5.00s$	Lick std
HD221148	LSS	$3 \times 1.00s$	Lick std
HD006695	LSS	$2 \times (3 \times 0.63s)$	Lick std

The spectra (science and standard stars) were reduced (i.e. bias subtracted, flat field corrected, optical distortion corrected and, wavelength calibrated) using the ESO Recipe Execution Tool v3.6 (ESO-REX)¹. Typical rms from the distortion corrections were of the order of 0.4 pixels and the wavelength calibration accuracy of the model applied during the wavelength calibration was of the order of 0.08Å.

In the following section we explain the radial velocity measurements. We only focus on the globular clusters because filler spectra were too faint to have reasonable radial velocity measurements.

4.3 Radial velocities

Radial velocities were first derived for the standard stars. Since each standard star was acquired in a set of 3 consecutive exposures, we derived the radial velocity on each single exposure. This was accomplished by cross correlating a zero velocity elliptical galaxy template from Quintana et al. (1996) with each spectrum using the *FXCOR* IRAF² task. Each single spectrum was shifted to zero radial velocity and combined into a high signal to noise standard star spectrum.

Globular cluster spectra taken in the same OB were combined, yielding 7 spectra for each globular cluster. Each one of them, in combination with the high signal to noise standard star spectra, were used to derive the globular cluster velocities through cross

¹<http://www.eso.org/sci/data-processing/software/cpl/esorex.html>

²IRAF is distributed by the National Optical Astronomical Observatory, which is operated by the Association of Universities for Research in Astronomy, Inc, under cooperative agreement with the National Science Foundation.

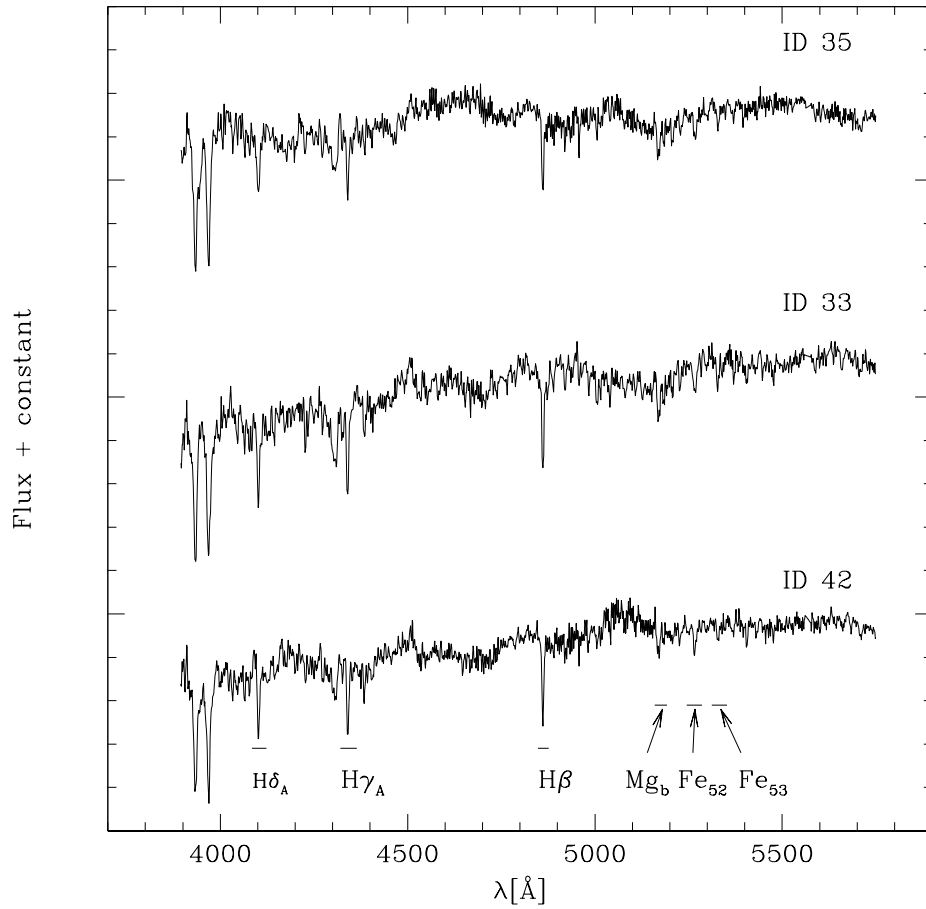


Figure 4.1: Samples of the spectra. The spectra have been shifted to the 0 radial velocity and an offset in flux has been added for best clarity of the sample. Some Lick-index passband are indicated at the bottom of the panel.

correlation using the *FXCOR* IRAF task. On each cross correlation we select a region of 200 Å width centered in the Ca II H+K, H β and, H γ features. An extra region from 5000 Å up to 5500 Å was also considered for cross correlation. We note that the cross correlations between standard-star types A and K; and the globular cluster spectra were particularly difficult, most likely because such stars provide a poorer match to the overall spectrum of a globular cluster. This effect, combined with the low signal-to-noise of the spectra (especially for the globular clusters ID 45 and ID 47) caused the velocity measurements to be more uncertain when based on these stars.

In Fig. 4.2 we show histograms of all the individual velocity measurements for each cluster. We adopted the average of the distribution as the final velocity value of each globular cluster. The error was obtained from the standard deviation divided by the square

root of the number of measurements. Values are listed in Table 4.2.

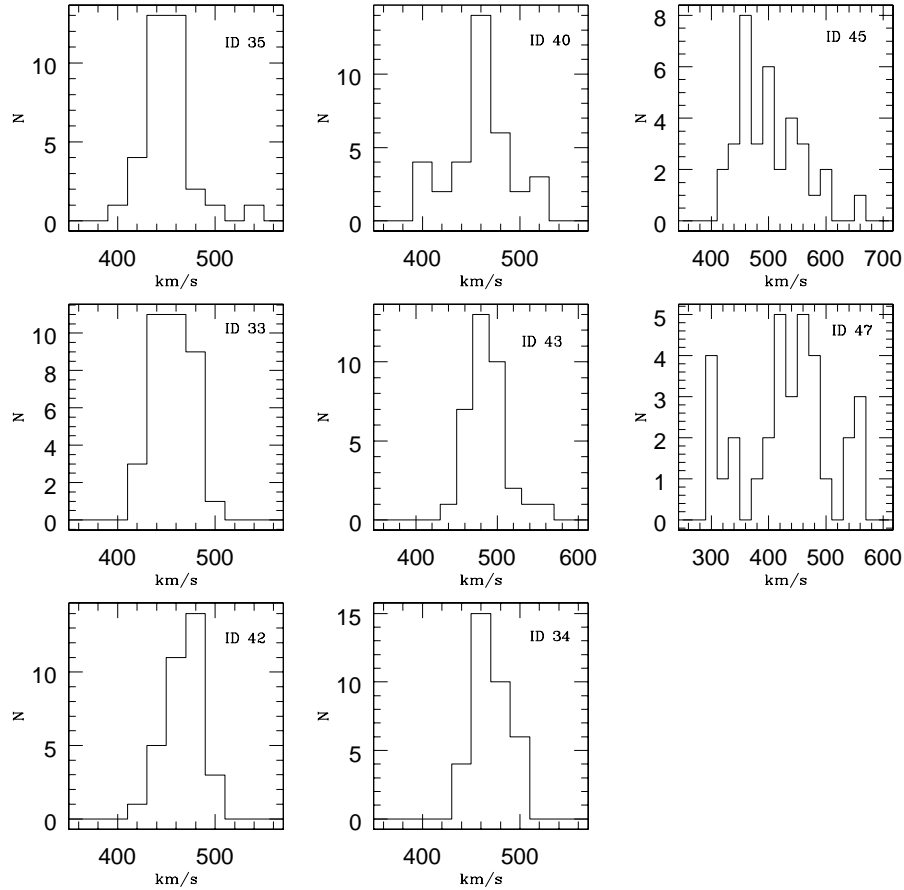


Figure 4.2: Distributions of velocity measurements of the globular clusters.

In Fig. 4.3 we show the position of the globular clusters with overplotted isovelocity contours from Chemin et al. (2006). The sub-panel on the bottom and the sub-panel on the right shows the projected velocity as function of RA and DEC. The panels show that our velocity measurements are consistent with no overall rotation of the globular cluster system. Globular clusters located near the center of the galaxy show velocities consistent with the observed H I gas velocities from Chemin et al. (2006). The greatest difference between the globular cluster velocities was $\Delta V = 71 \pm 16$ km/s. It corresponds to the difference of velocity between the globular cluster ID=45 and 47, which also show the largest errors. Therefore, globular cluster velocities are mainly concentrated between $V=430 - 480$ km/s, as is seen in Fig 4.3.

The velocities of the GCs clearly do not match the isovelocity contours of Chemin et al. (2006), and we thus exclude that the GCs are associated with the disk component

Table 4.2: Derived velocities of the globular clusters. σ is the standard deviation and N corresponds to the number of measurements.

ID	Vel(km/s)	σ	N
33	455 ± 3	19	37
34	470 ± 3	17	35
35	450 ± 4	25	35
40	459 ± 5	32	35
42	467 ± 3	17	34
43	485 ± 4	23	35
45	503 ± 9	55	33
47	432 ± 13	77	33

of NGC 45. The velocity dispersion is $\sigma = 20 \pm 4$ km/s, which is significantly larger than the measurement errors (Table 4.2) and smaller than other similar galaxies like M 33 (Chandar et al. (2002) found values of $\sigma = 54 \pm 8$ for disk/bulge globular clusters and $\sigma = 83 \pm 13$ km/s for halo globular clusters). Therefore, we conclude that the globular cluster velocities in NGC 45 are indicative of halo- or bulge like kinematics, with little or no overall rotation.

4.4 Lick index calibrations

In the following we estimate abundances for our globular cluster sample using the Lick/IDS system of absorption line indices. We used passband definitions from Trager et al. (1998) taken from G. Worthey’s web page³ which includes the old definitions from Worthey et al. (1994) and H_δ and H_γ definitions from Worthey & Ottaviani (1997).

The Lick/IDS system is designed to measure absorption features such as CN, $H\beta$, Fe, Mg, G (molecular bands) and blend of absorption lines present in old populations. These features were used to construct a library from several stars observed at the Lick observatory. Six of these standard stars were taken during the observations that are presented in this work. Due to our instrument configuration, the standard stars spectra, as well as the globular cluster spectra, have higher spectral resolution than the original Lick/IDS system. Thus, we must carefully degrade our spectra in order to match the Lick/IDS spectral resolution. One way to quantify the difference between our instrumental system and the original Lick/IDS spectra is to measure the FWHM of narrow spectral features. We measured the FWHM of the sky lines in our sky spectra and we found a typical FWHM=4.9 Å. This value was used as input for the code used for the index derivations.

The indices were measured using the GONZO code from Puzia et al. (2002). Briefly, GONZO degrades the spectra to the Lick/IDS index system with a wavelength-dependent Gaussian kernel in order to match the resolution from Worthey & Ottaviani (1997).

³<http://astro.wsu.edu/worthey/html/index.table.html>

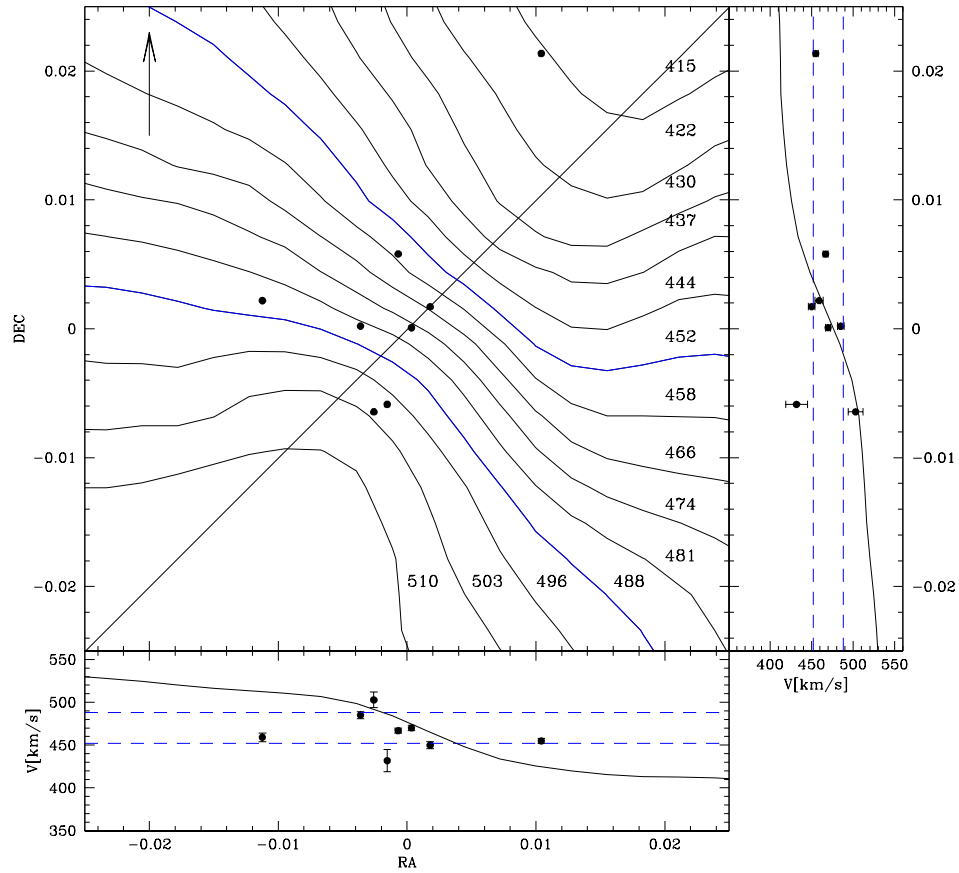


Figure 4.3: Main panel: Position of the bona fide globular clusters with overlaid isovelocity contours from Chemin et al. (2006). Arrow indicates the north and East is on the left. The sub panels on the bottom as well as on the right show the globular cluster velocity projections of the main panel as function of RA and DEC respectively. Blue lines indicate isovelocity lines for 480 km/s and 452 km/s. The straight line crossing the main panel has the purpose of illustrating the velocity changes when it is projected as function of RA and DEC on the sub panels. Numbers next to the isovelocity contours indicate the velocity in km/s.

GONZO also derives the uncertainties of the indices by considering the Poisson statistics on each pixel from the error spectra. These statistics are used in the addition of random noise when creating artificial science spectra and measuring the indices on these. For further details on GONZO, see Puzia et al. (2002).

In the comparisons between our standard stars and the Lick/IDS system, we assumed that the transformation between our measured Lick/IDS indices and the standard values

Table 4.3: Calibration summary of the Lick Indices. TiO_1 and TiO_2 were not measured due to the fact that our standard-star spectra do not cover the TiOs wavelength. ZP corresponds to the zero point needed in order to match the Lick/IDS system and σ corresponds to the error which was calculated considering the standard deviation divided by the square root of the number of measurements.

Index	ZP	σ	Units
CN ₁	0.0301	0.0123	<i>mag</i>
CN ₂	0.0364	0.0087	<i>mag</i>
Ca4227	0.3878	0.0830	Å
G4300	0.8417	0.2467	Å
Fe4383	0.6260	0.2155	Å
Ca4455	0.1553	0.1183	Å
Fe4531	0.3835	0.2359	Å
Fe4668	-0.0715	0.2840	Å
H β	0.0515	0.1234	Å
Fe5015	0.0583	0.2394	Å
Mg ₁	-0.0116	0.0034	<i>mag</i>
Mg ₂	-0.0149	0.0062	<i>mag</i>
Mg _b	0.2932	0.0501	Å
Fe5270	0.4598	0.0563	Å
Fe5335	0.2400	0.1041	Å
Fe5406	0.0729	0.0581	Å
Fe5709	0.1342	0.0667	Å
TiO ₁	-	-	<i>mag</i>
TiO ₂	-	-	<i>mag</i>
H δ_A	0.1376	0.3270	Å
H γ_A	-0.4629	0.3295	Å
H δ_F	0.6445	0.1504	Å
H γ_F	-0.1960	0.1333	Å

was linear with a slope of unity, so that only an offset is needed to match the standard Lick/IDS system. Also we avoided possible changes of the slopes due to outlier measurements (which were impossible to identify because of the small number of the observed standard stars).

The zero-point offsets are given in Table 4.3 and a comparison between our measurements and the Lick/IDS system is shown in Fig. 4.4. The reader may note that we do not list values for the TiO indices because the TiO indices were outside the wavelength coverage.

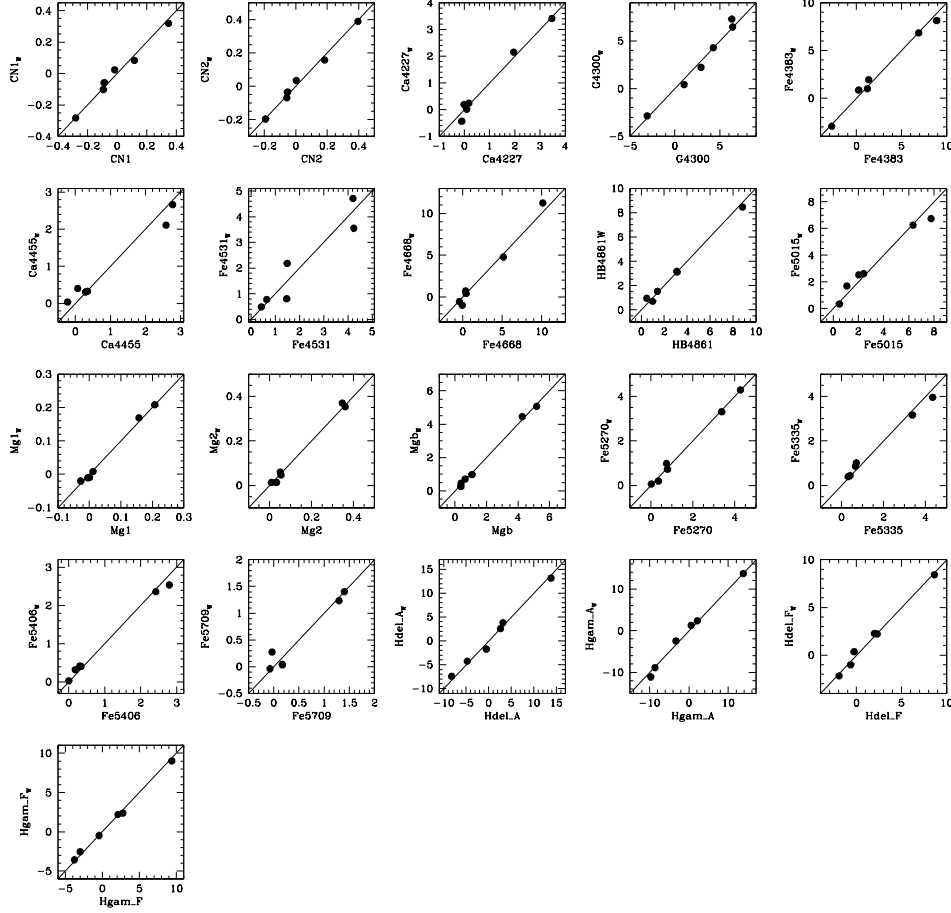


Figure 4.4: Comparison of Worthey Lick/IDS indices with the one measured by us after zero-point offset correction. Lines represent the one-to-one comparison.

4.5 Results

4.5.1 Age diagnostic plots

In this subsection we discuss the results of the indices measurements and their comparisons with α /Fe models from Thomas et al. (2003) and Thomas et al. (2004). We adopted the index $[\text{MgFe}]' = \sqrt{\text{Mgb} \times (0.72 \times \text{Fe5270} + 0.28 \times \text{Fe5335})}$ which is $[\alpha/\text{Fe}]$ independent defined by Thomas et al. (2003). We also adopted from González (1993) the $\langle \text{Fe} \rangle = (\text{Fe5270} + \text{Fe5335})/2$ index definition. Figure 4.5 show the age metallicity diagnostic plots for the Balmer line indices $\text{H}\beta$, $\text{H}\gamma_A$, $\text{H}\gamma_F$, $\text{H}\delta_A$ and, $\text{H}\delta_F$ against $[\text{MgFe}]'$. All our globular clusters show $[\text{MgFe}]'$ values less than or equal to 2 \AA , which makes them metal poor.

Ages are poorly constrained and depend on the Balmer line used for the comparison

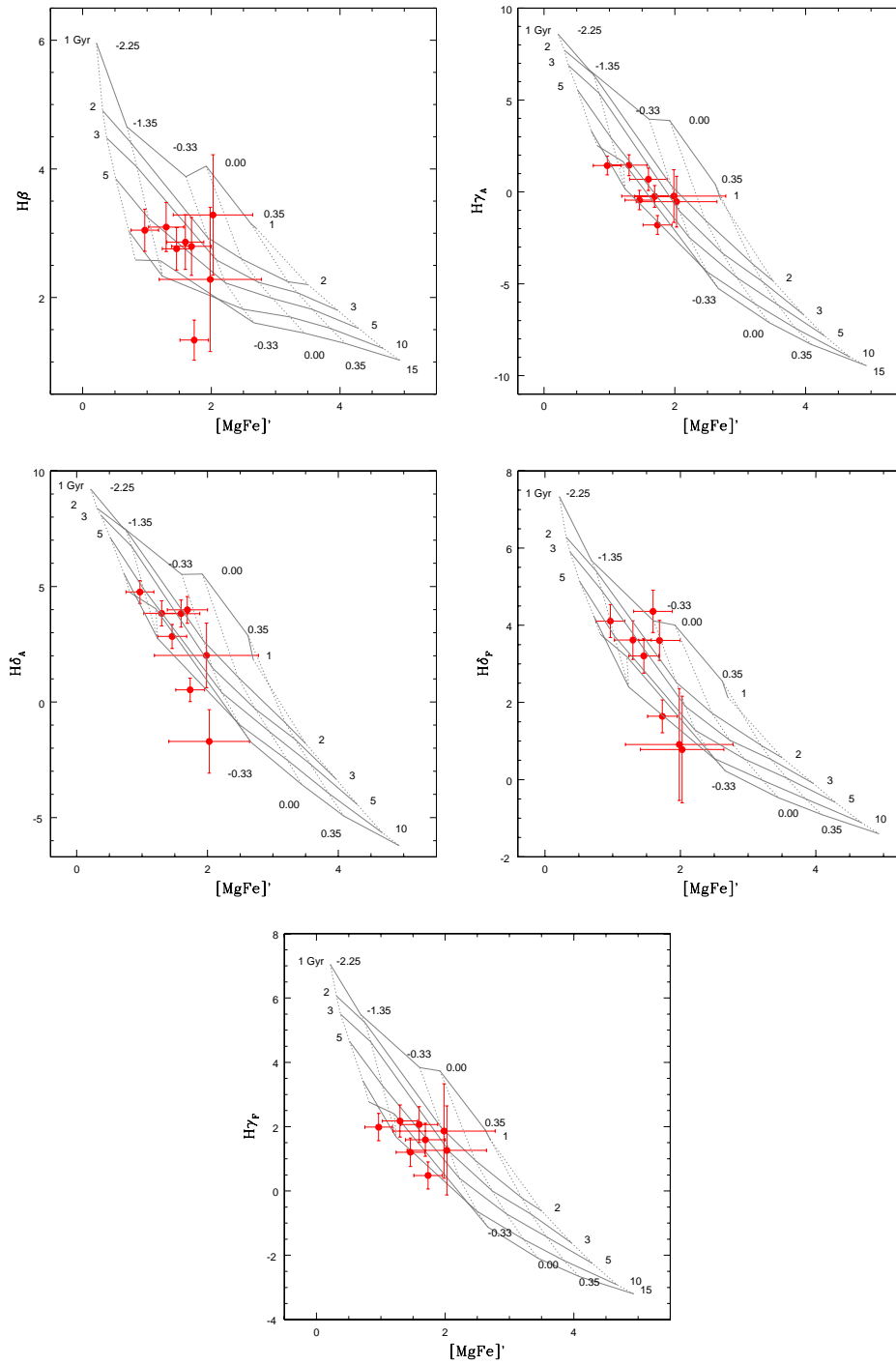


Figure 4.5: Age diagnostic plots. The over-plotted grid corresponds to SSP model from Thomas et al. (2004) for $[\alpha/Fe]= 0.0$. Dotted lines correspond to metallicities $[Z/H]= -2.25, -1.35, -0.33, 0.0, 0.35$ and, 0.67 dex. Solid lines correspond to ages of 1, 2, 3, 5, 10 and 15 Gyr.

with models, but the metallicities are consistently sub-solar with $[Z/H] < -0.33$. In the left panel of Fig. 4.6 we show the average iron versus Mg2 over-plotted with models from Thomas et al. (2004) for $[\alpha/Fe] = -0.3, 0.0$ and, 0.3 ; and ages of 5 and 15 Gyr. The panel shows globular clusters located in the sub-solar metallicity region with values lower than $[Z/H] = -0.33$ corroborating the same result of Fig. 4.5 and, despite the great uncertainties, the globular clusters seem to be better described by models with sub-solar $[\alpha/Fe] = 0.0, -0.3$ element ratios. This conclusion becomes less strong when the two Fe index are plotted separately versus Mgb as it is seen in the central and right panels of Fig. 4.6. For the Fe_{5270} index, globular clusters show $[\alpha/Fe] \leq 0.0$ while for the Fe_{5335} index, globular clusters are scattered between $-0.3 < [\alpha/Fe] < 0.3$. The derived values of $[\alpha/Fe]$ element ratios and metallicities seems to be consistent with values found by Olsen et al. (2004) in 4 Sculptor galaxies. They concluded that all globular clusters in the Sculptor group have $[Fe/H] \leq -1.0$ (we found values for NGC 45 $[Fe/H] \leq -0.3$) and values of $-0.3 \pm 0.15 < [\alpha/Fe] < 0.0 \pm 0.15$ for the measured globular clusters.

4.5.2 Comparison with photometric ages

In spite of the uncertainties of the star cluster metallicities and ages, it is worth to comment how ages and metallicities derived here compare with the previous ages and metallicities assumed in Mora et al. (2007). As a reminder, in Mora et al. (2007) we used GALEV models (Anders & Fritze-v. Alvensleben 2003) considering 4 metallicities: $Z=0.004, 0.008, 0.02,$ and 0.05 which are equivalent to $[Fe/H] = -0.7, 0.4, 0,$ and $+0.4$. In the present work, we have 3 globular clusters (ID=33, 34 and, 35) in common with our previous work.

In Table 4.4 we show the $[Z/H]$ values calculated for each index and its mean value calculated from the age diagnostic plots. We do not extrapolate ages nor metallicities of globular clusters lying outside the model grids. Errors were calculated considering the highest and lowest values for each index within the error bars. Also, if the error bar (or a part of it) lie outside the model grids, we do not extrapolate its value and we considered the farthest point of the grid as the maximum (or minimum) error value. Therefore, errors lie within the grid values. We found that the derived metallicities agree on each index and we concluded that the most adequate metallicity for age and mass derivations with photometry is $Z=0.004$ of the GALEV models.

In Table 4.5 we show individual ages derived from the age diagnostic plots for each Balmer index, and the mean value considering all Balmer indices. We do not extrapolated values outside the model grids and errors were calculated in the same way as we did in Table 4.4. The last two columns show the derived ages from GALEV (considering $Z=0.004$). Ages derived from photometry do not agree with the values derived using spectroscopy. Photometric ages were underestimated, compared with the spectroscopic ones. This underestimation is more dramatic for the globular cluster ID=35 where the photometric age do not share the same order of magnitude as the spectroscopic ones. This result is not entirely unexpected, since old globular clusters are faint in the U-band, which provides much of the leverage for age determinations. Furthermore, model uncertainties and degeneracies in age/metallicity/reddening all combine to produce larger uncertainties

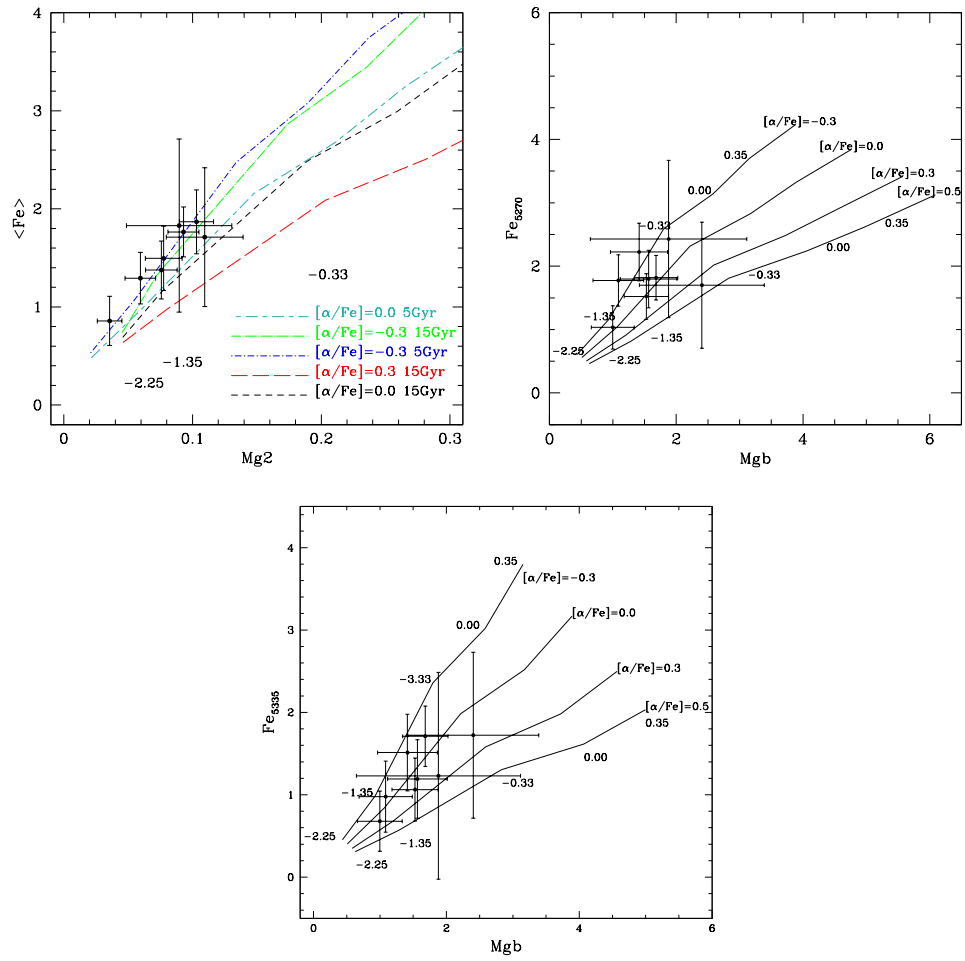


Figure 4.6: Top left panel: Iron $\langle Fe \rangle$ as function of $Mg2$. Top right panel: Fe_{5270} index versus Mgb . Bottom central panel: Fe_{5335} index versus Mgb .

Table 4.4: Metallicities from age diagnostic plots. Column (1): Globular cluster ID. Columns (2) to (6): Z/H. The index used for its derivation is shown between brackets. Column (7): average Z/H

(1)	(2)	(3)	(4)	(5)	(6)	(7)
ID	Z/H($H\beta$)	Z/H($H\gamma_A$)	Z/H($H\delta_F$)	Z/H($H\delta_A$)	Z/H($H\gamma_F$)	< [Z/H] >
33	$-1.1^{+0.40}_{-0.55}$	$-1.15^{+0.45}_{-0.60}$	$-1.0^{+0.65}_{-0.75}$	$-1.15^{+0.60}_{-0.55}$	$-1.2^{+0.40}_{-0.50}$	$-1.12^{+0.5}_{-0.59}$
34	–	$-0.9^{+0.2}_{-0.10}$	–	–	–	$-0.9^{+0.2}_{-0.1}$
35	$-0.85^{+0.45}_{-0.40}$	$-0.8^{+0.3}_{-0.50}$	–	$-0.65^{+0.30}_{-0.55}$	$-0.85^{+0.40}_{-0.40}$	$-0.79^{+0.36}_{-0.46}$
40	$-1.6^{+0.45}_{-0.65}$	–	$-1.4^{+0.45}_{-0.85}$	$-1.6^{+0.55}_{-0.65}$	–	$-1.53^{+0.48}_{-0.72}$
42	$-1.0^{+0.35}_{-0.35}$	$-1.15^{+0.35}_{-0.15}$	$-0.9^{+0.55}_{-0.45}$	$-1.05^{+0.40}_{-0.30}$	–	$-1.03^{+0.41}_{-0.31}$
43	$-0.75^{+0.40}_{-0.45}$	$-0.8^{+0.40}_{-0.40}$	$-0.4^{+0.30}_{-0.60}$	$-0.45^{+0.30}_{-0.60}$	$-0.8^{+0.40}_{-0.40}$	$-0.64^{+0.36}_{-0.49}$
45	$-0.15^{+0.65}_{-1.05}$	$-0.35^{+0.95}_{-0.85}$	–	–	$-0.4^{+0.70}_{-0.80}$	$-0.30^{+0.76}_{-0.9}$
47	$-0.6^{+0.65}_{-0.80}$	$-0.35^{+0.60}_{-1.05}$	–	$-0.35^{+0.55}_{-1.00}$	$-0.3^{+0.55}_{-1.10}$	$-0.40^{+0.59}_{-0.99}$

Table 4.5: Derived ages in Gyr from age diagnostic plots. Column (1): Globular cluster ID. Columns (2) to (6): Derived ages. The index used for its derivation is shown between brackets. Column (7): Average age. Columns (8) and (9): Ages derived from GALEV.

(1)	(2)	(3)	(4)	(5)	(6)	(7)	(8)	(9)
ID	Age($H\beta$)	Age($H\gamma_A$)	Age($H\delta_F$)	Age($H\delta_A$)	Age($H\gamma_F$)	< Age >	log(Age/yr)	Age
33	$4.7^{+4.4}_{-2.3}$	$5.8^{+9.2}_{-3.2}$	$3.5^{+10.0}_{-2.5}$	$5.4^{+8.8}_{-3.7}$	$7.2^{+6.3}_{-3.6}$	$5.32^{+7.74}_{-3.06}$	$9.06^{+0.39}_{-1.14}$	$1.14^{+1.67}_{-1.06}$
34	–	$9.9^{+0.8}_{-3.1}$	–	–	–	$9.90^{+0.80}_{-3.1}$	$9.10^{+0.91}_{-0.65}$	$1.25^{+8.97}_{-0.97}$
35	$4.6^{+4.5}_{-2.9}$	$4.3^{+10.4}_{-2.1}$	–	$2.3^{+5.1}_{-0.9}$	$4.6^{+9.0}_{-2.8}$	$4.52^{+6.09}_{-1.76}$	$6.91^{+1.43}_{-0.09}$	$0.008^{+0.27}_{-0.02}$
40	$7.0^{+6.4}_{-2.9}$	–	$4.5^{+10.5}_{-2.8}$	$6.9^{+8.1}_{-4.0}$	–	$6.13^{+8.30}_{-3.23}$	–	–
42	$5.9^{+9.1}_{-3.0}$	$9.5^{+3.6}_{-4.2}$	$3.8^{+11.2}_{-2.5}$	$6.9^{+7.9}_{-3.9}$	–	$6.52^{+7.95}_{-3.4}$	–	–
43	$4.4^{+5.1}_{-2.5}$	$5.6^{+8.5}_{-3.3}$	$1.4^{+3.2}_{-0.4}$	$1.7^{+3.7}_{-0.4}$	$5.5^{+8.4}_{-3.4}$	$3.72^{+5.78}_{-2}$	–	–
45	$1.6^{+7.9}_{-0.6}$	$2.7^{+10.8}_{-1.7}$	–	–	$3.4^{+8.5}_{-2.4}$	$2.56^{+9.06}_{-1.57}$	–	–
47	$6.9^{+8.1}_{-5.2}$	$2.5^{+11.3}_{-1.3}$	–	$2.6^{+7.4}_{-1.3}$	$2.0^{+11}_{-1.0}$	$3.50^{+9.45}_{-2.2}$	–	–

on the photometric ages for old globular clusters.

4.6 Discussion and conclusion

Although uncertainties on the age estimates for our sample of globular clusters in NGC 45 remain large, we were able to constrain their metallicities and α /Fe abundance ratios. These showed that the globular clusters in NGC 45 are metal poor, corroborating the metal poor population deduced from the globular cluster colors in Mora et al. (2007).

Assuming that the globular clusters are tracer of star formation events, considering that NGC 45 is an isolated galaxy, probably a background object and, not a true member of the Sculptor group (Puche & Carignan 1988), it is puzzling how these entities formed in this galaxy. Whiting (1999) suggested that NGC 45 once made a close pass by the Sculptor group, getting close to NGC 7793 and transferring angular momentum. This would have been excited the globular cluster formation in NGC 45 but there is no record

of this in the globular cluster population. Therefore, the formation of the globular clusters must be happen at early times probably when the galaxy assembled.

The globular cluster velocities and the velocity dispersion of the system argue in favor of a real association between the globular clusters and the galaxy bulge. The velocity distribution of the GC population seems to be dominated by random motions, although it would be desirable to corroborate this statement with further velocity measurements of the remaining 11 candidates.

The sub-solar $[\alpha/\text{Fe}]$ values derived here are unlike those typically observed in old GC populations (e.g. Puzia et al. 2005), including those in the Milky Way. However, we note that they are consistent with those derived by Olsen et al. (2004). It is also of interest to note that dwarf galaxies in the Local Group tend to show less alpha-enhanced abundance ratios than the Milky Way (Sbordone et al. 2005; Tolstoy et al. 2003). This may point to important differences in the early chemical evolution in these different types of galaxies, and is potentially an argument against the notion that a major fraction of the GCs in large galaxies could have been accreted from minor galaxies similar to those observed today.

One possible explanation for the relatively low $[\alpha/\text{Fe}]$ ratios of the GCs in NGC 45 is that the formation and assembly of the halo/bulge component took longer than in major galaxies like the Milky Way. This would allow time for Type Ia supernovae to appear and enrich the gas with greater amounts of Fe.

Acknowledgements:

We would like to thank Thomas Puzia for providing us the GONZO code, Steffen Mieske for providing us the elliptical galaxy spectra template and, Laurent Chemin for gently provide us the NGC 45 H I velocity field data.

Table 4.6: Measured indice. σ corresponds to the error from the random noise. σ_{vel} corresponds to the error due to the velocity uncertainties.

Indice \ ID		33	34	35	40
CN ₁ $\pm\sigma_{-vel}^{+vel}$	mag	$-0.021 \pm 0.005^{+0.046}_{-0.048}$	$-0.020 \pm 0.008^{+0.009}_{-0.003}$	$0.012 \pm 0.005^{+0.048}_{-0.050}$	$-0.017 \pm 0.004^{+0.020}_{-0.027}$
CN ₂ $\pm\sigma_{-vel}^{+vel}$	mag	$-0.038 \pm 0.003^{+0.004}_{-0.001}$	$0.012 \pm 0.005^{+0.000}_{-0.001}$	$0.001 \pm 0.004^{+0.000}_{-0.000}$	$0.004 \pm 0.003^{+0.003}_{-0.002}$
Ca4227 $\pm\sigma_{-vel}^{+vel}$	Å	$0.705 \pm 0.135^{+0.073}_{-0.000}$	$0.905 \pm 0.177^{+0.002}_{-0.005}$	$0.783 \pm 0.173^{+0.017}_{-0.020}$	$0.047 \pm 0.104^{+0.014}_{-0.042}$
G4300 $\pm\sigma_{-vel}^{+vel}$	Å	$4.632 \pm 0.195^{+0.854}_{-0.075}$	$5.399 \pm 0.214^{+1.144}_{-0.022}$	$4.876 \pm 0.257^{+0.173}_{-0.185}$	$2.167 \pm 0.134^{+0.075}_{-0.849}$
Fe4383 $\pm\sigma_{-vel}^{+vel}$	Å	$1.579 \pm 0.238^{+0.009}_{-0.043}$	$2.518 \pm 0.237^{+0.011}_{-0.041}$	$0.951 \pm 0.303^{+0.073}_{-0.108}$	$-0.462 \pm 0.174^{+0.399}_{-0.068}$
Ca4455 $\pm\sigma_{-vel}^{+vel}$	Å	$0.889 \pm 0.246^{+0.045}_{-0.015}$	$0.412 \pm 0.242^{+0.015}_{-0.081}$	$1.021 \pm 0.313^{+0.061}_{-0.027}$	$0.260 \pm 0.180^{+0.025}_{-0.023}$
Fe4531 $\pm\sigma_{-vel}^{+vel}$	Å	$2.112 \pm 0.258^{+0.056}_{-0.037}$	$2.847 \pm 0.257^{+0.025}_{-0.018}$	$1.342 \pm 0.323^{+0.005}_{-0.042}$	$0.174 \pm 0.197^{+0.014}_{-0.006}$
Fe4668 $\pm\sigma_{-vel}^{+vel}$	Å	$1.640 \pm 0.358^{+0.042}_{-0.055}$	$3.526 \pm 0.285^{+0.001}_{-0.026}$	$-1.152 \pm 0.404^{+0.072}_{-0.032}$	$-3.567 \pm 0.301^{+0.045}_{-0.225}$
H β $\pm\sigma_{-vel}^{+vel}$	Å	$3.045 \pm 0.360^{+0.003}_{-0.000}$	$1.287 \pm 0.287^{+0.016}_{-0.021}$	$2.810 \pm 0.407^{+0.019}_{-0.446}$	$2.995 \pm 0.302^{+0.009}_{-0.000}$
Fe5015 $\pm\sigma_{-vel}^{+vel}$	Å	$2.108 \pm 0.376^{+0.091}_{-0.046}$	$1.136 \pm 0.328^{+0.054}_{-0.034}$	$1.740 \pm 0.422^{+0.155}_{-0.977}$	$1.915 \pm 0.318^{+0.123}_{-0.048}$
Mg ₁ $\pm\sigma_{-vel}^{+vel}$	mag	$0.032 \pm 0.010^{+0.000}_{-0.000}$	$0.030 \pm 0.010^{+0.000}_{-0.000}$	$0.004 \pm 0.012^{+0.000}_{-0.009}$	$-0.041 \pm 0.007^{+0.000}_{-0.000}$
Mg ₂ $\pm\sigma_{-vel}^{+vel}$	mag	$0.090 \pm 0.010^{+0.000}_{-0.000}$	$0.107 \pm 0.010^{+0.000}_{-0.000}$	$0.092 \pm 0.012^{+0.000}_{-0.006}$	$0.050 \pm 0.007^{+0.000}_{-0.000}$
Mg _b $\pm\sigma_{-vel}^{+vel}$	Å	$0.793 \pm 0.398^{+0.042}_{-0.048}$	$1.389 \pm 0.337^{+0.013}_{-0.020}$	$1.270 \pm 0.444^{+0.004}_{-0.003}$	$0.705 \pm 0.333^{+0.036}_{-0.002}$
Fe5270 $\pm\sigma_{-vel}^{+vel}$	Å	$1.315 \pm 0.402^{+0.036}_{-0.021}$	$1.358 \pm 0.347^{+0.024}_{-0.050}$	$1.338 \pm 0.450^{+0.055}_{-0.053}$	$0.574 \pm 0.336^{+0.073}_{-0.052}$
Fe5335 $\pm\sigma_{-vel}^{+vel}$	Å	$0.737 \pm 0.417^{+0.043}_{-0.042}$	$1.470 \pm 0.350^{+0.042}_{-0.040}$	$0.952 \pm 0.464^{+0.054}_{-0.052}$	$0.439 \pm 0.350^{+0.029}_{-0.040}$
Fe5406 $\pm\sigma_{-vel}^{+vel}$	Å	$0.808 \pm 0.419^{+0.004}_{-0.013}$	$0.894 \pm 0.354^{+0.008}_{-0.010}$	$0.655 \pm 0.467^{+0.019}_{-0.013}$	$0.402 \pm 0.352^{+0.014}_{-0.010}$
Fe5709 $\pm\sigma_{-vel}^{+vel}$	Å	$0.380 \pm 0.419^{+0.004}_{-0.001}$	$0.770 \pm 0.356^{+0.001}_{-0.021}$	$0.704 \pm 0.468^{+0.003}_{-0.019}$	$0.172 \pm 0.353^{+0.008}_{-0.004}$
H δ_A $\pm\sigma_{-vel}^{+vel}$	Å	$3.696 \pm 0.435^{+0.038}_{-0.000}$	$0.388 \pm 0.387^{+0.053}_{-0.003}$	$3.686 \pm 0.490^{+0.008}_{-0.018}$	$4.621 \pm 0.367^{+0.032}_{-0.028}$
H γ_A $\pm\sigma_{-vel}^{+vel}$	Å	$1.915 \pm 0.468^{+0.092}_{-0.170}$	$-1.337 \pm 0.396^{+0.051}_{-0.066}$	$1.146 \pm 0.515^{+0.136}_{-0.172}$	$1.895 \pm 0.394^{+0.462}_{-0.040}$
H δ_F $\pm\sigma_{-vel}^{+vel}$	Å	$2.972 \pm 0.478^{+0.003}_{-0.008}$	$0.997 \pm 0.399^{+0.022}_{-0.011}$	$3.716 \pm 0.527^{+0.024}_{-0.027}$	$3.462 \pm 0.399^{+0.026}_{-0.035}$
H γ_F $\pm\sigma_{-vel}^{+vel}$	Å	$2.372 \pm 0.481^{+0.046}_{-0.342}$	$0.678 \pm 0.402^{+0.003}_{-0.008}$	$2.263 \pm 0.539^{+0.060}_{-0.081}$	$2.180 \pm 0.403^{+0.134}_{-0.146}$

Indice \ ID		42	43	45	47
CN ₁ ±σ ^{+σ_{vel}}	mag	-0.079 ± 0.007 ^{+0.013}	-0.155 ± 0.014 ^{+0.018}	-0.066 ± 0.017 ^{+0.001}	0.007 ± 0.029 ^{+0.052}
CN ₂ ±σ ^{+σ_{vel}}	mag	-0.052 ± 0.004 ^{+0.000}	-0.113 ± 0.008 ^{+0.001}	0.011 ± 0.012 ^{+0.002}	0.066 ± 0.021 ^{+0.050}
Ca4227 ±σ ^{+σ_{vel}}	Å	0.601 ± 0.178 ^{+0.002}	0.775 ± 0.331 ^{+0.012}	1.636 ± 0.430 ^{+0.022}	0.516 ± 0.716 ^{+0.501}
G4300 ±σ ^{+σ_{vel}}	Å	4.452 ± 0.220 ^{+0.020}	3.863 ± 0.338 ^{+0.030}	6.603 ± 0.500 ^{+0.117}	9.475 ± 0.792 ^{+0.333}
Fe4383 ±σ ^{+σ_{vel}}	Å	2.270 ± 0.248 ^{+0.029}	0.384 ± 0.366 ^{+0.089}	-1.343 ± 0.818 ^{+0.289}	-0.944 ± 0.889 ^{+0.538}
Ca4455 ±σ ^{+σ_{vel}}	Å	0.666 ± 0.253 ^{+0.046}	0.895 ± 0.370 ^{+0.048}	0.158 ± 0.844 ^{+0.040}	-0.935 ± 0.950 ^{+0.896}
Fe4531 ±σ ^{+σ_{vel}}	Å	2.438 ± 0.266 ^{+0.051}	2.881 ± 0.391 ^{+0.122}	1.085 ± 0.873 ^{+0.007}	3.993 ± 1.026 ^{+0.875}
Fe4668 ±σ ^{+σ_{vel}}	Å	1.541 ± 0.301 ^{+0.037}	0.464 ± 0.431 ^{+0.018}	-2.511 ± 0.921 ^{+0.226}	4.999 ± 1.101 ^{+2.516}
H _β ±σ ^{+σ_{vel}}	Å	2.707 ± 0.304 ^{+0.004}	2.743 ± 0.433 ^{+0.005}	3.233 ± 0.928 ^{+0.028}	2.230 ± 1.115 ^{+0.100}
Fe5015 ±σ ^{+σ_{vel}}	Å	2.563 ± 0.336 ^{+0.093}	2.716 ± 0.442 ^{+0.214}	5.323 ± 0.954 ^{+0.200}	0.887 ± 1.157 ^{+0.761}
Mg ₁ ±σ ^{+σ_{vel}}	mag	-0.006 ± 0.010 ^{+0.000}	0.075 ± 0.011 ^{+0.000}	0.066 ± 0.029 ^{+0.026}	-0.024 ± 0.040 ^{+0.028}
Mg ₂ ±σ ^{+σ_{vel}}	mag	0.074 ± 0.010 ^{+0.000}	0.118 ± 0.011 ^{+0.000}	0.124 ± 0.029 ^{+0.032}	0.104 ± 0.040 ^{+0.042}
Mg _b ±σ ^{+σ_{vel}}	Å	1.235 ± 0.345 ^{+0.014}	1.120 ± 0.447 ^{+0.041}	2.111 ± 0.984 ^{+0.095}	1.586 ± 1.233 ^{+0.198}
Fe5270 ±σ ^{+σ_{vel}}	Å	1.062 ± 0.355 ^{+0.038}	1.764 ± 0.451 ^{+0.114}	1.240 ± 0.993 ^{+0.047}	1.968 ± 1.239 ^{+0.111}
Fe5335 ±σ ^{+σ_{vel}}	Å	0.823 ± 0.368 ^{+0.378}	1.272 ± 0.454 ^{+0.013}	1.483 ± 1.001 ^{+0.045}	0.990 ± 1.250 ^{+0.332}
Fe5406 ±σ ^{+σ_{vel}}	Å	0.965 ± 0.371 ^{+0.028}	1.123 ± 0.456 ^{+0.009}	1.169 ± 1.012 ^{+0.062}	1.941 ± 1.258 ^{+1.184}
Fe5709 ±σ ^{+σ_{vel}}	Å	0.742 ± 0.372 ^{+0.014}	0.674 ± 0.457 ^{+0.033}	0.598 ± 1.032 ^{+0.073}	1.910 ± 1.270 ^{+1.108}
Hδ _A ±σ ^{+σ_{vel}}	Å	2.698 ± 0.405 ^{+0.059}	3.850 ± 0.477 ^{+0.077}	-1.843 ± 1.330 ^{+1.655}	1.876 ± 1.361 ^{+0.105}
Hγ _A ±σ ^{+σ_{vel}}	Å	0.014 ± 0.413 ^{+0.056}	0.220 ± 0.489 ^{+0.203}	-0.069 ± 1.345 ^{+0.129}	0.234 ± 1.397 ^{+1.350}
Hδ _F ±σ ^{+σ_{vel}}	Å	2.560 ± 0.418 ^{+0.019}	2.962 ± 0.494 ^{+0.019}	0.135 ± 1.372 ^{+0.508}	0.266 ± 1.443 ^{+0.239}
Hγ _F ±σ ^{+σ_{vel}}	Å	1.400 ± 0.421 ^{+0.000}	1.786 ± 0.496 ^{+0.000}	1.456 ± 1.378 ^{+0.090}	2.060 ± 1.462 ^{+0.283}

Chapter 5

Conclusions

The work presented here deals with star clusters in five unperturbed spiral galaxies and aims to explore the star cluster formation (and their properties) in environments similar to our galaxy. We think that the most spectacular results come from the most unperturbed galaxy, NGC 45. Despite its small young star cluster population, NGC 45 shows a rich number of globular clusters with properties similar to the irregular galaxies in the Local Group.

We would like to stress the homogeneity of the data used in this thesis. It allowed comparisons without introducing bias due to different observing instruments, observing conditions and analysis techniques. It is for this reason that the comparison of the global star cluster properties become an important point of this thesis. A remarkable result of this thesis is the expansion of the star cluster studies towards the low mass ones. For the first time we are observing star clusters with masses and properties similar to the Milky Way open star clusters. Herewith, the principal results of this thesis are listed and the future perspectives discussed.

5.1 Synopsis

In this section the results of this work are summarized.

Ages and Masses: Low mass star clusters were found in all galaxies. They were interpreted as Milky Way open star cluster counterparts. In the upper mass extreme, only two galaxies showed star clusters with masses greater than 10^5 solar masses. These clusters are located in a starburst galaxy (NGC 5236) and in a galaxy with a strange morphology (NGC 1313).

The environment and the star cluster formation: Comparisons of cumulative age distributions from different galaxies and regions, lead us to the conclusion that the star cluster formation is a process that strongly depends on the local conditions. Two galaxies showed similar star formation histories: NGC 45 and NGC 4395 Although, both galaxies

share the lowest number of detected star clusters. Therefore, their similar star formation histories can be a result of low number statistics.

Sizes: Star cluster sizes were derived in this work. There is a shallow tendency that most massive star clusters tend to be more extended.

Luminosity functions: On each galaxy the luminosity function shows a slope $\sim \alpha = -2$, supporting the idea of an universal mechanism of star cluster formation. The detection of the brightest star cluster on each galaxy is explained as a consequence of the random sampling of the luminosity function.

Disruption times: The present data do not allow us to derive the disruption time, nor discriminate between whether the disruption scenario is mass-dependent or mass-independent. Nevertheless, in this work it is pointed out that star cluster age distributions are influenced by more than one filter and this caveat must be considered in further analysis.

Globular Clusters: Globular clusters were detected in 4 of the 5 galaxies and extensively analyzed in one galaxy: NGC 45. This galaxy hosts a rich population of globular clusters. The analysis of the observed colors showed a unimodal distribution which corresponds to a metal poor population. This was later confirmed for 8 globular clusters through spectroscopical analysis. Their spectra showed alpha abundance ratios lower than the observed in the Milky Way, M31 and M33; but similar to dwarf galaxies in the local group, suggesting that globular clusters in NGC 45 formed after the appearance of the Type Ia supernova.

The kinematics of NGC 45 globular clusters is compared with previous studies of the H I velocity distribution. We noted that globular clusters in NGC 45 do not follow the H I rotation map. Therefore, it is concluded that globular clusters do not show signs of overall rotation and their kinematics correspond to halo or bulge like kinematics.

5.2 Outlook

During the research of this work, several questions were posed. Those questions, I believe, are the main directions for future researches.

- How unperturbed are the unperturbed environments? It is still an open question that needs to be further investigated. The question can be addressed by looking at the star cluster populations in low luminosity galaxies using a combination of ground based and space observations. HST archive, the upgraded HST or/and the new space telescope (JWST) can be used to identify the star clusters on these galaxies. Depending on the available passbands, similar researches to the work presented here can be done and the masses and ages of the star clusters can be derived. Ground based spectroscopical observations will be used to obtain kinematic

information of the detected star clusters. 3D spectroscopy can be used to understand properties of the surrounding media on which star clusters lie. I.e. Does the surrounding media show a chaotic kinematics compared with the kinematics of the star clusters? How do the star cluster kinematics compare among them? So far we do not fully understand the relations between the environment kinematics and star cluster ages. First approach are studies of embedded star clusters (Lada & Lada 2003) and the disruption time approach, however if there are limiting environmental conditions which prevent star clusters to be bound, remain to be further investigated as well as the relation between star cluster ages and the kinematics of their surrounding media.

- Is the star cluster disruption a mass-limited or mass-independent process? This point is related with the previous one. A mass-limited disruption scenario will indicate that star clusters will be disrupted according to their mass. Massive star clusters (more gravitationally bounded) will have better chances to survive interactions with the surrounding media compared with the ones with lower masses (less gravitationally bounded), hinting a relation between the surrounding environment and the star clusters. However, a mass-independent disruption scenario will hint that star clusters disruption is independent of the level of gravitational boundness and thus not being affected by the surrounding media.
- Globular clusters in low luminosity galaxies need to be systematically investigated. Spectroscopical observation aiming at the star cluster kinematics and globular cluster abundances are needed to answer the questions: How they were formed? Are they metallicities similar/different to the host galaxy? Do the globular clusters in this kind of galaxy have a kinematic hot halo? Is there a relation between the more massive star cluster and the lowest mass one? Do they form by the same mechanism?

Since the detection of globular clusters in low luminosity galaxies are done considering magnitudes and sizes criteria HST (or JWST) telescopes are the ideal tool since they are not affected by the distortion of the earth atmosphere, making the identification of extended objects (such as globular clusters) reliable. Globular clusters lying on those galaxies are faint, large telescope are needed (VLT, ELTs) in order to obtain reliable spectra and answer the posed questions.

- The early stages of star cluster formation in spiral galaxies are almost unknown. A natural evolution on the research presented here will be the studies of the dust clouds in spiral galaxies and their embedded star clusters. Unfortunately in order to investigate this we have to wait a few years until ALMA is available.

5.3 Concluding remarks

This thesis is a record of the exiting times that we are living. A time where human kind was starting to observe star clusters similar to the Pleiades, a time where we were trying to

understand if the Milky Way was typical or unique spiral galaxy. A time which may lead to the understanding of the processes involved in the disruption of the star clusters and how their stars finally end up being single stars like the sun. I hope that this contribution helps to better understand the formation and evolution of stars in spiral galaxies. However, it has posed more questions than answers. I hope that those question and answers will inspire new researches.

Acknowledgments

There are many people which I would like to thank, which without them, this work would have not been possible. First, I would like to express my gratitude to my two supervisors Markus Kissler-Patig and Søren Larsen for their excellent support, guidance, teaching, help and insightful conversations about science, ethics and several issues. Also I would like to thank to the people who made my landing in Germany soft and smooth, which also opened their home when I was homeless: Jorge Cuadra and Patricia Arévalo. My office-mates: Maren Hempel, for teaching me all the “secrets and hidden offices at ESO”, Jaroslaw Rzepecki, for hours of fun inside the office and outside work, also for teaching me “some” polish words. Karina Kjær for many thinks which will not fit in one page. Special thanks to the “AstroWG” crew: Anja von der Linden, Michael Bauer and Karina Kjær (yes, you again!) for their company, parties (including toilet dancing) and their help in everything related with work and the German day-to-day life. Mariya Lyubenova, for helping me with administrative matters, for many interesting conversations, coffees, and your contagious laughing. Special thank to Mark Gieles and Constanza Gómez, for hosting me when I was in Utrecht. Margrethe Wold, for her “Freak-out parties” and ”Rocky Horror” movies. Arjan Bik, for many hours of 3D-fit explanations, excellent company in several clubs (including Mittelalterparties) and many coffee breaks. Constanza Araujo, for lending us a room at her place during the last month in München and her aid to recover my health. Also, I would like to thank my friends Rasmus Voss, Cecilia Scannapieco, Andre Waelkens, Daniela Villegas, Yuri Belestky, Steffen Mieske, the “italian mafia” and the ESO students. To the people at the morning coffee, for their interesting and stimulating conversations about almost everything. To Matthias Schreiber for his german translation of the abstract. To my parents and sister for all their support. Last but not least, to my wife Carolina, for her support, love and cheer ups each time I was depressed. Gracias por compartir tu vida con la mía, Te amo.

Marcelo D. Mora Genskowsky
May 2008

Bibliography

- Anders, P. & Fritze-v. Alvensleben, U. 2003, A&A, 401, 1063
- Arp, H. & Sandage, A. 1985, AJ, 90, 1163
- Ashman, K. M. & Bird, C. M. 1993, AJ, 106, 2281
- Ashman, K. M. & Zepf, S. E. 1992, ApJ, 384, 50
- Ashman, K. M. & Zepf, S. E. 1998, Globular Cluster Systems (Globular cluster systems / Keith M. Ashman, Stephen E. Zepf. Cambridge, U. K. ; New York : Cambridge University Press, 1998.)
- Barbuy, B., Bica, E., & Ortolani, S. 1998, A&A, 333, 117
- Barmby, P., Huchra, J. P., Brodie, J. P., et al. 2000, AJ, 119, 727
- Barmby, P., Perrett, K. M., & Bridges, T. J. 2002, MNRAS, 329, 461
- Barth, A. J., Ho, L. C., Filippenko, A. V., & Sargent, W. L. 1995, AJ, 110, 1009
- Bastian, N., Gieles, M., Efremov, Y. N., & Lamers, H. J. G. L. M. 2005a, A&A, 443, 79
- Bastian, N., Gieles, M., Lamers, H. J. G. L. M., Scheepmaker, R. A., & de Grijs, R. 2005b, A&A, 431, 905
- Bastian, N., Hempel, M., Kissler-Patig, M., Homeier, N. L., & Trancho, G. 2005c, A&A, 435, 65
- Beasley, M. A., Brodie, J. P., Strader, J., et al. 2004, AJ, 128, 1623
- Beasley, M. A., Brodie, J. P., Strader, J., et al. 2005, AJ, 129, 1412
- Bertelli, G., Bressan, A., Chiosi, C., Fagotto, F., & Nasi, E. 1994, A&AS, 106, 275
- Bertin, E. & Arnouts, S. 1996, A&AS, 117, 393
- Bica, E., Bonatto, C., Barbuy, B., & Ortolani, S. 2006, A&A, 450, 105

- Bik, A., Lamers, H. J. G. L. M., Bastian, N., Panagia, N., & Romaniello, M. 2003, *A&A*, 397, 473
- Billett, O. H., Hunter, D. A., & Elmegreen, B. G. 2002, *AJ*, 123, 1454
- Binney, J. & Tremaine, S. 1987, *Galactic dynamics* (Princeton, NJ, Princeton University Press, 1987, 747)
- Bohlin, R. C. & Gilliland, R. L. 2004, *AJ*, 127, 3508
- Bottinelli, L., Gouguenheim, L., Paturel, G., & de Vaucouleurs, G. 1985, *ApJS*, 59, 293
- Bottinelli, L., Gouguenheim, L., Paturel, G., & Teerikorpi, P. 1995, *A&A*, 296, 64
- Boutloukos, S. G. & Lamers, H. J. G. L. M. 2003, *MNRAS*, 338, 717
- Bresolin, F. & Kennicutt, Jr., R. C. 2002, *ApJ*, 572, 838
- Brodie, J. P. & Strader, J. 2006, *ARA&A*, 44, 193
- Bruzual, G. & Charlot, S. 2003, *MNRAS*, 344, 1000
- Burstein, D., Faber, S. M., Gaskell, C. M., & Krumm, N. 1984, *ApJ*, 287, 586
- Buzzoni, A. 1989, *ApJS*, 71, 817
- Carignan, C. 1985, *ApJS*, 58, 107
- Carlson, M. N., Holtzman, J. A., Watson, A. M., et al. 1998, *AJ*, 115, 1778
- Carney, B. W. 2001, in *Saas-Fee Advanced Course 28: Star Clusters*, ed. L. Labhardt & B. Binggeli
- Cassisi, S., Castellani, V., degl'Innocenti, S., & Weiss, A. 1998, *A&AS*, 129, 267
- Chabrier, G. 2003, *PASP*, 115, 763
- Chandar, R., Bianchi, L., & Ford, H. C. 1999, *ApJS*, 122, 431
- Chandar, R., Bianchi, L., & Ford, H. C. 2001, *A&A*, 366, 498
- Chandar, R., Bianchi, L., Ford, H. C., & Sarajedini, A. 2002, *ApJ*, 564, 712
- Chandar, R., Fall, S. M., & Whitmore, B. C. 2006, *ApJ*, 650, L111
- Chandar, R., Whitmore, B., & Lee, M. G. 2004, *ApJ*, 611, 220
- Charlot, S. & Bruzual, A. G. 1991, *ApJ*, 367, 126
- Chemin, L., Carignan, C., Drouin, N., & Freeman, K. C. 2006, *AJ*, 132, 2527
- Chiosi, C., Bertelli, G., & Bressan, A. 1988, *A&A*, 196, 84

- Christian, C. A. & Schommer, R. A. 1982, *ApJS*, 49, 405
- Christian, C. A. & Schommer, R. A. 1988, *AJ*, 95, 704
- Conti, P. S. & Vacca, W. D. 1994, *ApJ*, 423, 97
- Côté, P. 1999, *AJ*, 118, 406
- Côté, P., Blakeslee, J. P., Ferrarese, L., et al. 2004, *ApJS*, 153, 223
- Cote, S., Freeman, K. C., Carignan, C., & Quinn, P. J. 1997, *AJ*, 114, 1313
- Crampin, J. & Hoyle, F. 1961, *MNRAS*, 122, 27
- Crampton, D., Cowley, A. P., Schade, D., & Chayer, P. 1985, *ApJ*, 288, 494
- Da Costa, G. S. & Armandroff, T. E. 1995, *AJ*, 109, 2533
- de Grijs, R., Anders, P., Bastian, N., et al. 2003, *MNRAS*, 343, 1285
- de Grijs, R., Anders, P., Lamers, H. J. G. L. M., et al. 2005, *MNRAS*, 359, 874
- de Marchi, G., Clampin, M., Greggio, L., et al. 1997, *ApJ*, 479, L27
- de Vaucouleurs, G. 1963, *ApJ*, 137, 720
- de Vaucouleurs, G. 1979, *AJ*, 84, 1270
- Dolphin, A. E. 2000, *PASP*, 112, 1397
- Elmegreen, B. G. 1994, *ApJ*, 433, 39
- Elmegreen, B. G. & Efremov, Y. N. 1997, *ApJ*, 480, 235
- Elson, R. A. W. & Fall, S. M. 1985, *ApJ*, 299, 211
- Eskridge, P. B., de Grijs, R., Anders, P., et al. 2008, *AJ*, 135, 120
- Faber, S. M. 1972, *A&A*, 20, 361
- Faber, S. M. 1973, *ApJ*, 179, 731
- Fagotto, F., Bressan, A., Bertelli, G., & Chiosi, C. 1994a, *A&AS*, 104, 365
- Fagotto, F., Bressan, A., Bertelli, G., & Chiosi, C. 1994b, *A&AS*, 105, 29
- Fagotto, F., Bressan, A., Bertelli, G., & Chiosi, C. 1994c, *A&AS*, 105, 39
- Fall, S. M. 2004, in *ASP Conf. Ser. 322: The Formation and Evolution of Massive Young Star Clusters*, ed. H. J. G. L. M. Lamers, L. J. Smith, & A. Nota, 399
- Fall, S. M. 2006, *ApJ*, 652, 1129

- Fall, S. M., Chandar, R., & Whitmore, B. C. 2005, *ApJ*, 631, L133
- Fall, S. M. & Rees, M. J. 1985, *ApJ*, 298, 18
- Fall, S. M. & Zhang, Q. 2001, *ApJ*, 561, 751
- Gebhardt, K. & Kissler-Patig, M. 1999, *AJ*, 118, 1526
- Gieles, M., Athanassoula, E., & Portegies Zwart, S. F. 2007a, *MNRAS*, 376, 809
- Gieles, M., Bastian, N., Lamers, H. J. G. L. M., & Mout, J. N. 2005, *A&A*, 441, 949
- Gieles, M., Lamers, H. J. G. L. M., & Portegies Zwart, S. F. 2007b, *ApJ*, 668, 268
- Gieles, M., Larsen, S. S., Bastian, N., & Stein, I. T. 2006a, *A&A*, 450, 129
- Gieles, M., Portegies Zwart, S. F., Baumgardt, H., et al. 2006b, *MNRAS*, 371, 793
- Girardi, L., Bressan, A., Bertelli, G., & Chiosi, C. 2000, *A&AS*, 141, 371
- Girardi, L., Bressan, A., Chiosi, C., Bertelli, G., & Nasi, E. 1996, *A&AS*, 117, 113
- Girardi, L., Chiosi, C., Bertelli, G., & Bressan, A. 1995, *A&A*, 298, 87
- González, J. 1993, PhD Thesis (Univ. of California.)
- Goodwin, S. P. 1997, *MNRAS*, 286, 669
- Gorgas, J., Faber, S. M., Burstein, D., et al. 1993, *ApJS*, 86, 153
- Goudfrooij, P., Alonso, M. V., Maraston, C., & Minniti, D. 2001, *MNRAS*, 328, 237
- Harris, J., Calzetti, D., Gallagher, III, J. S., Smith, D. A., & Conselice, C. J. 2004, *ApJ*, 603, 503
- Harris, W. E. 1991, *ARA&A*, 29, 543
- Harris, W. E. & Pudritz, R. E. 1994, *ApJ*, 429, 177
- Harris, W. E. & van den Bergh, S. 1981, *AJ*, 86, 1627
- Hiltner, W. A. 1960, *ApJ*, 131, 163
- Hodge, P. W. 1979, *AJ*, 84, 744
- Hodge, P. W., Mateo, M., Lee, M. G., & Geisler, D. 1987, *PASP*, 99, 173
- Holtzman, J. A., Faber, S. M., Shaya, E. J., et al. 1992, *AJ*, 103, 691
- Holtzman, J. A., Watson, A. M., Mould, J. R., et al. 1996, *AJ*, 112, 416
- Hubble, E. 1932, *ApJ*, 76, 44

- Hunter, D. A., Elmegreen, B. G., Dupuy, T. J., & Mortonson, M. 2003, *AJ*, 126, 1836
- Hunter, D. A., O'Connell, R. W., Gallagher, J. S., & Smecker-Hane, T. A. 2000, *AJ*, 120, 2383
- Iglesias, C. A., Rogers, F. J., & Wilson, B. G. 1992, *ApJ*, 397, 717
- Johnson, J. A., Bolte, M., Stetson, P. B., Hesser, J. E., & Somerville, R. S. 1999, *ApJ*, 527, 199
- Jordán, A., Côté, P., Blakeslee, J. P., et al. 2005, *ApJ*, 634, 1002
- Jordán, A., McLaughlin, D. E., Côté, P., et al. 2006, *ApJ*, 651, L25
- Karachentsev, I. D. & Drozdovsky, I. O. 1998, *A&AS*, 131, 1
- Karachentsev, I. D., Grebel, E. K., Sharina, M. E., et al. 2003, *A&A*, 404, 93
- King, I. 1962, *AJ*, 67, 471
- Kinman, T. D. 1959, *MNRAS*, 119, 538
- Kissler-Patig, M. 2000a, in *Reviews in Modern Astronomy*, Vol. 13, *Reviews in Modern Astronomy*, ed. R. E. Schielicke, 13
- Kissler-Patig, M. 2000b, in *ASP Conf. Ser. 211: Massive Stellar Clusters*, ed. A. Lançon & C. M. Boily, 55
- Kissler-Patig, M., Ashman, K. M., Zepf, S. E., & Freeman, K. C. 1999, *AJ*, 118, 197
- Koekemoer, A. M., Fruchter, A. S., Hook, R. N., & Hack, W. 2002, in *The 2002 HST Calibration Workshop*, ed. S. Arribas, A. Koekemoer, & B. Whitmore, 337
- Krienke, O. K. & Hodge, P. W. 2007, *PASP*, 119, 7
- Krist, J. 1993, in *ASP Conf. Ser. 52: Astronomical Data Analysis Software and Systems II*, ed. R. J. Hanisch, R. J. V. Brissenden, & J. Barnes, 536
- Kroupa, P., Tout, C. A., & Gilmore, G. 1993, *MNRAS*, 262, 545
- Kumai, Y., Basu, B., & Fujimoto, M. 1993, *ApJ*, 404, 144
- Kundu, A. & Whitmore, B. C. 2001, *AJ*, 121, 2950
- Lada, C. J. & Lada, E. A. 2003, *ARA&A*, 41, 57
- Lamers, H. J. G. L. M., Bastian, N., & Gieles, M. 2004, in *ASP Conf. Ser. 322: The Formation and Evolution of Massive Young Star Clusters*, ed. H. J. G. L. M. Lamers, L. J. Smith, & A. Nota, 409
- Lamers, H. J. G. L. M., Gieles, M., Bastian, N., et al. 2005a, *A&A*, 441, 117

- Lamers, H. J. G. L. M., Gieles, M., & Portegies Zwart, S. F. 2005b, *A&A*, 429, 173
- Larsen, S. S. 1999, *A&AS*, 139, 393
- Larsen, S. S. 2002, *AJ*, 124, 1393
- Larsen, S. S. 2004a, *A&A*, 416, 537
- Larsen, S. S. 2004b, in *ASP Conf. Ser. 322: The Formation and Evolution of Massive Young Star Clusters*, ed. H. J. G. L. M. Lamers, L. J. Smith, & A. Nota, 19
- Larsen, S. S., Brodie, J. P., Huchra, J. P., Forbes, D. A., & Grillmair, C. J. 2001, *AJ*, 121, 2974
- Larsen, S. S., Mora, M. D., Brodie, J. P., & Richtler, T. 2007, *astro-ph/0701697*
- Larsen, S. S. & Richtler, T. 1999, *A&A*, 345, 59
- Larsen, S. S. & Richtler, T. 2000, *A&A*, 354, 836
- Lee, S., Schramm, D. N., & Mathews, G. J. 1995, *ApJ*, 449, 616
- Lejeune, T., Cuisinier, F., & Buser, R. 1997, *A&AS*, 125, 229
- Lejeune, T., Cuisinier, F., & Buser, R. 1998, *A&AS*, 130, 65
- Lutz, D. 1991, *A&A*, 245, 31
- Maíz-Apellániz, J. 2001, *ApJ*, 563, 151
- Maraston, C. 1998, *MNRAS*, 300, 872
- Maraston, C., Bastian, N., Saglia, R. P., et al. 2004, *A&A*, 416, 467
- Melnick, J. & D'Odorico, S. 1978, *A&AS*, 34, 249
- Melnick, J., Moles, M., & Terlevich, R. 1985, *A&A*, 149, L24
- Meurer, G. R., Heckman, T. M., Leitherer, C., et al. 1995, *AJ*, 110, 2665
- Miller, G. E. & Scalo, J. M. 1979, *ApJS*, 41, 513
- Minniti, D. 1995, *AJ*, 109, 1663
- Mochejska, B. J., Kaluzny, J., Krockenberger, M., Sasselov, D. D., & Stanek, K. Z. 1998, *Acta Astronomica*, 48, 455
- Mora, M. D., Larsen, S. S., & Kissler-Patig, M. 2007, *A&A*, 464, 495
- Morgan, W. W. 1959, *AJ*, 64, 432
- O'Connell, R. W., Gallagher, III, J. S., & Hunter, D. A. 1994, *ApJ*, 433, 65

- O'Connell, R. W., Gallagher, III, J. S., Hunter, D. A., & Colley, W. N. 1995, *ApJ*, 446, L1
- Olsen, K. A. G., Miller, B. W., Suntzeff, N. B., Schommer, R. A., & Bright, J. 2004, *AJ*, 127, 2674
- Paturel, G., Petit, C., Prugniel, P., et al. 2003, *A&A*, 412, 45
- Peebles, P. J. E. & Dicke, R. H. 1968, *ApJ*, 154, 891
- Perrett, K. M., Bridges, T. J., Hanes, D. A., et al. 2002, *AJ*, 123, 2490
- Puche, D. & Carignan, C. 1988, *AJ*, 95, 1025
- Puzia, T. H., Kissler-Patig, M., Thomas, D., et al. 2005, *A&A*, 439, 997
- Puzia, T. H., Saglia, R. P., Kissler-Patig, M., et al. 2002, *A&A*, 395, 45
- Quintana, H., Ramirez, A., & Way, M. J. 1996, *AJ*, 111, 603
- Rafelski, M. & Zaritsky, D. 2005, *AJ*, 129, 2701
- Renzini, A. 1994, in *Galaxy Formation*, ed. J. Silk & N. Vittorio, 303
- Renzini, A. & Buzzoni, A. 1986, in *Spectral evolution of galaxies*, p. 195 - 235, 195–235
- Rhode, K. L., Zepf, S. E., Kundu, A., & Larner, A. N. 2007, *AJ*, 134, 1403
- Rieke, G. H. & Lebofsky, M. J. 1985, *ApJ*, 288, 618
- Rose, J. A. 1985, *AJ*, 90, 1927
- Salpeter, E. E. 1955, *ApJ*, 121, 161
- Santos, M. R. 2003, in *Extragalactic Globular Cluster Systems*, ed. M. Kissler-Patig, 348
- Sarajedini, A., Geisler, D., Schommer, R., & Harding, P. 2000, *AJ*, 120, 2437
- Sbordone, L., Bonifacio, P., Marconi, G., Buonanno, R., & Zaggia, S. 2005, *A&A*, 437, 905
- Schlegel, D. J., Finkbeiner, D. P., & Davis, M. 1998, *ApJ*, 500, 525
- Schulz, J., Fritze-v. Alvensleben, U., Möller, C. S., & Fricke, K. J. 2002, *A&A*, 392, 1
- Schweizer, F. 1987, in *Nearly Normal Galaxies. From the Planck Time to the Present*, ed. S. M. Faber, 18
- Schweizer, F. 1997, in *Astronomical Society of the Pacific Conference Series, Vol. 116, The Nature of Elliptical Galaxies; 2nd Stromlo Symposium*, ed. M. Arnaboldi, G. S. Da Costa, & P. Saha, 447

- Schweizer, F., Miller, B. W., Whitmore, B. C., & Fall, S. M. 1996, *AJ*, 112, 1839
- Schweizer, F. & Seitzer, P. 1998, *AJ*, 116, 2206
- Searle, L., Wilkinson, A., & Bagnuolo, W. G. 1980, *ApJ*, 239, 803
- Searle, L. & Zinn, R. 1978, *ApJ*, 225, 357
- Shapley, H. & Lindsay, E. M. 1963, *Irish Astronomical Journal*, 6, 74
- Sirianni, M., Jee, M. J., Benítez, N., et al. 2005, *PASP*, 117, 1049
- Spitzer, L. 1987, *Dynamical evolution of globular clusters* (Princeton, NJ, Princeton University Press, 1987.)
- Spitzer, L. J. & Harm, R. 1958, *ApJ*, 127, 544
- Stetson, P. B. 1993, in *Astronomical Society of the Pacific Conference Series*, Vol. 48, *The Globular Cluster-Galaxy Connection*, ed. G. H. Smith & J. P. Brodie, 14
- Thomas, D., Maraston, C., & Bender, R. 2003, *MNRAS*, 339, 897
- Thomas, D., Maraston, C., & Korn, A. 2004, *MNRAS*, 351, L19
- Tinsley, B. M. 1968, *ApJ*, 151, 547
- Tolstoy, E., Venn, K. A., Shetrone, M., et al. 2003, *AJ*, 125, 707
- Trager, S. C., Worthey, G., Faber, S. M., Burstein, D., & Gonzalez, J. J. 1998, *ApJS*, 116, 1
- van den Bergh, S. 1971, *A&A*, 12, 474
- van den Bergh, S. 1981, *A&AS*, 46, 79
- van Zee, L., Salzer, J. J., Haynes, M. P., O'Donoghue, A. A., & Balonek, T. J. 1998, *AJ*, 116, 2805
- VandenBerg, D. A., Swenson, F. J., Rogers, F. J., Iglesias, C. A., & Alexander, D. R. 2000, *ApJ*, 532, 430
- Vázquez, G. A., Leitherer, C., Heckman, T. M., et al. 2004, *ApJ*, 600, 162
- Watson, A. M., Gallagher, III, J. S., Holtzman, J. A., et al. 1996, *AJ*, 112, 534
- Whiting, A. B. 1999, *AJ*, 117, 202
- Whitmore, B. C. 2003, in *A Decade of Hubble Space Telescope Science*, ed. M. Livio, K. Noll, & M. Stiavelli, 153–178
- Whitmore, B. C., Chandar, R., & Fall, S. M. 2007, *AJ*, 133, 1067

- Whitmore, B. C. & Schweizer, F. 1995, *AJ*, 109, 960
- Whitmore, B. C., Schweizer, F., Leitherer, C., Borne, K., & Robert, C. 1993, *AJ*, 106, 1354
- Worthey, G. 1994, *ApJS*, 95, 107
- Worthey, G., Faber, S. M., Gonzalez, J. J., & Burstein, D. 1994, *ApJS*, 94, 687
- Worthey, G. & Ottaviani, D. L. 1997, *ApJS*, 111, 377
- Zepf, S. E. & Ashman, K. M. 1993, *MNRAS*, 264, 611
- Zepf, S. E., Ashman, K. M., English, J., Freeman, K. C., & Sharples, R. M. 1999, *AJ*, 118, 752
- Zhang, Q. & Fall, S. M. 1999, *ApJ*, 527, L81
- Zinn, R. 1985, *ApJ*, 293, 424

Curriculum Vitae : Marcelo Mora

PERSONAL

Last name: Mora Genskowsky
First name: Marcelo Daniel
Date of birth: October 16th, 1976, Santiago Chile
Nationality : Chilean
Languages : Spanish (native)
English (good)
German (basic)
Hobbies Music and Poetry
Professional Address : European Southern Observatory,
Karl-Schwarzschild-Strasse 2, 85748
Garching bei München, Germany.
email : mmora@eso.org

EDUCATION

- 2008-** : Post Doc. at Universidad de Valparaíso Chile.
- 2004-2008** : PhD in Astronomy at the Ludwig-Maximilians-Universität München
Home institution: European Southern Observatory (ESO).
Advisors: Markus Kissler-Patig and Søren larsen
- 2001-2004** : Magister en Física (Master on Physics). P. Universidad Católica de Chile,
Santiago, Chile.
- 1995-2001** : Physics degree: Licenciatura en Físicas. Pontificia Universidad Católica
de Chile. Santiago, Chile.

ASTROPHYSICS SCHOOLS

Nov-Dec 2005 : XVII Canary Island Winter School of Astrophysics,
“3-D Spectroscopy” Puerto de la Cruz, Tenerife, Spain.

Jan-Mar 2002 : Cerro Tololo Inter-American Observatory (CTIO).
“Práctica de investigación en astronomía” (PIA) :
K Corrections in Type Ia supernovae .
Advisor: Dr. Nicholas B. Suntzeff.

OBSERVATIONAL EXPERIENCE

Oct 2002 : Two night at VLT at Paranal (ESO)
Aug 2002 : Two night with 3.8m telescope and NTT at La Silla (ESO)
Jan 2002 : Two night observing with 0.9m telescope
at CTIO as part of the PIA/REU program.

PI

2008 PI of *Interacting star cluster in Centaurus A*
ID 081.D-0705
2006 PI of *Globular clusters in the low luminosity spiral galaxy*
NGC 45 ID 077.D-0403

TEACHING EXPERIENCE:

- Teaching assistance of lectures and laboratories at the Facultad de Física of the Pontificia Universidad Católica de Chile from 1998-2004 : Physics I, Stellar Astrophysics, Classic Physics, and Electromagnetism.

COMPUTING SKILLS:

- Operating system: UNIX, Windows.
- Data reduction softwares: IRAF.(Spectra and photometry reductions), ISIS, SExtractor, Daophot II.
- Programming: scripts on C, bash, Perl, Python, and SuperMongo plots.

PUBLICATIONS:

- **Mora, M. D.**; Larsen S. S. & Kissler-Patig, M. “*Spectroscopy of globular clusters in the low-luminosity spiral galaxy NGC 45*” 2008, A&A 489, 1065
- **Mora, M. D.**; Larsen S. S. & Kissler-Patig, M. “*Imaging of star clusters in unperturbed spiral galaxies with the Advanced Camera for Surveys. I. The low luminosity galaxy NGC 45*” 2007, A&A 464, 495

- Magrini, L; Corradi, R.L.M.; Greimel, R., Leisy, P.; Mampaso, A.; Perinotto, M.; Walsh, J.R.; Walton, N.A.; Zijlstra, A.A.; Minniti, D.; **Mora, M** 2005, MNRAS, 361, 571
- Guldenschuh, K.A.; Layden, A.C.; Wan Y.; Withing, A.; van der Bliet, N.; Baca, P.; Carlin, J.; Freimuth, T.; **Mora, M.**; Salyk, C.; Vera, S.; Verdugo, M.; Young, A. 2005, PASP, 117, 721

CONFERENCES ATTENDED:

- 2006, May 29-June 1: Mass loss from stars and stellar clusters: Lunteren, The Netherland.
Poster contribution : *Star Clusters in NGC 5236*
- 2006, March 6-10: Globular Clusters : Guide to Galaxies, Concepción, Chile.
Poster contribution : *Two star cluster population in NGC 45*
- 2005, November 21- December 2 XVII Canary Island Winter School of Astrophysics, “3-D Spectroscopy” Puerto de la Cruz, Tenerife, Spain.
- 2005, July 23-8 Island Universes: the structure and evolution of Disk Galaxies, Terschelling, The Netherlands.
Poster contribution : *Continuous star formation cluster formation in NGC 45*
- 2003, January 5-10 21th AAS meeting Seattle, USA.
Poster Contribution : *K corrections in Type IA supernovae*
- 2002, March 11-14: *Massive star formation*. La Serena, Chile.

Marcelo D. Mora Genskowsky